공학박사학위논문

Regulation of human embryonic stem cell fate *via* generation of size-controlled human embryoid bodies using magnetic nanoparticles

자성나노입자를 이용한 인간배아체의 크기 조절 구현 및 이를 통한 인간배아줄기세포의 분화 조절

2019 년 2 월

서울대학교 대학원

공과대학 화학생물공학부

손 보 람

Abstract

Regulation of human embryonic stem cell fate *via* generation of size-controlled human embryoid bodies using magnetic nanoparticles

Boram Son

School of Chemical and Biological Engineering

The Graduate School

Seoul National University

Human embryonic stem cells (hESCs) possess unique properties in terms of self-renewal and differentiation, which make them particularly well-suited for use in tissue engineering and regenerative medicine. The differentiation of hESCs in the

form of human embryoid bodies (hEBs) recapitulates early embryonic development, and hEBs may provide useful insight into the embryological development of humans.

Herein, cell-penetrating magnetic nanoparticles (MNPs) were utilized to form hEBs with defined sizes and the differentiation patterns were analyzed. The MNPs were sufficiently delivered into hESCs, when feeder-free culture system of the hESCs was applied. Then the suspended and magnetized hESCs efficiently clustered into hEBs driven by magnetic pin-based concentrated magnetic force system. The size of hEBs was controlled by varying the suspended cell numbers which were added in a well of the concentrated magnetic force system. After 3 days of differentiation in a suspended condition, ectodermal differentiation was enhanced in small hEBs (150 μm in diameter) while endodermal and mesodermal differentiation was enhanced in large hEBs (600 μm in diameter).

In the spontaneous differentiation of size-controlled hEBs, some of small-sized hEBs, which showed glial fibrillary acidic protein (GFAP)-positive staining, sprouted neurite-like outgrowth. In fact, many researchers have tried to induce neural differentiation of the hEBs due to the similarity of tissue elasticity to the brains and the correspondence of the enhanced intercellular interactions with the actual nerve cells. In this work, to improve the neural development of small-sized hEBs, neural induction medium (NIM) was applied for 5 days (IV) and they were compared with 3 other groups of hESCs; the undifferentiated hESCs which maintained their pluripotency (I), the hESCs neurally induced in NIM for 5 days (II) and the hESCs neurally induced in NIM with the MNPs for 5 days (III). Neurally

induced small hEBs showed significantly improved neural induction compared to the other groups. Furthermore, the MNPs themselves demonstrated neurogenic effect synergic with NIM. Additionally, signaling pathways of the accelerated neural induction of IV were detected through expression of representative proteins; WNT proteins, dopaminergic neuronal proteins, proteins related to intercellular communications, and proteins related mechanotransduction.

To summarize, MNP-based size-controlled hEB generation method was devised and using this technique, it was revealed that the size of hEBs is one of the important factors that determine the direction of early differentiation of hESCs. In addition, small-sized hEBs, generated *via* the MNP-based methodology, were neurally induced and the neural induction was effectively improved, reducing the time required for early neural induction. Furthermore, it was confirmed that this process followed the WNT3 signaling pathways and dopaminergic neuronal pathways. Additionally, it was revealed that this result was caused by the enhancement of the intercellular interactions and mechanotransduction, resulting from the hEB generation technique using MNPs. Therefore, the MNP-based hEB size control method proposed in this study would be useful for inducing lineage-specific differentiation of hESCs and determining the cell fate. If this technology could be used to induce the differentiation of hESCs into a variety of cell types, applications to tissue engineering and simulations of embryogenesis would be possible.

Keywords: human embryonic stem cells (hESCs), embryoid bodies (EBs), EB size

control, lineage-specific differentiation, cell fate regulation, magnetic nanoparticles (MNPs), iron oxide nanoparticles

Student Number: 2012-20953

Contents

List of figures

List of tables

List of abbreviations

ALP: alkaline phosphatase

AM: acetoxymethyl

bFGF: basic fibroblast growth factor

BME: β-mercaptoethanol

BM-hMSC: bone marrow-derived human mesenchymal stem cell

BSA: bovine serum albumin

CCK-8: cell counting kit-8

CD31: cluster of differentiation 31

cDNA: complementary deoxyribonucleic acid

CLSM: confocal laser scanning microscopy

DAPI: 4',6-diamidino-2-phenylindole

DMEM: Dulbecco’s modified eagle medium

DMEM/F-12: Dulbecco’s modified eagle medium: nutrient mixture F-12

DMSO: dimethyl sulfoxide

E8: essential 8 medium

ECM: extracellular matrix

ESC: embryonic stem cell

EthD-1: ethidium homodimer-1

FAK: focal adhesion kinase

FBS: fetal bovine serum

FF: feeder-free

GAP43: growth associated protein 43

GAPDH: glyceraldehyde 3-phosphate dehydrogenase

GDNF: glial cell line-derived neurotrophic growth factor

GFAP: glial fibrillary acidic protein

hEB: human embryoid body

hESC: human embryonic stem cell

hMSC: human mesenchymal stem cell

HRP: horseradish peroxidase

ICC: immunocytochemistry

ICP-AES: inductively coupled plasma atomic emission spectroscopy

KOSR: knockout serum replacement

MAP2: microtubule-associated protein 2

mESC: mouse embryonic stem cell

MMC: mitomycin C

MNP: magnetic nanoparticle

mRNA: messenger ribonucleic acid

MSGM: magnetic spirillum growth medium

NCAM: neural cell adhesion molecule

NdFeB: neodymium iron boron

NEAA: nonessential amino acid

NES: nestin

NIM: neural induction medium

NPC: neural progenitor cell

OCT4: octamer-binding transcription factor 4

OTX2: orthodenticle homologue 2

PAX6: paired box 6

PBS: phosphate buffered saline

PBST: triton X-100 in phosphate buffered saline

PCR: reverse transcription polymerase chain reaction

PDX1: pancreatic and duodenal homeobox 1

PFA: paraformaldehyde

PROX1: prospero homeobox protein 1

PS: penicillin and streptomycin

PSC: pluripotent stem cell

ROCK: rho-associated protein kinase

RT-PCR: reverse transcription polymerase chain reaction

RUNX1: runt-related transcription factor 1

SDS-PAGE: sodium dodecyl sulfate polyacrylamide gel electrophoresis

SOX1: sex determining region Y-box 1

SOX2: sex determining region Y-box 2

SOX17: sex determining region Y-box 17

T: brachyury

TE: trypsin-ethylenediaminetetraacetic acid

TEM: transmission electron microscopy

TUBB3: tubulin beta 3 class III

Chapter 1.

Research background and objectives

Chapter 1. Research background and objectives

Since the discovery of their existence, stem cells have been consistently considered as a hope for the treatment of incurable diseases due to the self-renewal ability and pluripotency [1, 2], which are inherent characteristics of the stem cells [3-5]. In particular, human embryonic stem cells (hESCs) isolated from human embryos (in detail, inner cell mass of the blastocysts) have the potential to become almost all cell types in our body [6, 7]. Therefore, efforts have been made to induce differentiation of the hESCs into specific cells, which are difficult to recover and regenerate once damaged, represented as neurons and cardiomyocytes [8, 9].

Researchers have tried to make efficient use of these potentials of the stem cells, that is to say, the differentiation of stem cells into specific cells was never easy [10-12]. Although embryogenesis of *in vivo* embryos has completely differentiated stem cells into various cells, there have been limitations to differentiate the hESCs *in vitro* [13, 14]. In order to induce the differentiation of stem cells into specific cells, it is difficult to achieve homogeneous differentiation in which all cells undergo the same differentiation [15, 16], even if the hESCs are treated with chemical inducers [17-20]. To control the hESCs differentiating into different types under the same conditions, the researchers became interested in the physical environment applied to the stem cells [21-23].

The approach to the physical environments of the hESCs began with mimicking actual hESCs, to emulate the *in vivo* condition in which embryos are cultured [15, 24-27]. Therefore, there have been various attempts to aggregate the hESCs to

produce three-dimensional (3D) form of the hESCs, called hEBs [28, 29].

In this study, through hEB generation with a novel and efficient method, the fate of the hESCs was regulated by differentiating them into specific lineages, and to improve the directing efficiency. In order to produce hEBs, nanotechnology of magnetic nanoparticles (MNPs) was utilized because this method was considered as a solution to overcome the limitations of the conventional cell assembling; non-uniformity of cell aggregates and different sizes [30-34]. The uniform and size-controlled hEB generation was required to investigate whether the differentiation direction differs according to the diameter of hEBs, furthermore, whether this initial direction of differentiation could improve the neural induction of the hESCs.

If the fate of hESCs in early stage can be regulated and thus the efficiency of lineage-specific differentiation could be enhanced, this technology would be applicable not only to treat the degenerative diseases, but also to understand the embryogenesis of the hESCs *in vivo*.

Chapter 2.

Literature review

Chapter 2. Literature review

2.1 Stem cell

2.1.1 Embryonic stem cell (ESC) and adult stem cell

Stem cells have the potential to be distinguished from many other mammalian cells which are already given their own functions and are already performing well [35, 36]. A stem cell has its own ability to transform into various cell types that constitute a specific tissue or organ in the body [6, 7]. These stem cells are classified into two types depending on the collection timing (Figure 2.1.1.1) [37]. If the donor decides to provide cells before birth, the stem cells extracted from the inner cell mass of embryo at the blastocystic stage are called “embryonic stem cells (ESCs)”. Otherwise, when the donor decides to provide cells after birth, the stem cells extracted from the adult are called “adult stem cells”. Since the characteristics of adult stem cells differ depending on the actual extraction location of the body, usually origin comes along; fat-derived, bone marrow-derived and etc [38-40].

Stem cells differ in their ability to change, depending on their type. As ESCs are extracted from the developmental stage of embryos, they can be transformed into almost all kinds of cells that make up our body, and this ability is called “pluripotency” [37]. Since adult stem cells have already been separated in a particular lineage, there are several possibilities for divergence, called “multipotency” [38-40]. Regardless of their degrees of the potentials, researchers have tried to utilize the stem cells for clinical applications in tissue engineering and regenerative medicine,

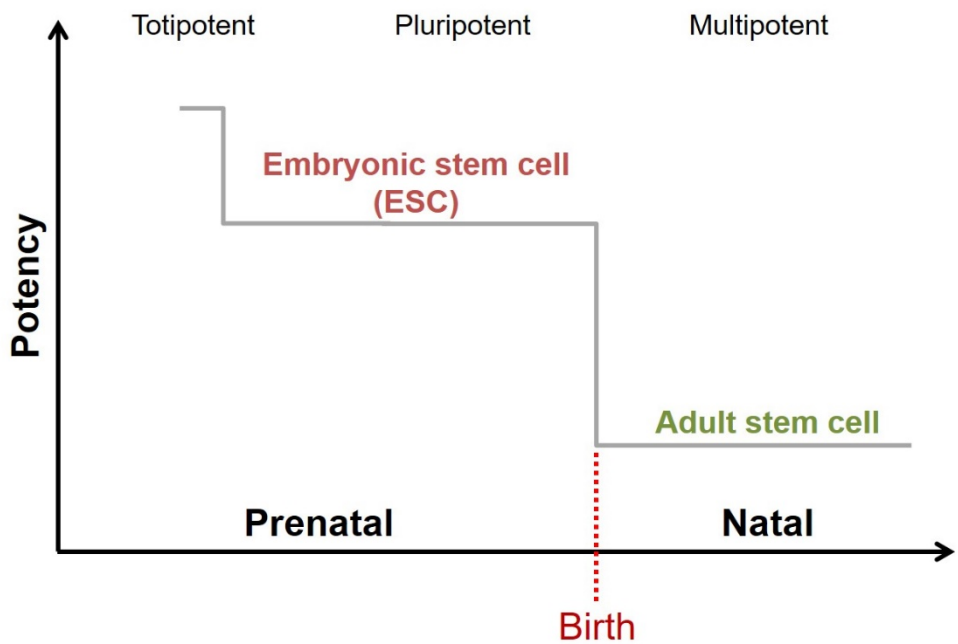

Figure 2.1.1.1 ESCs and adult stem cells.

because of the advantages that stem cells can be transformed into various cells. It would be possible to transform stem cells into specific cells of damaged tissue in the body in order to use them in therapy by reconstructing damaged organs and also in order to generate a model that mimics the body *in vitro* [41, 42].

However, for these studies, the transformation of stem cells needs to be controlled precisely. This transformation is called “differentiation”, and research using stem cells focuses on narrowing and limiting the direction of this differentiation, and increasing its efficiency [15, 16]. If the differentiation of stem cells cannot be precisely controlled, there may be a mixture of unintended cell types, as well as the cells of a specific tissue intended by the researcher. The result of this heterogeneous differentiation is a direct cause of tumor formation and also is a major obstacle in clinical research using stem cells. Therefore, in order to take full advantage of the attractive properties of the stem cells, it is important to develop chemical and physical methods that homogeneously differentiate the stem cells into targeted cell types.

2.1.2 Regulation of stem cell differentiation

In studies using stem cells, researchers have tried to differentiate stem cells into specific cell types suitable for application to particular tissues [7, 10-13]. In this process, elaborate regulation is required for the cell differentiation into homogeneous cell types. However, the methods of precise differentiation control should be improved to achieve high efficiency on homogeneous performance. Although the details of the mechanisms involved in stem cell differentiation have not been fully elucidated, there have been considerable progresses in research on chemical factors that influence the direction of differentiation. Thus, the chemical factors, represented as particular growth factors and cytokines that induce designated signaling pathways through chemical cues, have widely been used commercially for controlled differentiation of stem cells into targeted tissue-specific cells.

Recently, there is an academic interest in the physical factors that act as regulators of stem cell differentiation [43, 44]. Determination of cell fate based on various methods and degree of physical stimuli, which stem cells perceive from extracellular environment, is important for researchers studying the direction of stem cell differentiation.

Physical factors transmit specific signals to stem cells through mechanical stimulations [45]. When a physical factor-recognizing receptor on the surface of a cell receives stimulation, intracellular cytoskeletons connected to the receptor are stimulated sequentially [46, 47]. This is initially a physical force, such as simple pull or push, but it is converted into a signal that causes a conformational change of

particular downstream proteins. Then, it affects the expression of specific genes in the nucleus of a cell, resulting in regulation of stem cell differentiation. Thus, physical factor-based control of stem cell fate is capable *via* cell-level perception of external physical stimuli and then cytoskeleton-derived particular cascades. Therefore, in order to differentiate stem cells in a desired direction, it is important to precisely control the physical stimulations and the microenvironments of stem cells.

2.1.3 Stem cell in three-dimension (3D)

To achieve regulated differentiation of ESCs, there have been attempts to make the cells in the form of 3D mimicking the embryos [48]. Comparing with two-dimensional (2D) ESC cultivation and differentiation method, which is still conventionally used in laboratory, 3D embryoid body (EB) generation and differentiation method has been proposed as an ideal method for efficient differentiation of the ESCs [24-29]. Since the EBs are modeled on the morphology of embryos, ESCs in the form of EBs are spontaneously induced to differentiate into a variety of directions.

Researchers have tried to generate EBs through various cell clustering methods including the hanging-drop method, which has been widely used for a long time, non-sticking surface culture method, and porous 3D scaffold culture method (Figure 2.1.3.1) [30-33, 49-51]. However, such conventional cell clustering methods have

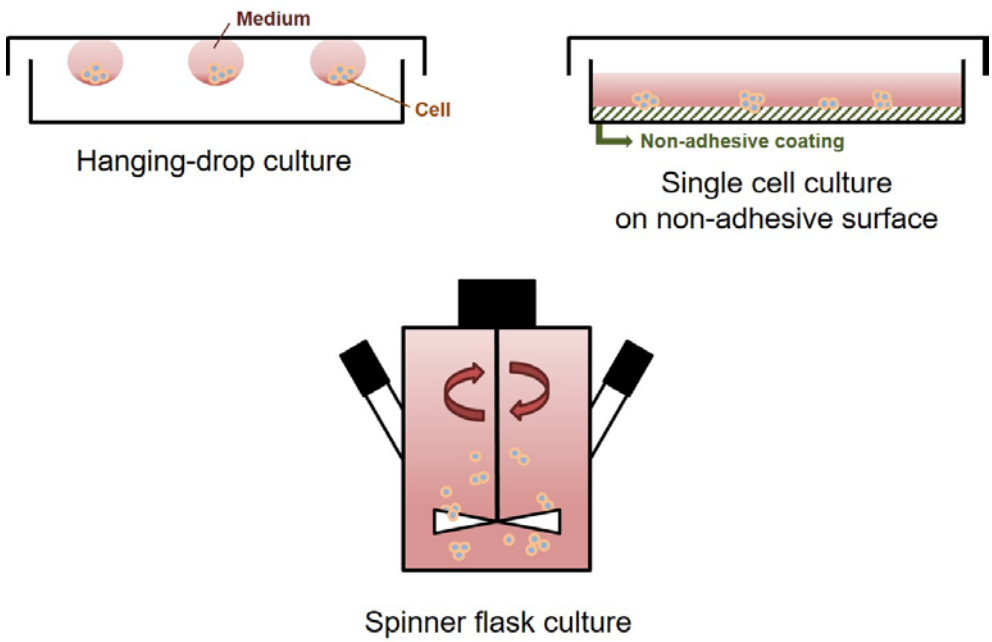

Figure 2.1.3.1 Previously utilized EB generation methods.

limitations in producing cell aggregates of uniform size, and thus it may be difficult to use these methods for exquisite ESC differentiation. Recently, microscale technology has been applied to EB production to overcome this problem (Figure 2.1.3.2) [34, 52-57]. Microfluidic devices [52-54] and microwells [55-57] were used as elaborate methods for EB generation of uniform diameter. However, the EB fabrication method using the microscale technique still has limitations on the efficiency of the platform fabrication, the time required for the final EB generation, and the uniformity of the shape and size of the EBs.

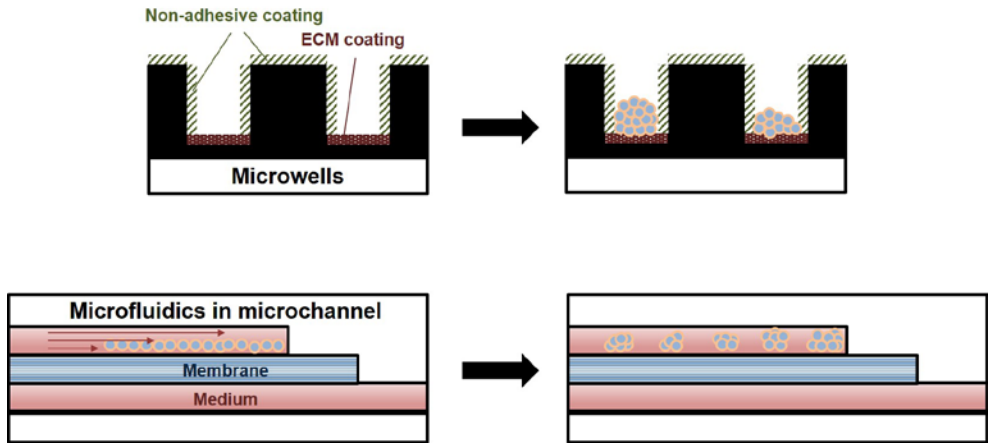

Figure 2.1.3.2 EB generation using microscale technologies.

2.2 Magnetic nanoparticles (MNPs)

2.2.1 Characteristics of MNPs

There are many kinds of magnetic particles used in biochemistry. Properties such as size, magnetism and surface are controlled according to biochemical uses [58-62]. Most of the magnetic particles are applied for the mechanotransduction of cells since they are mostly sized to nanoscale in order to enable intracellular delivery and accumulation [62-67]. Those nano-sized magnetic particles, called “magnetic nanoparticles (MNPs)” that are incorporated in cells, physically stimulate the intracellular organelles, resulting in determination of the cell fate [68]. Magnetic properties of the MNPs are usually dependent on their size, thus they possess various properties ranging from superparamagnetism to ferromagnetism, according to their size [69-74]. This property is important in the interaction with an extracellular magnetic field, which would be artificially provided for controlling the differentiation of cells, based on magnetic force [75-83]. The MNPs are produced by chemical or biological synthesis. Chemical synthesis of the MNPs is a common method of manufacturing to ensure uniformity of dimensions and various surface coatings [58-60]. Meanwhile, biological synthesis of the MNPs from magnetic bacteria solves the problem of biocompatibility [23, 84].

Among the various biological usages, application of the MNPs for stem cell research and tissue engineering has been popularized [85]. This is because MNP-based activation has proven to be effective for controlling stem cell differentiation efficiency [75-83]. In this research field, the MNPs commonly used possess iron

oxide as a core due to the convenience in coprecipitation of iron salt and also in surface modification with various functional materials [58-61].

When the synthesized MNPs are applied to stem cells, they can attach to the cell surface *via* receptor-ligand binding, or can incorporate into the cells through endocytosis [62-67]. MNPs bound to the cell surface physically influence the cell membranes, and thus intracellular organelles by the manipulation of magnetic field outside the cell [68]. This allows elaborate regulation of stem cell differentiation by inducing acute mechanotransduction processes. And the MNPs incorporated into the cells contribute to magnetization of the cells [84, 86]. When a cell is magnetized, it acts like a small magnet, thus its movement can be controlled by external magnetic force. Therefore, cell aggregates can be simply produced, and such methods can be applied to tissue engineering and regenerative medicine using stem cells.

2.2.2 Benefits of using MNPs in biological applications

2.2.2.1 Controllability of elaborate differentiation

As discussed above, in the studies using stem cells, differentiation of stem cells into specific cells of a desired tissue has important significance in tissue engineering and regenerative medicine [35, 41, 87]. Thus, methods have been studied to control the fate of stem cells and, consequently, to increase the efficiency of homogenous differentiation into restricted cell types [42]. Various types of stimuli or factors

have been applied to the stem cells for the effective stem cell differentiation [88, 89]. These factors may be chemical factors such as growth factors or physical factors, that provide mechanical stimulation. Since physical factors can be managed finely and thus useful for investigating unknown mechanisms of chemical factors, researchers have paid attention to the physical cues [43, 44]. These physical factors could be applied to stem cells without any chemical factors, or in combination with some chemical factors for synergistic effects on stem cell differentiation [43, 44, 90].

In various types of physical stimuli, the effects of magnetic stimulation on the regulation of stem cell differentiation have been studied [45-47, 90]. Magnetic stimulation uses the MNPs and exterior magnetic force. Since the magnitude of the magnetic force can be easily manipulated, it is possible to control the differentiation simply by applying magnetic force to MNP-incorporated stem cells [85]. Although the mechanisms causing the differentiation of stem cells have not been elucidated in detail, it is known that the differentiation is roughly based on the regulation of downstream protein expression in cytosols and the regulation of gene expression in nuclei [46, 47]. Because the MNPs are nanoscale in size, they can be applied to these downstream protein levels, which can lead to sensitive differentiation regulation through elaborate stimulation regulation.

2.2.2.2 Efficient cell maintenance during transplantation

The ultimate goal of tissue engineering is to repair a damaged tissue or organ [3-5]. Thus, stem cells that are differentiated into a specific cell types of the targeted tissue, are eventually injected into the body in order to replace the damaged tissue area [91, 92]. Therefore, successful engraftment of cells is crucial when such surgical implantation is required in clinical practice. Due to the speed of the moving fluid (body fluids containing blood), most injected cells are scattered by the liquid before they provide a healing effect [93]. Thus, increasing the cell maintenance efficacy of damaged areas is an important limitation for successful transplantation.

There have been many attempts to immobilize the cells to the desired area [94, 95]. Because immobilization of cells depends on physical cues, a variety of physical forces are used to stably bind the cells *in situ*. Among the various physical stimulation methods, the magnetic force-based cell maintenance method has gained popularity with its simplicity and effectiveness [93, 96, 97]. If the cells are magnetized by the incorporation of the MNPs, this method becomes simpler. This is because the mobility of the injected magnetized cells can be sufficiently controlled by the external magnetic force. Recently, studies on tissue engineering using MNP-based cell maintenance method have shown that the grafted cells can be effectively immobilized at desired points by external magnetic forces [84, 86]. Therefore, strategies using MNPs and magnetic force can be applied not only to differentiation of stem cells but also to tissue engineering including grafting of the cells.

2.2.3 MNP-based stem cell fate commitments

The application of physical force using the MNPs is advantageous for precise control of stem cell fate [88, 89]. Since the MNPs are magnetically managed, fine control of the cell commitments by delivering a physical effect into cells is possible through exquisite regulation of exterior magnetic force under MNPs-cells combined condition [62-67]. By modulating the magnetic force outside the cells, the MNPs bound to the cells can be clustered or dispersed to each other, and also can be pulled or rotated in a specific direction [66, 69, 83]. It may lead to morphological changes of the cells such as lengthening or twisting of the cellular structure, resulting in changes in the intracellular organelles, especially the cytoskeletons which ultimately affects the intracellular signaling pathways into the cells. The physical stimuli delivered to the intracellular organelles is a significant factor that determines the phosphorylation of some downstream proteins, and through this, a specific cascade could be expressed or inhibited, which ultimately affects gene expression in the nuclei [98-106]. As a result, it is possible to derive such precise results through the technology of an external artificial magnetic field control and the MNP synthesis technique, by which the characteristics of MNPs such as size, magnetic force, and surface materials can be regulated.

Alternatively, the MNPs can be incorporated into stem cells inducing the cells to behave like a small magnet for the regulation of cell fate [23, 62-67, 84, 86]. By the MNP introduction, the cells with MNPs are magnetized and those magnetized cells are responsive to external magnetic forces. When a magnetized cell is

attached to a substrate and is subjected to a pulling force to specific direction by a static magnetic force, the cell may experience artificial pressure or tension [83]. On the other hand, free-floating magnetized cells may have mobility due to an external magnetic field to specific direction [66, 69, 83]. At this time, they may be exposed to a rotating stimulus by an external variable magnetic field, which causes shear stress to the cells in the fluid [23]. In such a process it is difficult to distinguish which of the complex interconnected factors specifically influence the regulation of cell fate commitments. However, it is clear that the effects on the cells and thus the changes in cell fate depend on the physical stimulation applied.

Chapter 3.

Experimental procedures

Chapter 3. Experimental procedure

3.1 Cell culture

3.1.1 Conventional culture of human embryonic stem cells (hESCs)

Human embryonic stem cells (hESCs, SNUhES31) were donated at passage 23 from the Seoul National University Medical Research Center after obtaining approval from the Seoul National University Institutional Review Board (IRB No.1402/002-006). Human ESCs were maintained in a pluripotent state under the standard hESC growth condition following previously described protocols [10, 16, 107]. Briefly, the hESCs were grown with mitotically inactivated STO mouse fibroblast cells (STO) on 0.2% gelatin-coated tissue culture dishes in Dulbecco's Modified Eagle Medium: Nutrient Mixture F-12 (DMEM ⁄ F-12, Gibco, USA) supplemented with 20% KnockOut™ Serum Replacement (KOSR, Gibco, USA), 4 ng/ml basic fibroblast growth factor (bFGF, Invitrogen, USA), 0.1 mM β-mercaptoethanol (BME, Sigma, USA), 0.1 mM nonessential amino acids (NEAA, Gibco, USA) and 50 units/ml penicillin, and 50 μg/ml streptomycin (PS, Gibco, USA). Five to seven days after the initial plating, the hESC colonies were mechanically dissociated by modified Pasteur pipettes and re-plated on a fresh feeder layer. Human ESCs were culture at 37 °C in a humidified CO_2 incubator and the medium for the hESCs with feeder was exchanged every single day.

STO was grown and prepared for use as feeder cells as described in previous studies [10, 107]. In brief, STO was treated with 5 μg/ml Mitomycin C (MMC, Sigma, USA) to inactivate the cell division, and then 2.5×10^5 cells were transferred onto a gelatinized 35 mm dish after detaching *via* 0.25% trypsin-ethylenediaminetetraacetic acid (EDTA) (TE, Sigma, USA) to feed the hESCs.

3.1.2 Feeder-free culture of hESCs

To minimize the STO contribution to generation of human embryoid bodies (hEBs) and differentiation of hESCs, a feeder-free system was applied. Conventionally cultured hESCs were transferred mechanically to dishes coated with Geltrex™ (Gibco, USA) and they were cultured in Essential 8™ Medium (Gibco, USA) as described in prior studies, without any adverse effects on pluripotency [107]. The medium for the hESCs without feeder was exchanged every single day.

3.1.3 Culture of human mesenchymal stem cells (hMSCs)

Bone marrow-derived human mesenchymal stem cells (hMSCs) were purchased at passage 2 from Lonza (Switzerland). hMSCs were maintained in 75 cm^2 tissue culture flasks in mesenchymal stem cell growth medium (MSCGM™) supplemented with MSCGM™ SingleQuots™ Kit (Lonza, Switzerland) at 37 °C in a humidified CO_2 incubator. Cells were detached using 0.25% TE when they

have reached approximately 95% cellular confluence and re-seeded for transfer. Passage 3 to 5 cells were used for experiments.

3.1.4 Culture of mouse embryonic stem cells (mESCs)

Mouse embryonic stem cells (mESCs, R1) were maintained with feeder layers of MMC-treated mouse embryonic fibroblast (MEF) on gelatin-coated tissue culture dishes. The culture medium for mESC was knockout-DMEM (KO-DMEM, Gibco, USA) supplemented with 15% fetal bovine serum (FBS, Gibco, USA), 103 units/ml of leukemia inhibitory factor (LIF, Chemicon, USA), 0.1 mM BME, 100 mM NEAA and 50 units/ml penicillin, and 50 μg/ml streptomycin in a humidified incubator with 5% CO_2 at 37 °C. Mouse ESCs were transferred to fresh feeder cells every 3 days.

3.2 Preparation of magnetic nanoparticles (MNPs)

3.2.1 Preparation of *Magnetospirillum* sp. AMB-1

The magnetic bacterium, *Magnetospirillum* sp. AMB-1 (ATCC 700264) was purchased from ATCC and then cultured in magnetic spirillum growth medium (MSGM), revised according to Blakemore's paper [86, 108]. One liter of the modified MSGM contained 10 ml of Wolfe's vitamin solution, 5 ml of Wolfe's mineral solution, 0.02 g of ferrous sulfate (Sigma, USA), 0.45 mL of 0.1% resazurin (Sigma, USA), 0.68 g of monopotassium phosphate (KH_2PO_4, Yakuri, Japan), 0.12 g of sodium nitrate ($NaNO_3$, Junsei, Japan), 0.035 g of ascorbic acid (Sigma, Japan), 0.37 g of tartaric acid (Sigma, Japan), 0.37 g of succinic acid (Sigma, Japan) and 0.05 g of sodium acetate (Sigma, Japan). The pH of the medium was adjusted to 6.75 with a 0.5 N sodium hydroxide (NaOH, Junsei, Japan) solution before sterilization.

AMB-1 cells were anaerobically pre-cultured in 50 ml of a growth medium in a shaking incubator at 27 °C and 150 rpm overnight. And then, the pre-cultured bacteria were inoculated into fermenter containing 3 ml of MSGM, after medium saturation with nitrogen gas for 30 min to provide anaerobic condition. The bacteria were anaerobically fermented for 5 days at 27 °C with stirring and feeding. One liter of feeding solution contained 1 ml of distilled water supplemented with 50 g of succinic acid, 80 g of sodium nitrate, 20 ml of nitric acid (HNO_3, Junsei, Japan) and 1.5 g of ferrous sulfate. When fermentation was finished, the color of fermented solution changed from bright pink to muddy water color.

3.2.2 Isolation and purification of MNPs

Ferromagnetic nanoparticles (MNPs, Fe_3O_4) were gained from anaerobically fermented magnetotactic bacteria (Figure 3.2.2.1) [23, 84]. After the 5-day long fermentation, AMB-1 cells were gathered *via* 11,300×g centrifugation for 20 min. And then the bacterial cells were ruptured *via* sonication with 35% amplification for 15 min (VCX500, Sonics & Materials, USA). The MNPs were isolated from the total solution using neodymium-iron-boron (NdFeB) magnets. The NdFeB magnets were attached beneath the Petri dishes, and the solution containing the MNPs was poured out on the magnet-installed Petri dishes. Contrary to other debris, only the MNPs in the solution were stuck onto the areas of the magnets, and flowing solution was discarded by pipettes except for the MNPs anchored to the magnets. After detaching the NdFeB magnets, the MNPs flowed down, and gathered. The isolated MNPs were washed using phosphate buffered saline (PBS, Welgene, Korea), and the magnetic isolation following PBS washing was repeated 3 times for purification. The MNPs were sterilized using an autoclave as a dispersion in PBS. After measuring the concentration using ICP-AES (ICPS-7500, Shimadzu, Japan), the MNPs were concentrated to 1 mg/ml in PBS and then stored at 4 °C. Just before application to the mammalian cells for experimental purpose, the MNPs were entirely dispersed using an ultrasonicator (JAC 1002, Kodo Technical Research, Japan) for 10 min at room temperature.

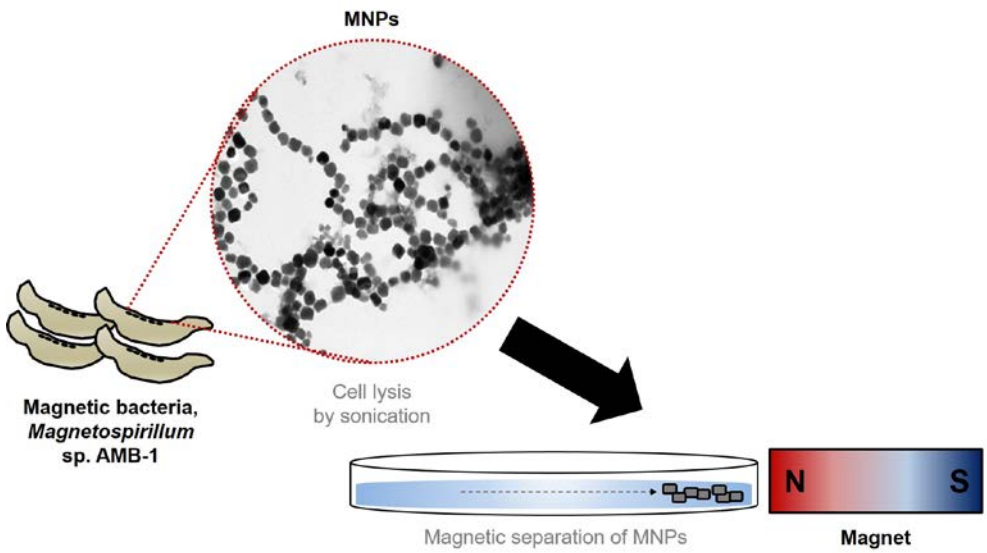

Figure 3.2.2.1 Preparation of MNPs.

3.3 Spheroid generation using MNPs

The hMSCs, mESCs and hESCs were respectively incubated with 20 μg/ml cell-penetrating MNPs at 37 °C in a humidified CO_2 incubator for 24 h. The MNPs were incorporated into cells, resulting in magnetization of the cells. Then the MNP-incorporated cells on dishes were detached from the plate with 0.25% TE or Accutase™ Solution (Millipore, USA). The cells were suspended in a medium and then added into the concentrated magnetic force system, which was manufactured following the previous work [84]. In brief, the lids of 96-well plates were prepared with static magnets (10 mm×5 mm×2 mm) placed on the cover and iron pins attached to the magnets under the lids. The 130 to 135 ml of cell suspension was added into each well at different cell number. The magnetized cells were driven to move toward the iron pin, at which magnetic force was concentrated (450 mT), resulting in construction of spheroids underneath the medium surface.

3.4 Differentiation of stem cells

3.4.1 Spontaneous differentiation of human embryoid bodies (hEBs)

For spontaneous induction of early differentiation, the human embryoid bodies (hEBs) were cultured in suspended condition for 3 days at 37 ℃ in a humidified CO_2 incubator in a hEB medium. In a hEB medium, bFGF was excluded from standard hESC growth medium. Therefore, the hEB medium was composed of DMEM／F-12, supplemented with 20% KOSR, 0.1 mM BME, 0.1 mM NEAA, 50 units/ml penicillin, and 50 μg/ml streptomycin.

3.4.2 Neural induction of hESCs and hEBs

For neural induction, the hESCs were cultured in neural induction medium (NIM, Gibco, USA) for 5 days at 37 ℃ in a humidified CO_2 incubator. The medium was exchanged every 3 days. Also, the hEBs were neurally induced *via* NIM in suspended condition for 5 days.

3.5 Cell viability test

3.5.1 Cell counting kit-8 (CCK-8) assay

To examine the cytotoxicity of the MNPs on hMSCs and hESCs respectively, Cell Counting Kit-8 (CCK-8, Dojindo, USA) was used following the manufacturer's instruction. In brief, after the incubation of the cells with MNPs for 24 h at 37 °C in a humidified CO_2 incubator, CCK-8 solution was added at 10% concentration. The absorbance of each well was measured at 450 nm, following an additional incubation in the incubator for 2 h.

3.5.2 Fluorescence-based live and dead assay

In order to detect the live and dead hESCs in hEBs, LIVE/DEAD cell viability kit (Molecular Probes, USA) was used. The hEBs were treated with a mixed solution of 2 μM acetoxymethyl ester of calcein (calcein AM) and 4 μM ethidium homodimer-1 (EthD-1). After incubation for 1 h at 37 °C in a humidified CO_2 incubator, green fluorescence for live cells and red fluorescence for dead cells were observed.

3.6 Intracellular uptake of MNPs

3.6.1 Transmission electron microscopy (TEM) analysis

The MNPs endocytosed in hMSCs and hESCs were observed *via* transmission electron microscopy (TEM), respectively. After incubation with 20 μg/ml cell-penetrating MNPs, the cells were fixed with paraformaldehyde-glutaraldehyde solution (Karnovsky's Fixative) for 2 h at 4 °C. The cells were then washed with 0.05 M sodium cacodylate buffer. Subsequently, the cells were fixed with 2% osmium tetroxide with 0.1 M cacodylate buffer for 2 h and washed using distilled water, followed by overnight 0.5% uranyl acetate treatment for negative staining at 4 °C. After serial dehydration with sequentially concentrated ethanol from 30% to 100%, the cells were treated with propylene oxide to remove the residual ethanol. Finally, they were penetrated by propylene oxide with resin mixture and then the cells were embedded in resin. The embedded samples were cut using an ultramicrotome (EM UC7, Leica, Germany) and were then observed *via* TEM (JEM1010, JEOL, Japan).

3.6.2 Prussian blue staining

The endocytosed MNPs into hMSCs and hESCs were detected using a Prussian blue staining kit (Sigma, USA) according to the manufacturer’s instruction. After washing the cells with PBS, they were fixed with 4% paraformaldehyde (PFA) for 5 min at room temperature. The cells were then washed with distilled water followed

by permeabilization using 0.25% Triton X-100 in phosphate buffer saline (PBST) for 10 min at room temperature. After washing with distilled water, the cells were treated with 1:1 mixture of potassium ferrocyanide and hydrochloric acid for 10 min at room temperature. Then, the cells were washed with distilled water and were counterstained with 2% pararosaniline solution for 5 min at room temperature. After washing with distilled water and drying, the cells incorporated with MNPs were observed by microscopy.

3.7 Real time reverse transcription-polymerase chain reaction (RT-PCR)

To analyze differentiation of the hESCs and hEBs, the expression of related mRNA was measured through reverse transcription-polymerase chain reaction (RT-PCR) method. In order to detect early differentiation of small and large hEBs, the relative expression of gastrulational genes specifying the ectoderm, endoderm and mesoderm was measured. And to identify degree of neural induction of hESCs and hEBs, the relative expression of neural genes was detected.

The total RNA was extracted using TRIzol® RNA Isolation Reagents (Invitrogen, USA) according to the manufacturer's instructions. After cell gathering by centrifugation, cells were lysed by TRIzol solution and they were incubated at room temperature for 5 min for nuclear complex dissociation. Chloroform (Millipore, Germany) was added at 20% concentration and total solution was shook 15 sec, then subsequently incubated at room temperature for 2 to 3 min. After 12,000×g centrifugation for 15 min at 4 ℃, the solution was separated into 3 phases and the colorless upper aqueous phase was transferred to fresh tube. Then, isopropyl alcohol (2-propanol, Millipore, Germany) was added to the transferred supernatant at 1:1 volume and they were centrifuged at 12,000×g for 10 min at 4 ℃ for RNA precipitation. After centrifugation, supernatant was discarded and then RNA was washed by vortex with 75% ethanol (Millipore, Germany). After centrifugation of the solution at 7,500×g for 5 min at 4 ℃ and the supernatant removal, RNA pellet was dried for 1 h at room temperature and resolved in RNase free water (iNtRON

Biotechnology, South Korea), subsequently incubated at 55 to 60 °C for 10 min.

Reverse transcription was then carried out using 500 ng of total RNA with each reaction of a M-MLV cDNA synthesis kit (Enzynomics, South Korea), following the manufacturer's instructions. Real-time RT-PCR was performed with TOPreal™ qPCR 2X PreMIX (Enzynomics, South Korea), utilizing a StepOnePlus™ Real-Time PCR System (Applied Biosystems, USA).

Each of the expressed genes was normalized by glyceraldehyde 3-phosphate dehydrogenase (*GAPDH*), an endogenous reference gene, and were then analyzed using relative quantification methods. The pluripotency of the hESCs and hEBs was determined respectively by detecting octamer-binding transcription factor 4 (*OCT4*) expression. The relative expression values were represented as the fold changes in the gene expression relative to the pluripotent hESCs as control.

For the primer detecting the ectodermal differentiation, glial fibrillary acidic protein (*GFAP*), sex determining region Y-box 1 (*SOX1*), orthodenticle homolog 2 (*OTX2*) and paired box 6 (*PAX6*) were used while sex determining region Y-box 17 (*SOX17*), brachyury (*Brachyury*), runt-related transcription factor 1 (*RUNX1*), pancreatic and duodenal homeobox 1 (*PDX1*) and cluster of differentiation 31 (*CD31*) were used as the endodermal and mesodermal differentiation markers.

And for detection of neural induction, growth associated protein 43 (*GAP43*), β3-tubulin (*TUBB3*), nestin (*NES*) and *GFAP* were used as representative neural induction markers.

3.8 Immunocytochemical analysis (ICC)

The hESCs and hEBs were fixed with 4% PFA for 10 min at room temperature. After permeabilization using 0.25% PBST for 10 min at room temperature, the cells were blocked by 3% bovine serum albumin (BSA) in 0.1% PBST for 1 h at room temperature on a rocker. The primary antibodies targeting especial maker proteins were diluted with 1% BSA in 0.1% PBST according to the manufacturer's instructions, and the cells were treated with primary antibodies in solution, overnight, at 4 °C on a rocker. In order to investigate pluripotency and self-renewal ability, anti-sex determining region Y-box 2 (SOX2) antibody (D6D9, Cell Signaling Technology, USA) and anti-NANOG antibody (D73G4, Cell Signaling Technology, USA) were used. For the detection of ectodermal differentiation, anti-GFAP antibody (GF5, ab10062, Abcam, England) was used, while anti-Brachyury antibody (ab20680, Abcam, England) was used to confirm the endodermal and mesodermal commitments. To identify neural induction, anti-GFAP antibody, anti-PAX6 antibody (ab5790, Abcam, England) and anti-prospero homeobox protein 1 (PROX1) antibody (ab101851, Abcam, England) were used. For detection of mechanisms of the accelerated neural induction, anti-glial cell line-derived neurotrophic factor (GDNF) antibody (ab18956, Abcam, England), anti-neural cell adhesion molecule (NACM) antibody (3606S, Cell Signaling Technology, USA), anti-microtubule-associated protein 2 (MAP2) antibody (ab111267, Abcam, England) and anti-focal adhesion kinase (FAK) antibody (ab81298, Abcam, England) were utilized. The hESCs and hEBs, exposed to primary antibodies, were subsequently treated with secondary antibodies for 1 h at room temperature and also with 4',6-diamidino-2-

phenylindole (DAPI) for 5 min and then observed by confocal laser scanning microscopy (CLSM, Leica, Germany).

3.9 Western blotting

After centrifuging the 3×10^5 cells at 1,200×g for 5 min, supernatant was discarded and the hESCs were re-suspended in 2 mM EDTA with PBS. The cells were lysed *via* sonication with 23% amplification for 1 min (VCX500, Sonics & Materials, USA). Then the lysates of the hESCs were separated into supernatant and pellets by centrifugation at 12,000×g for 20 min at 4 ℃. The pellets were incubated at 100 ºC for 5 min in 2 mM EDTA with sulfate-polyacrylamide gel electrophoresis (SDS-PAGE) protein loading buffer (Intron Biotechnology, USA). Then the pellets were separated by electrophoresis on 10% SDS-PAGE gel and transferred to nitrocellulose blotting membranes (GE Healthcare Life science, Germany). The blot was blocked with 5% BSA in 0.1% PBST for 1 h at room temperature and then incubated with primary antibody solution (1% BSA in 0.1% PBST with diluted primary antibody) at 4 ºC, overnight. After incubation with horseradish peroxidase (HRP)-conjugated secondary antibody solution (5% BSA in 0.1% PBST) for 1 h at room temperature, the signals were detected with Luminata™ Western HRP Chemiluminescence Substrates (Millipore, USA) and G:BOX Chemi XL system (Syngene, Cambridge, UK). The primary antibodies used for western blot analysis were anti-β-actin antibody (1:1000, ab8227, Abcam, England), anti-WNT3 antibody (1:1000, ab32249, Abcam, England) and anti-WNT5a antibody (1:1000, ab72583, Abcam, England).

3.10 Statistical analysis

The statistical analysis was conducted by using repeatedly drawn results from samples of all the groups. The numbers of repetitions were 3 for genetical analysis, 10 for quantification of ICC and 150 for morphological neurite analysis, respectively. The statistical significance was determined using an analysis of variance (t-test, SigmaPlot) with * for $p < 0.05$, ** for $p < 0.01$ and *** for $p < 0.001$.

Chapter 4.

Generation of size-controlled human embryoid bodies using magnetic nanoparticles

Chapter 4. Generation of size-controlled human embryoid bodies (hEBs) using magnetic nanoparticles (MNPs)

4.1 Introduction

Stem cells have been investigated for the clinical applications such as tissue engineering and regenerative medicine [3-5]. The development of stem cell-based treatments for incurable diseases has been thought to be promising. In particular, human embryonic stem cells (hESCs) have been applied in tissue regeneration because of their unique ability for differentiation [6, 7]. Under defined conditions, the hESCs can differentiate into various cell types. In spite of their prospective characteristics, hESCs are difficult to use in the practical applications because there have been unsolved problems that may arise after stem cell *in vivo* injection due to tumor formation as a result of heterogeneous differentiation [10-14]. Therefore, in order to make use of the fascinating properties of the hESCs, improved methods need to be developed for homogeneous differentiation of the hESCs into intended cell types.

Recently, the hESC differentiation into specific and homogeneous cell types was accomplished. However, achieving a high efficiency with homogeneous differentiation still remains a work in progress [15, 16]. To improve the control for particular lineages, hESC differentiation has made use of various chemical cues to induce designated signaling pathways [17-20]. In addition to such chemical factors, recently, controlling physical cues is also considered as a novel method in order to

delicately regulate the fate of the hESCs [21-23]. In particular, generating human embryoid bodies (hEBs), three-dimensional (3D) cell aggregates of the hESCs, is recognized as an ideal method to efficiently differentiate hESCs [15, 24-27]. Since the hEBs are generated in order to mimic the morphological similarity of developing embryos, hESCs in the form of hEBs are spontaneously induced into differentiation [28, 29].

In recent studies, researchers have suggested that the size of hEBs could play a significant role in the directing hESC lineage, because the hEBs with different diameters have shown distinct differentiation results [109-113]. Accordingly, the hEB generation has been attempted *via* various cell-clustering methods, including hanging-drop culture, non-adhesive surface culture, and porous 3D scaffold culture [30-33]. However, conventional cell-clustering methods have limitations in generating uniformly sized cell aggregates, and therefore microscale techniques have been suggested to achieve a more elaborate regulation [34]. Though the microfluidic devices [52-54] and microwells [55-57] have been widely used to generate uniform hEBs, there are still some limitations in microwells for hEB size control.

In this study, the magnetic nanoparticle (MNP)-based magnetic force system was used to overcome those hurdles. Major advantage of the MNP-based system is that it can instantaneously assemble the hESCs to make various sizes of hEBs. Shorter time for cell gathering is critical because non-adherent single cells may undergo apoptosis during incubation. Moreover, compared with microwells, precise

regulation of the hEB size is possible through the MNP-based concentrated magnetic force system, resulting in uniform hEB generation. Anti-apoptotic assistants such as rho-associated protein kinase (ROCK) inhibitor are vital in the hEB generation using microwells, because the hESCs are prone to apoptosis when they are detached to be single cells. However, the hEBs can be generated successfully using the MNP-based magnetic force system without the assistance of anti-apoptotic factors.

4.2 Spheroid generation with human mesenchymal stem cells (hMSCs) and mouse ESCs (mESCs)

To efficiently generate uniform spheroids of human mesenchymal stem cells (hMSCs) and mouse embryonic stem cells (mESCs), the MNPs isolated from magnetic bacteria and the concentrated magnetic force system were used (Figure 4.2.1). After purification, the MNPs dispersed in PBS were mixed with the cell culture medium, and the mixture was then applied to monolayered hMSCs and mESC, respectively. Then, the MNPs were simply endocytosed into the cells. This intracellular delivery of MNPs was performed without additional modifications on MNP surfaces. Then the magnetized cells, in which the MNPs were accumulated, were detached from the culture dishes using 0.25% trypsin-ethylenediaminetetraacetic acid (TE) and added into the well of concentrated magnetic force system. The concentrated magnetic force system was manufactured following the previous work [84]. Static magnets (10 mm × 5 mm × 6 mm) were placed on the cover of the plates, and iron pins were held by the magnetic force, under the cover. The magnetically induced cells were driven toward the magnetized iron pinpoint after the lid had been closed, and the spheroids of hMSCs and mESCs that were generated respectively, floating just below the medium surface (Figure 4.2.2). The size of the generated spheroids of stem cells was regulated in a reproducible manner by adjusting the cell number added in the well.

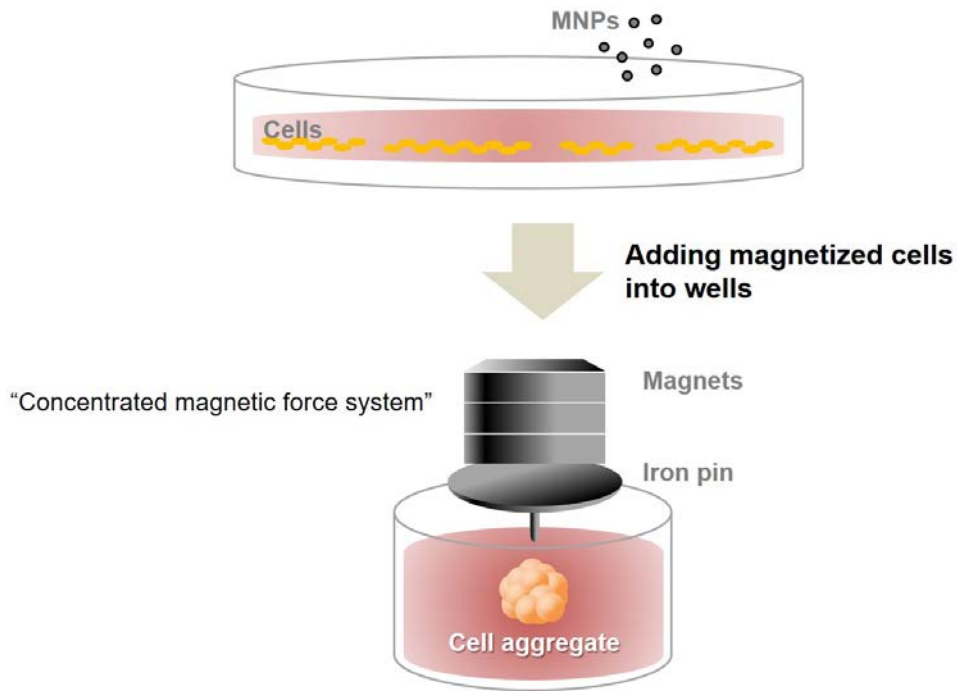

Figure 4.2.1 Spheroid generation method using MNPs and concentrated magnetic force system. After intracellular incorporation of the MNPs into the cells, the magnetized cells were added into a well of the concentrated magnetic force system. Then the cells move toward the concentrated magnetic force, resulting in generation of cell aggregates.

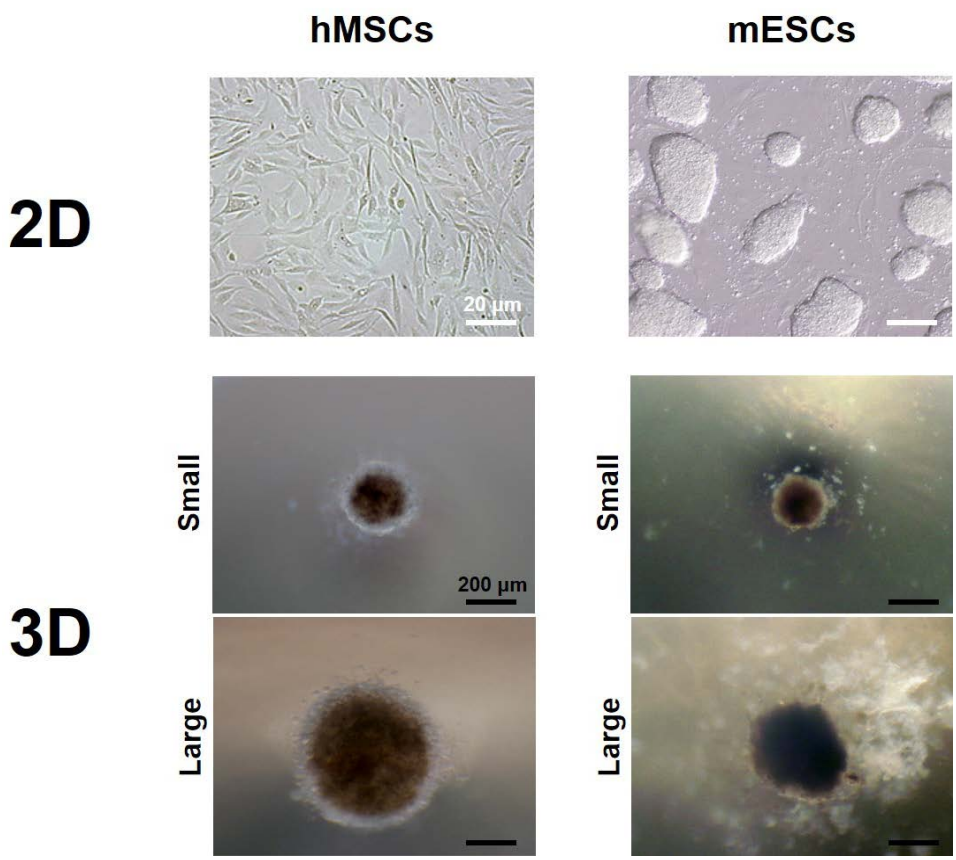

Figure 4.2.2 Size-controlled spheroid generation with hMSCs and mESCs. Small and large spheroids of the hMSCs and mESCs were produced, respectively. And their size was regulated by controlling the number of cells added in a well of the concentrated magnetic force system. White scale bars indicate 20 μm, and black scale bars indicate 200 μm, respectively.

4.3 Limitation of hEB generation

Like the spheroid generation method with hMSCs and mESCs which was mentioned above, the MNPs isolated from magnetic bacteria and the concentrated magnetic force system were utilized in order to efficiently generate precisely regulated and uniform hEBs. However, different from the spheroid generation with hMSCs and mESCs, hEB generation *via* MNPs had a problem.

A mixed solution of MNP-dispersed PBS and the hESC culture medium was treated with colony-shaped hESCs which were cultured as a monolayer with feeder cells according to the conventional culture method of the hESCs. Similar to the spheroid generation with hMSCs and mESCs described previously, MNPs were treated overnight with the hESCs and then chemicals were treated with the hESCs to detach them from the culture dishes. First, when cells were separated by TE treatment as in other cells, the feeder cell, STO, fell off together, making it difficult to use only the hESCs. Therefore, collagenase was treated for 30 min to isolate only colony-typed hESCs first. Additionally, the isolated hESC colonies were disrupted at the single cell level through accutase treatment. Thus the magnetized hESCs obtained were added into the wells of the concentrated magnetic force system.

Considering that the time taken for cell moving toward the concentrated magnetic force and then the cell aggregate formation was several seconds to several minutes in case of hMSCs and mESCs, the hEB generation was not observed after several hours. Although floating hESCs were observed near the pinpoint, they did not form a solid hEBs and most of the hESCs added into the well were observed to sink to the

bottom (Figure 4.3.1). The color of the floating cells at the pinpoint just below the surface of the medium were black or dark gray, whereas the sunken cells were white. This indicates that the hESCs which were incorporated with the MNPs (the color of the cells were dark) existed in a floating form below the surface and the amount was small compared with the amount of total cells added into a well. However, majority of the added hESCs were non-magnetized cells (the color of the cells were bright) which did not have incorporated-MNPs, and they were sunk to the bottom of the wells.

After cell adding to wells of the concentrated magnetic force system, suspended cells were observed continuously for several hours to several days, but still organized hEBs were not generated.

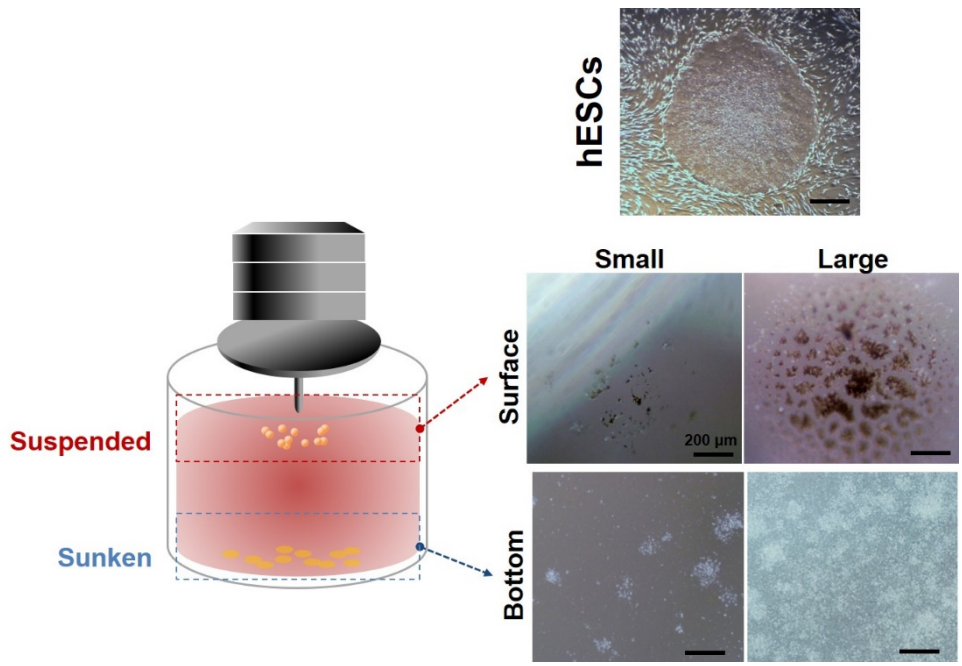

Figure 4.3.1 Limitation of hEB generation using MNPs and concentrated magnetic force system. The sufficiently magnetized cells (dark colored) were suspended just below the medium surface by the concentrated magnetic force, while non magnetized cells (bright colored) were sunken at the bottom of wells. And the amount of the sunken cells was large compared with the suspended cells. Scale bars indicate 200 μm.

4.4 Cytotoxicity and intracellular incorporation of MNPs

Because majority of the hESCs to which the MNPs were treated remained non-magnetized (the color of the cells were white), intracellular properties of the MNPs to the hESCs were investigated through cytotoxicity test and intracellular incorporation analysis.

First, cytotoxicity of the MNPs on hESCs was compared with hMSCs (Figure 4.4.1). After the MNPs had been directly applied to the hMSCs and hESCs over a wide range of concentrations, they were incubated with cells for 24 h, respectively. And the cell viability was then detected. The concentration of the MNPs, which were mixed with the cell culture medium as dispersed form in PBS, ranged from 5 to 50 μg/ml. The cell viability of the hMSCs decreased along increase of the MNP concentrations. When the concentration of the MNPs over 40 μg/ml, cell viability was reduced under 85%. However, the hESCs did not show significant cell death regardless of the MNP concentrations when compared to the non-treated cells.

Based on this, presence and the location of MNPs introduced into the hESCs were investigated comparing with the hMSCs (Figure 4.4.2). The transmission electron microscopy (TEM) analysis and Prussian blue staining analysis were conducted to verify the difference in the MNP incorporation. In a hMSC, plenty of the MNPs were located within vesicle-like structures. However, there was no MNPs observed in a hESC. Furthermore, intracellularly delivered MNPs showed positive for Prussian blue iron detection staining in hMSCs, whereas hESCs did not show any

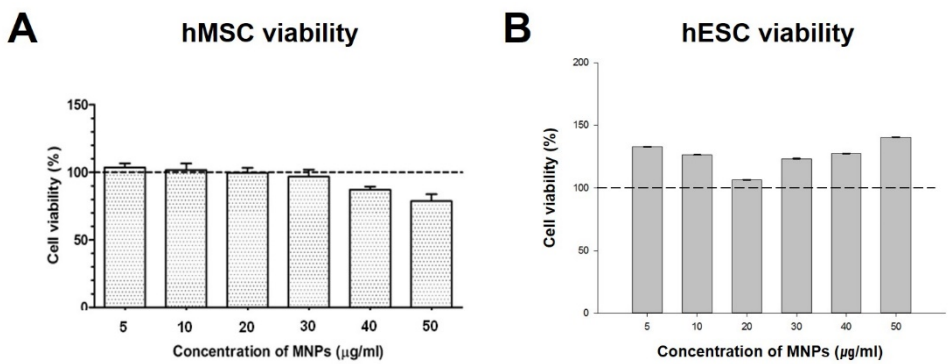

Figure 4.4.1 Cytotoxicity of MNPs on hMSCs and hESCs, respectively. (A) The hMSCs showed decreased cell viability under 100% (which was the cell viability of the untreated cells), when more than 30 μg/ml of the MNPs were treated to the cells. (B) On the other hand, the hESCs did not show any decrease of the cell viability under 100% in all the concentrations of MNPs (from 5 to 50 μg/ml).

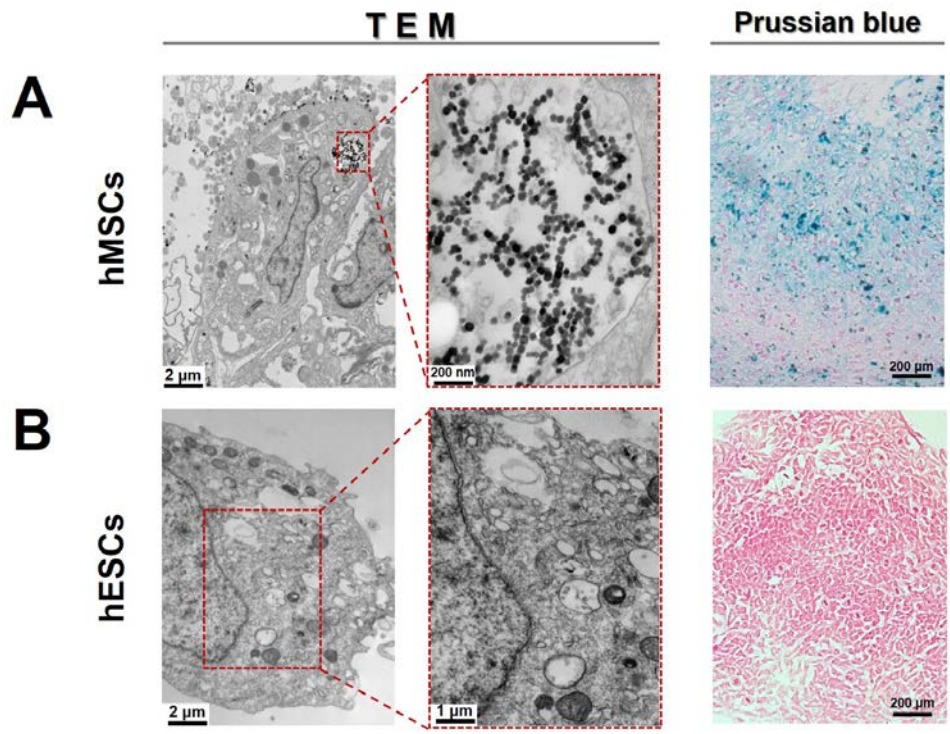

Figure 4.4.2 Intracellular incorporation of MNPs in hMSCs and hESCs, respectively. (A) The TEM image of the hMSCs showed a lot of the MNPs incorporated in the cells, in vesicle-like structures. Rectangles of red dotted lines represent expanded image from left to right. In the Prussian blue staining image, the iron ion from the MNPs included in the hMSCs were stained as blue, when the hMSCs were counterstained as red. (B) In the TEM image of the hESCs cultured with feeder cells, the MNPs incorporated in the cells were not observed. Also in Plussian blue staining image, only the counterstained hESCs were observed, while there was no blue colored MNPs. Scale bars indicate 2 μm, 200 nm, 1 μm and 200 μm, respectively.

blue staining all over the colonies. Therefore, poor incorporation of the MNPs into hESCs was identified comparing with hMSCs.

4.5 Effect of feeder cells on intracellular uptake of MNPs into hESCs

In the preceding study, intracellular delivery of MNPs into the hMSCs and mESCs was easy and simple, whereas the MNPs were not easily introduced into the hESCs. In order to identify the cause of this problem, especially occurring only in the hESCs different from other stem cells, and to find a solution, the specific culture condition of hESCs was considered. According to the conventional culture method of the hESCs, they were cultured with other cells called “feeders” or “feeder cells” to remain pluripotency (Figure 4.5.1) [107]. After inner cell mass was isolated from embryo at blastocystic stage, the cells were transferred to *in vitro* cell culture dish in which feeder cells were attached in advance [10, 16, 107, 114]. With the feeders, the hESCs maintaine their pluripotency, even though the accurate effect and the role of the feeder cells on the hESC culture have been unknown.

In this conventional method, the hESCs existed in the form of colonies, in which the cells were in close proximity to each other, resulting in a small cytosolic volume. Thus, cultivation of the hESCs with feeder cells, inducing the decrease of cellular volume, needed to be improved for the intracellular incorporation of the MNPs. As a novel culture method for hESCs, feeder-free system was applied, in which the hESCs were cultured without feeder cells but extracellular matrices (ECM), represented as Geltrex™, were used instead of the feeders. Without the feeders, the colonies of hESCs were made loose and thus the cytosolic volume of the hESCs increased. To verify the difference in MNP incorporation depending on the

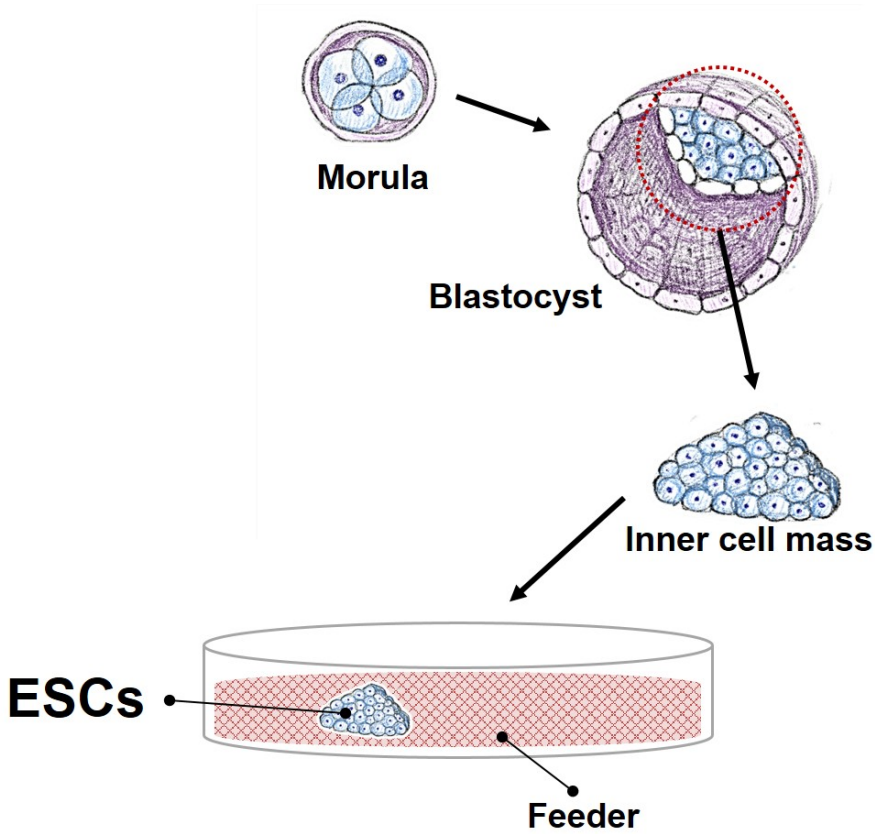

Figure 4.5.1 Conventional culture of hESCs. Schematics of the hESC isolation and cultivation indicates that the hESCs were conventionally cultured with feeder cells.

existence of feeder cells and thus in order to detect the effect of feeder cells on intracellular introduction of the MNPs into the hESCs, conventional hESC culture method and the feeder-free system were compared through Prussian blue staining and TEM analysis (Figure 4.5.2 A and B, respectively). According to the Prussian blue staining, unlike the hESCs in compact colonies with feeder cells, feeder-free hESCs showed improved incorporation of the MNPs. In conventional culture, only the MNP-introduced feeder cells were stained as blue, which were surrounding the hESC colonies. However, a lot of feeder-free hESCs were stained as blue. In TEM images, a conventionally cultured hESC did not show any MNPs which were accumulated in a cell, whereas a hESC cultured without feeder cells possessed some clusters of the MNPs located in vesicle-like structures. As a result of the reduced compact junction between cells, the cytosolic volume of the cells increased, and therefore the permeation of the MNPs into the hESCs improved in the feeder-free system.

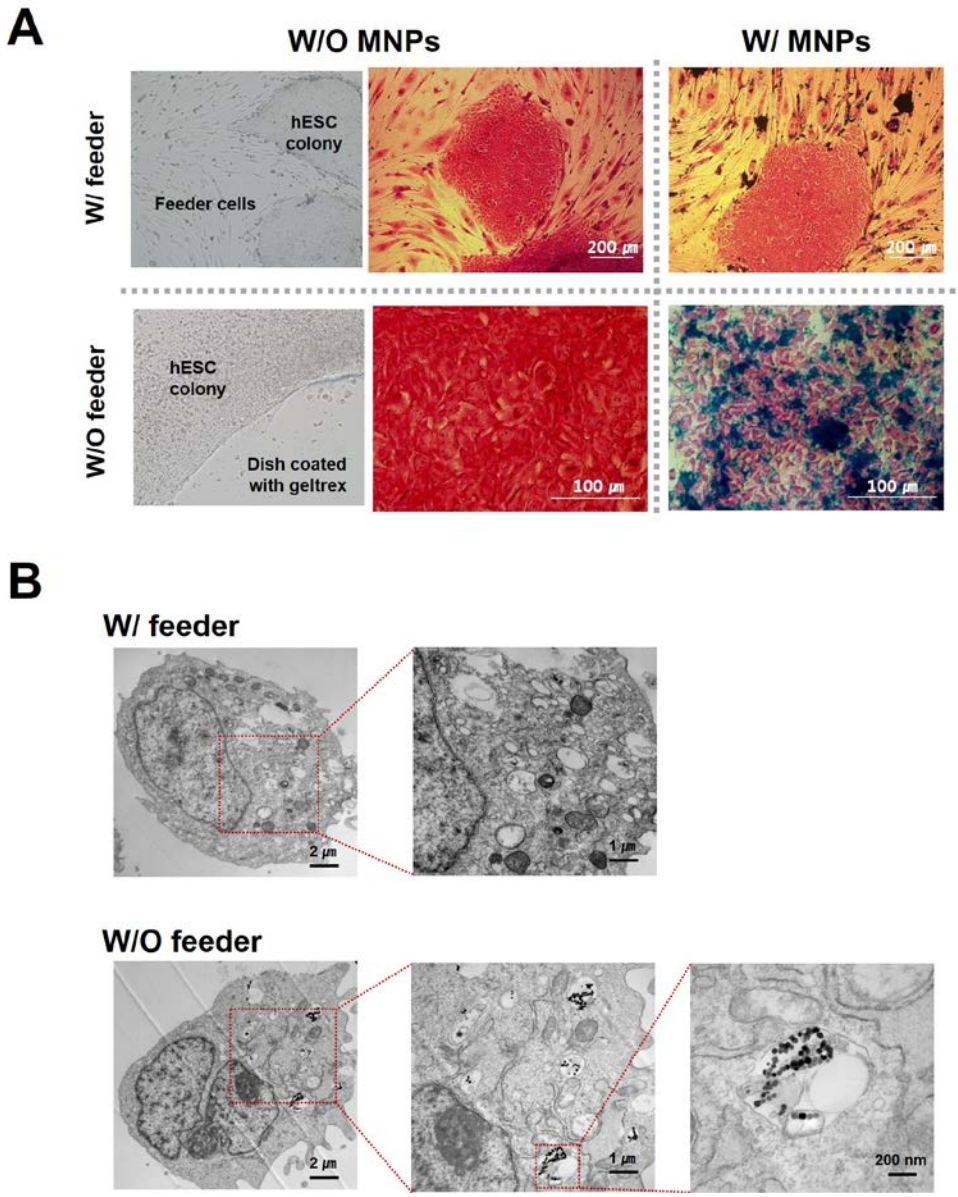

Figure 4.5.2 Effect of feeder cells on MNP incorporation into hESCs. The MNP incorporation in hESCs with or without the feeder cells was compared through Prussian blue staining (A) and TEM analysis (B). Scale bars indicate 200 μm, 100 μm, 2 μm, 1 μm and 200 nm, respectively.

4.6 Optimization of hEB generation method

As previously described, MNP accumulation into the cytosols of the hESCs was enhanced by removing the compact colony construction *via* feeder-free system. Therefore, the hEB generation method using the MNPs and the concentrated magnetic force system was optimized as below (Figure 4.6.1). The hESCs were cultured with feeder cells to maintain their pluripotency and the hESCs without feeder cells were used for the MNP addition procedure for the efficient hEB generation. Thus, the hESCs cultivated with feeders were transferred onto feeder-free system, 5 to 7 days before the MNP treatment. Then the hESCs without feeders were magnetized through intracellular incorporation of the MNPs. Even though the intracellular delivery of MNPs was improved through feeder-free system, the hESCs need sufficient cytosolic incorporation of the MNPs for complete magnetization by which the hEB generation using MNPs would be practical. Actually, because of the small cytosolic volume of the hESCs compared with other mammalian cells, only about 10% of the hESCs, to which the MNPs were treated, were sufficiently incorporated with MNPs. Thus, the sufficiently magnetized hESCs were separated using magnetic force. After the overnight incubation with the MNPs, the hESCs were detached and the suspending cells were transferred to fresh 1.5 ml tube. Then, the 200 mT static magnets were applied to the tube containing the cell solution for 1 min. Only the sufficiently magnetized hESCs moved toward the magnets. Since only the hESCs possessing magnetically driven mobility were retained at the tube wall by the NdFeB magnets, other cells remaining in the solution were discarded. After separation, the static magnets were removed

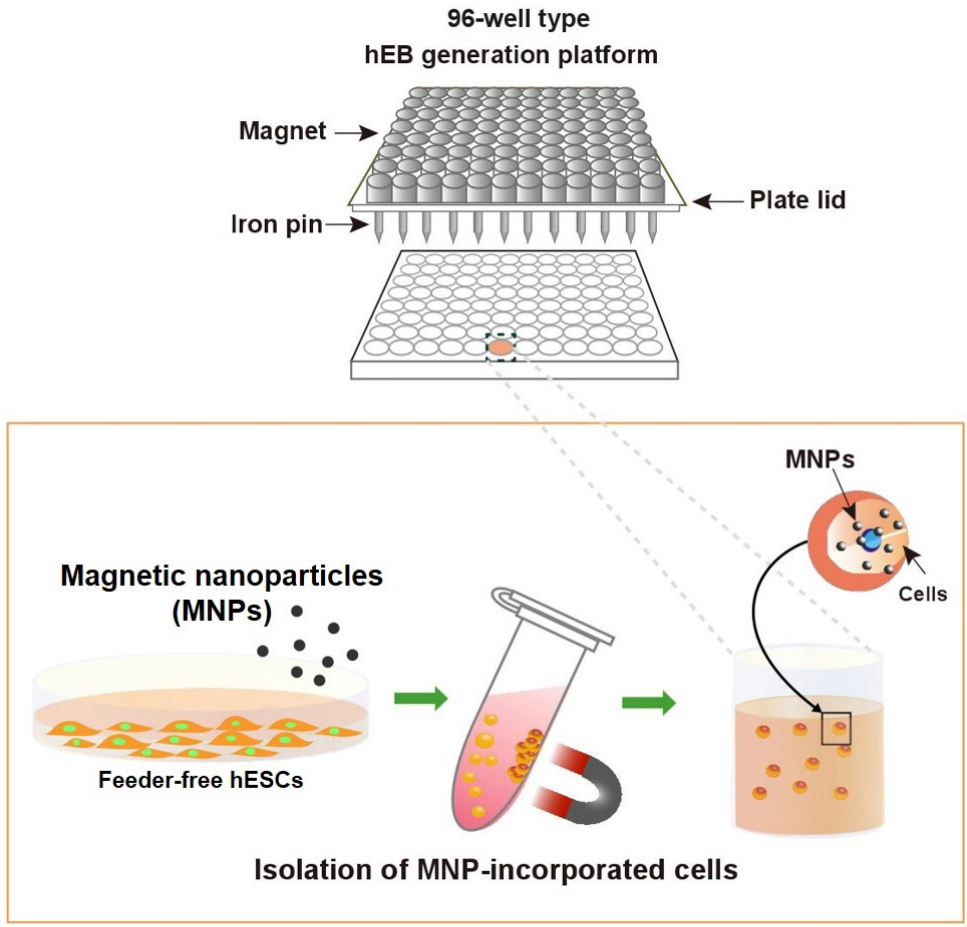

Figure 4.6.1 Optimized hEB generation method using MNPs and concentrated magnetic force system. For improved intracellular delivery of the MNPs into the hESCs, the feeder-free system was applied. Furthermore, only the sufficiently magnetized hESCs were magnetically isolated and then they were added into the wells of the concentrated magnetic force system.

from the tube, and the magnetized cells were re-suspended in hEB medium. These sorted hESCs were then added into wells of the concentrated magnetic force system to generate the hEBs.

In the process of MNP treatment to the hESCs, the MNP concentration was fixed depending on amount of the cells which were sufficiently magnetized through magnetic sorting of the hESCs. Even when the concentration of the MNPs was higher than 20 μg/ml, the proportion of the sufficiently magnetized hESCs did not exceed 10%. Therefore, 20 μg/ml of the MNPs were used to magnetize the hESCs.

4.7 Generation of hEBs depending on cell concentration and incubation time

The MNPs and the optimized concentrated magnetic force system which was described above were used to generate hEBs efficiently. And the size of the hEBs could be regulated by controlling the number of cells added in a well. The correlation of the number of cells added in a well and the diameter of the hEBs was investigated depending on the incubation time after cell addition to the concentrated magnetic force system. As shown in Figure 4.7.1, the size of the hEBs was determined by the total number of cells added into a well. The hEB produced from 5,000 cells of the hESCs was 100 μm in diameter, and 10,000 cells of the hESCs generated a hEB, diametered 150 μm. The hEB made from 50,000 hESCs was 300 μm in diameter, and the hEB generated with 500,000 cells was 800 μm in diameter. Furthermore, we found that larger hEBs required a longer incubation time for a tighter cell aggregation. Up to ten thousand cells of hESCs were concentrated in several seconds, and they were easily gathered within 3 days. On the other hand, more than 10,000 cells of the hESCs were not immediately concentrated but they assembled gradually for 3 days, resulting in compact masses. The construction of the hEBs was solidly rearranged according to the incubation time. After 3 days of hEB generation, the hESCs were adequately aggregated independently of the cell numbers, and the cells were compactly agglomerated from the core of hEBs.

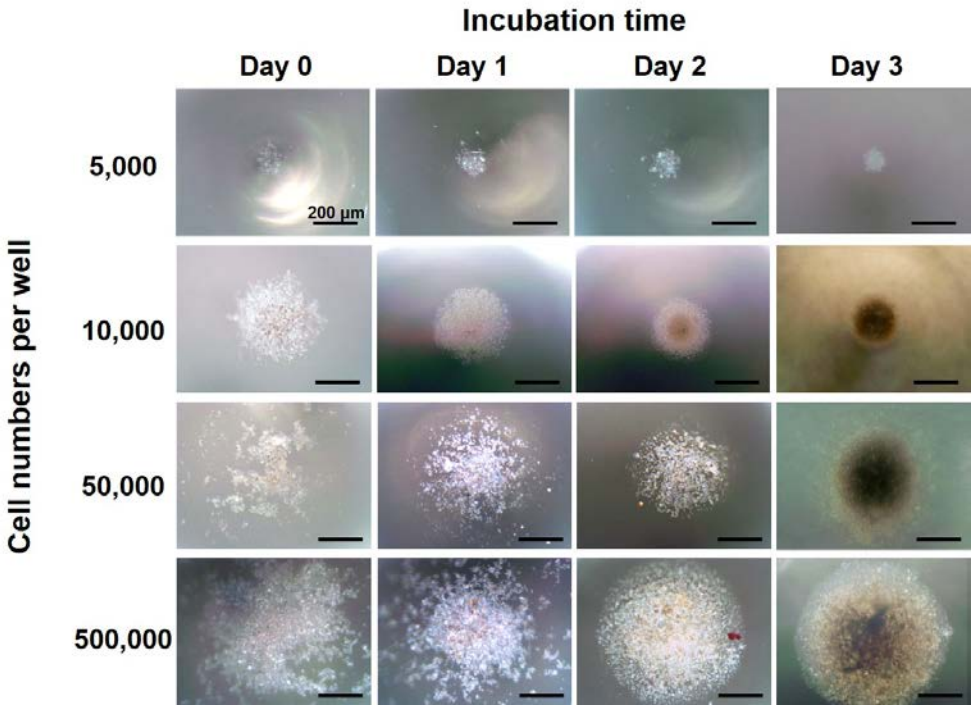

Figure 4.7.1 Effect of cell numbers and incubation time on hEB generation. The hEBs were organized depending on the cell numbers added into a well of the concentrated magnetic force system, and they were observed according to the incubation time after the cell addition. As the number of added cells increased, the final size of the hEBs also increased. And the hEBs were reorganized, resulting in compactly agglomerated hEBs as time passed. Scale bars indicate 200 μm.

4.8 Small and large hEB generation

According to previous studies reporting that the initial size of the hEBs might be a critical factor influencing the early differentiation of the hESCs, a size of 300 μm was hypothesized as a significant point to determine the direction of the lineage-specific differentiation. Consequently, the criteria for the hEB size were defined as below. For a small hEB, the diameter was determined as 150 μm which means half of the 300 μm, and for a large hEB, the diameter was decided as 600 μm which is twice of the 300 μm.

A theoretical calculation on the basis of the correlation between the cell number per well and the hEB size was used to determine accurate cell numbers for small and large hEBs. The number of magnetically induced cells which were added into a well of the concentrated magnetic force system was 1×10^4 for a small hEB whose diameter was 150 μm. And 16×10^4 cells of the hESCs were utilized to generate a large hEB, 600 μm in a diameter. Based on these, the small and large hEBs were generate respectively, and the core of the compactly agglomerated hEBs appeared to be dark because of their thickness (Figure 4.8.1).

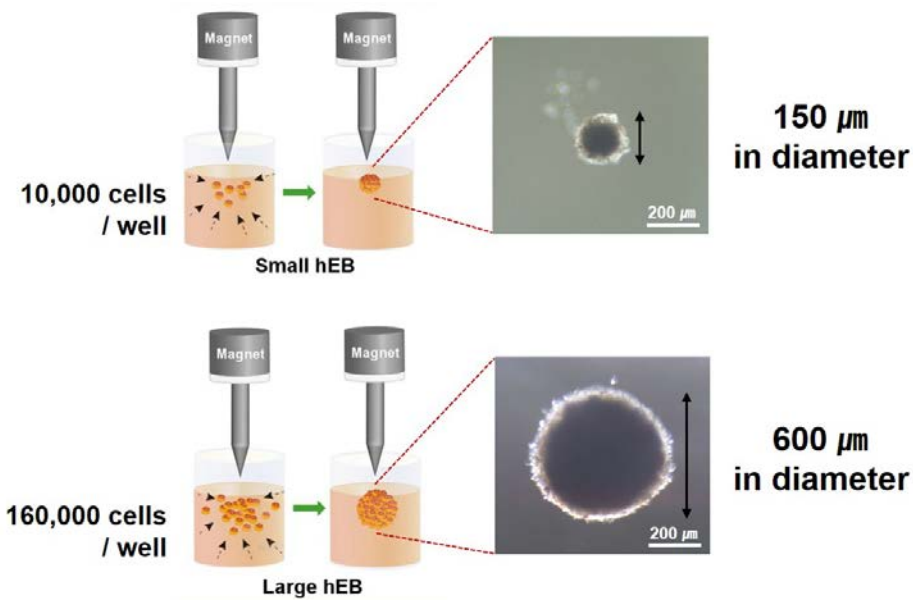

Figure 4.8.1 Small and large hEB generation. Based on the calculated correlation of the cell number added in a well and the hEB size, size-controlled hEBs were produced. 10,000 cells of the sufficiently magnetized hESCs were added in a well of the concentrated magnetic force system to generated small hEBs (150 μm in diameter). And 160,000 cells were added for large hEBs (600 μm in diameter). Scale bars indicate 200 μm.

4.9 Conclusions

In this study, uniformly shaped spheroids of stem cells were generated using the MNPs isolates and then purified from magnetic bacteria, *Magnetospirillum* sp. AMB-1. By treating the MNPs to hMSCs and mESCs overnight, MNPs were incorporated into the cells and thus the stem cells were efficiently magnetized. Then, the magnetized cells were added into wells of the concentrated magnetic force system to produce spheroids of hMSCs and mESCs, respectively. Because the MNP-introduced cells were moved by driven force of the concentrated magnetic force system, cells were gathered generating cell aggregates at the pinpoint. By controlling the cell numbers added in a well, the size of the spheroids of hMSCs and mESCs was easily regulated.

Unlike other stem cells represented as hMSCs and mESCs, the hESCs were difficult to generate as spheroids, called “hEBs”, due to the small amount of the MNPs accumulated therein. Only small proportion of the hESCs, which were treated with the MNPs, were magnetized and suspended below the surface of the medium in the concentrated magnetic force system. On the other hand, majority of the added cells were not magnetized and sank at the bottom of the wells.

Thus intracellular properties of the MNPs were detected in hESCs compared with hMSCs. The cytotoxicity of the MNPs on hESCs was not observed regardless of MNP concentrations, whereas the cell toxicity of the MNPs increased in hMSCs according to their concentrations. And the MNPs were not observed in hESCs, while there was large amount of the MNPs in hMSCs *via* TEM analysis and Prussian

blue staining.

Typically, the hESCs have been cultured in the form of compact colonies surrounded by feeder cells, which have been considered to be essential for maintaining pluripotency of the hESCs. In those colonies, the hESCs were in close proximity to each other leading to decreased surface area and volume. Thus, intracellular delivery and cytosolic accumulation of the MNPs were difficult in those colony-shaped hESCs. To solve this insufficient incorporation of the MNPs and inadequate magnetization of the hESCs, feeder-free system was applied. By replacing the feeder cells as Geltrex™, the colonies of the hESCs was made loose, resulting in the improved intracellular incorporation of the MNPs.

To generate hEBs efficiently using the MNPs, the hESCs without feeders were utilized during MNP treatment process, and then sufficiently magnetized cells were isolated by static magnet separation. Through this optimization of the MNP-based concentrated magnetic force system, the hEBs could be generated efficiently.

The size of the hEBs was uniformly regulated by controlling the cell numbers added into a well of the concentrated magnetic force system. Through verifying the number of hESCs which were sufficiently magnetized, and the incubation time after adding the cells into a well, the correlation of the cell number and hEB size was detected. As the number of the magnetized cells added into a well increased, diameter of the hEBs expanded. And the resulting hEBs were compactly organized according to the incubation time.

As a result, based on theoretical calculations, the hEBs of two sizes were generated;

10,000 cells for small one, 150 μm in diameter and 160,000 cells for large one, 600 μm in diameter.

Chapter 5.

Lineage-specific differentiation by controlling the size of human embryoid bodies

Chapter 5. Lineage-specific differentiation by controlling the size of human embryoid bodies (hEBs)

5.1 Introduction

As briefly mentioned above, controlling the size of human embryoid bodies (hEBs) is crucial for homogeneous and lineage-specific differentiation of the human embryonic stem cells (hESCs) [109-113]. In chapter 4, the magnetic nanoparticle (MNP)-based concentrated magnetic force system, which was optimized with feeder-free system and magnetic cell sorting, was utilized for the assembly of hESCs into hEBs with uniform size distribution. This precise formation based on magnetic control allowed facile and prompt hEB generation. It also facilitates high-throughput and largescale hEB generation. This advanced hEB generation method improves cell-to-cell contact by external magnetic force and thus, the size of fabricable hEB was wide in range (up to 600 μm in diameter) without assistance of anti-apoptotic assistants such as rho-associated protein kinase (ROCK) inhibitor. Furthermore, the hEB size could be controlled with accurate cell number added in a well of the concentrated magnetic force system, because the percentage of the aggregated cells among total cells added in a well constantly remained at 85%.

In this study, the effect of the hEB size on early commitments of the hESCs was detected. And thus, the homogeneous cell population was obtained in terms of the specific germ lineage.

5.2 Down regulation of pluripotency in hEBs

In chapter 4, precisely sized hEBs were generated using the MNPs and the concentrated magnetic force system. And their sized were determined based on the studies reporting the effect of initial hEB size on lineage specification of the hESCs. According to the previous work, a size of 300 μm in a diameter was hypothesized as a significant point to determine the direction of the lineage-specific differentiation [109-113]. So, small hEBs were generated, 150 μm in a diameter smaller than 300 μm, and large hEBs were produced, 600 μm in a diameter larger than 300 μm.

In order to define the direction of differentiation in the hEBs of two sizes, spontaneous differentiation was induced and differentiation aspects were investigated. The differentiation of small and large hEBs was induced for 3 days in hEB medium without any chemical inducers. And then the differentiation patterns were observed *via* genetic analysis and immunocytochemical analysis (ICC). The primers used in real time reverse transcription-polymerase chain reaction (RT-PCR) for genetical analysis are as in Table 5.1.

First, the pluripotency (i.e., the ability of cell to differentiate into various cell types) was investigated because it is one of the most significant properties of natural hESCs. As in previous studies, pluripotency is an intrinsic feature of the hESCs and would therefore, decrease as differentiation proceeds [10, 16, 107]. Regarding the effect of the MNPs themselves on differentiation, we observed that the hESCs with MNPs did not show significant difference in pluripotency, when cultured in stem cell culture medium. After a 3-day-long differentiation, however, the change in the

Table 5.1 Primer sequences for genetical analysis.

	Marker	Sequence (5' → 3') Forward / Reverse
Endogenous reference	*GAPDH*	ccatgacaactttggcatcg / cctgcttcaccaccttctt
Pluripotency	*OCT4*	agcgaaccagtatcgagaac / ctctcgttgtgcatagtcg
Ectoderm	*GFAP*	gagaacaacctggctgccta / ctcatactgcgtgcggatct
	SOX1	cacaactcggagatcagcaa / ggtacttgtaatccgggtgc
	OTX2	aaccgccttacgcagtcaat / cttaaaccatacctgcaccc
	PAX6	tctaatcgaagggccaaatg / tgtgagggctgtgtctgttc
Endoderm and Mesoderm	*SOX17*	gaacgctttcatggtgtggg / ttccacgacttgcccagcat
	PDX1	cctttcccatggatgaagtc / ggaactccttctccagctcta
	Brachyury	atgatggaggaacccgga / taggtgggctggcattgt
	CD31	cgcctgtgaaataccaacct / cctgtctttcagccttcagc

pluripotency of the hEBs was detected according to the expression level of *OCT4* using RT-PCR (Figure 5.2.1). The *OCT4* expression in small and large hEBs was significantly down-regulated, compared to undifferentiated hESCs. Furthermore, pluripotency and self-renewal ability of the hESCs and the hEBs were detected using ICC for other pluripotency markers such as SOX2 and NANOG (Figure 5.2.2). Contrary to the undifferentiated hESCs, the hEBs did not show any expression of both SOX2 and NANOG, indicating the lost of pluripotency with the progress of differentiation. Consequently, hESCs in the form of hEBs were definitely induced to differentiate into specific lineages, regardless of their size.

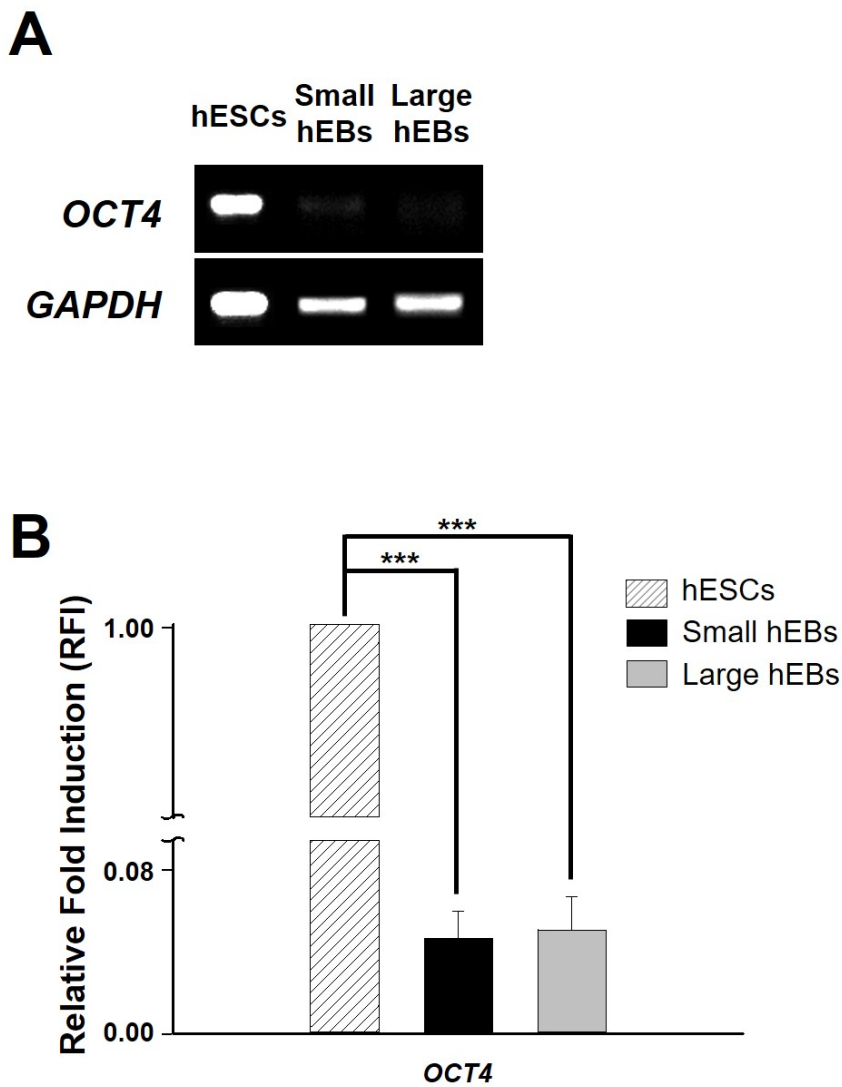

Figure 5.2.1 Genetical analysis of pluripotency in hESCs and hEBs. According to the agarose gel data of RT-PCR (A), and the quantitative data of real time RT-PCR (B), the pluripotency represented by genetical expression level of *OCT* significantly decreased in both sizes of hEBs compared with undifferentiated hESCs. *** indicates $p < 0.001$.

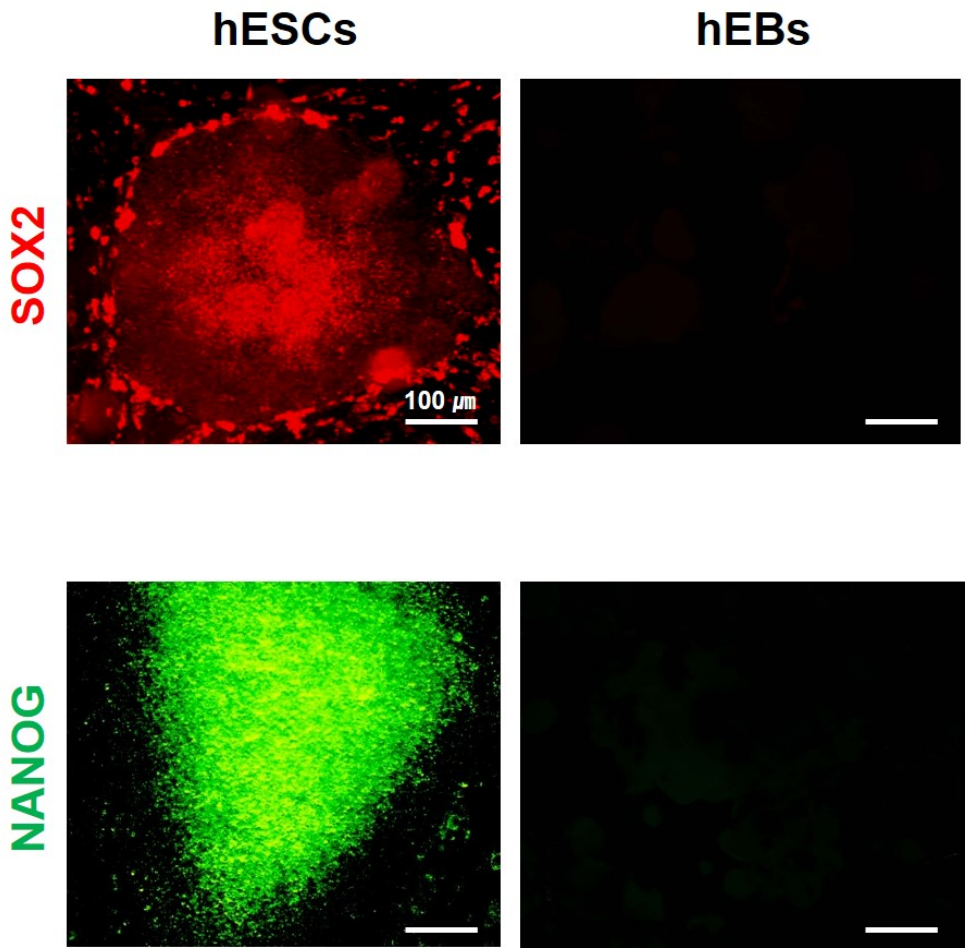

Figure 5.2.2 ICC of pluripotency in hESCs and hEBs. The pluripotency represented by protein expression of SOX2 (red fluorescence) and NANOG (green fluorescence) obviously decreased in hEBs compared with undifferentiated hESCs.

5.3 Ectodermal differentiation of hEBs

Although both small and large hEBs underwent down regulation in their pluripotency, their fate was determined differently. The fate of the hESCs was evaluated by representative markers of three germ layers; ectoderm, endoderm and mesoderm.

First, the expression of ectodermal marker genes, including glial fibrillary acidic protein (*GFAP*), sex determining region Y-box 1 (*SOX1*), orthodenticle homolog 2 (*OTX2*) and paired box 6 (*PAX6*), was investigated in the hESCs, small and large hEBs (Figure 5.3.1). Through the agarose gel band after electrophoresis, expression of the ectodermal markers was enhanced in small hEBs compared with the undifferentiated hESCs and large hEBs. And according to the quantitative analysis *via* real time RT-PCR in which the results were normalized by each value of the control, both small and large hEBs showed a remarkable increase in the expression of *GFAP* and *SOX1* relative to the undifferentiated hESCs. Furthermore, their expression in small hEBs indicated statistically significant differences compared to the large hEBs. The *GFAP* expression level increased by 2.5-fold in small hEBs compared with the large hEBs, and the *SOX1* expression level increased by 5.2-fold in small hEBs relative to large hEBs. In addition, the expression of the ectodermal protein, GFAP, was analyzed *via* the ICC (Figure 5.3.2). The nuclei were described in both the small and large hEBs as a blue fluorescence while the GFAP expression was identified only in the small hEBs as a green fluorescence.

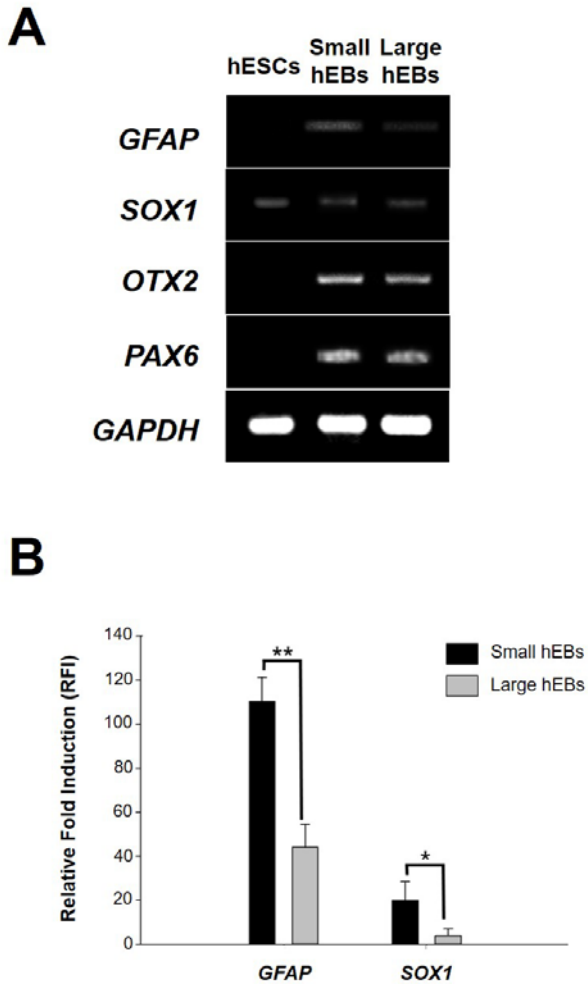

Figure 5.3.1 Genetical analysis of ectodermal differentiation in small and large hEBs. (A) According to the agarose gel data of RT-PCR, the ectodermal differentiation represented by the expression of *GFAP*, *SOX1*, *OTX2* and *PAX6* was enhanced in small hEBs compared to the hESCs and large hEBs. (B) In quantitative data of real time RT-PCR, the ectodermal differentiation indicated by relative expression level of *GFAP* and *SOX1* significantly increased in small hEBs when compared with large hEBs. * indicates $p < 0.05$ and ** indicates $p < 0.01$.

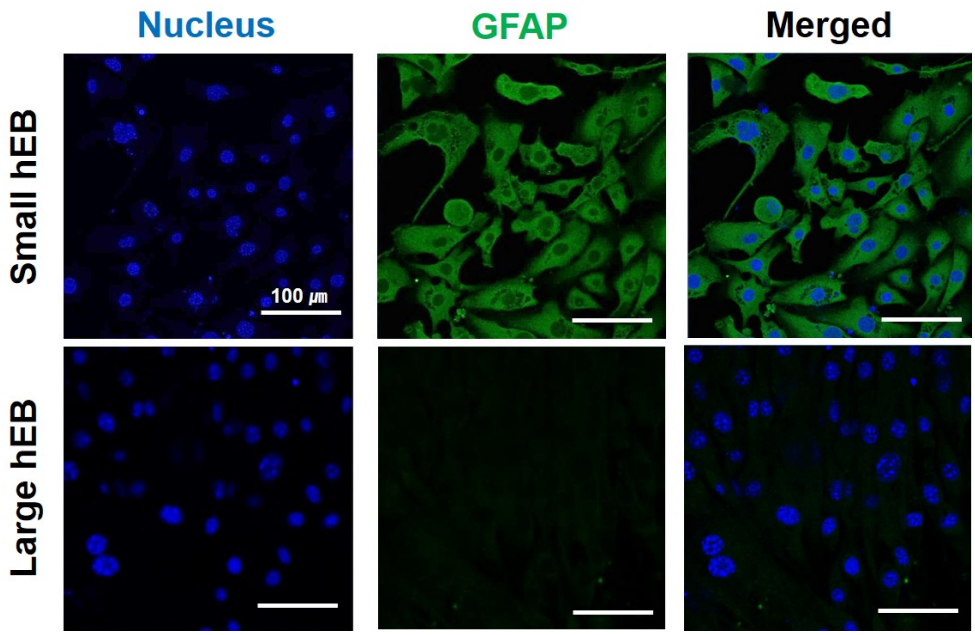

Figure 5.3.2 ICC of ectodermal differentiation in small and large hEBs. The ectodermal differentiation represented by protein expression of GFAP (green fluorescence) was enhanced in the small hEBs compared with the large hEBs. The nuclei were stained as blue. Scale bars indicate 100 μm.

5.4 Endodermal and mesodermal differentiation of hEBs

The endodermal and mesodermal differentiation in both small and large hEBs was genetically analyzed as in Figure 5.4.1. The expression of endodermal and mesodermal differentiation marker genes, including sex determining region Y-box 17 (*SOX17*), brachyury (*Brachyury*), runt-related transcription factor 1 (*RUNX1*), pancreatic and duodenal homeobox 1 (*PDX1*) and cluster of differentiation 31 (*CD31*), was investigated in the hESCs, small and large hEBs. Through the agarose gel band after electrophoresis, expression of the endodermal and mesodermal markers was obviously enhanced in large hEBs compared with the undifferentiated hESCs and small hEBs. The result of quantitative analysis *via* real time RT-PCR indicated that both small and large hEBs clearly showed an enhanced expression of *SOX17*, *Brachyury* and *RUNX1* when compared with the undifferentiated hESCs. Furthermore, their expression in large hEBs indicated statistically significant increases compared to the small hEBs. The *SOX17* expression level increased by 1.8-fold in large hEBs when compared with small hEBs. Moreover, the *Brachyury* expression level increased by 1.7-fold, and the *RUNX1* expression level increased by 3.2-fold in large hEBs compared with the small hEBs. The expression of a typical mesodermal protein, Brachyury, was analyzed *via* ICC (Figure 5.4.2). The nuclei were described in both the small and large hEBs as a blue fluorescence while the Brachyury expression was identified only in the large hEBs as a red fluorescence.

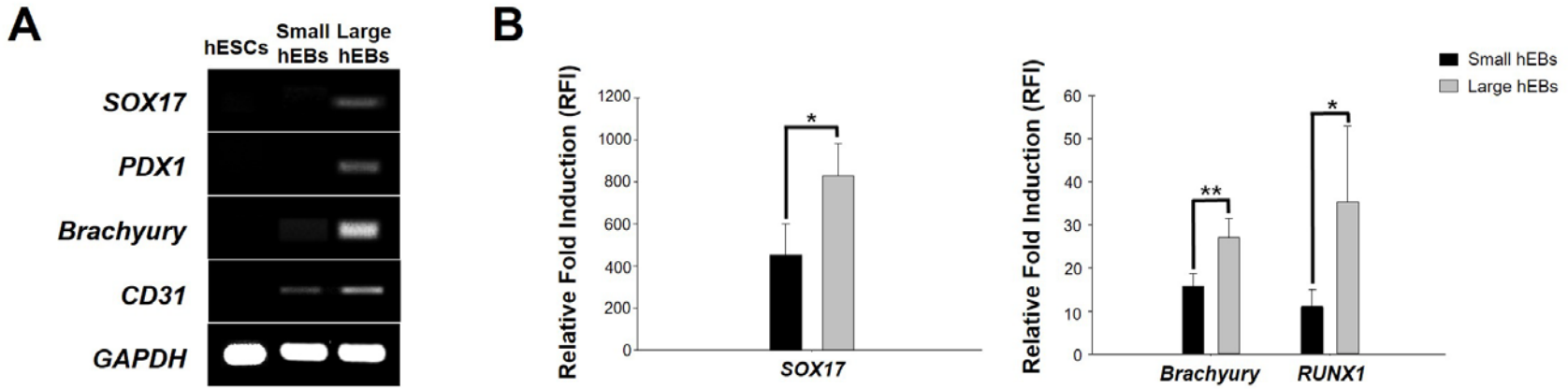

Figure 5.4.1 Genetical analysis of endodermal and mesodermal differentiation in small and large hEBs. (A) According to the agarose gel data of RT-PCR, the endodermal and mesodermal differentiation represented by the expression of *SOX17*, *PDX1*, *Brachyury* and *CD31* was enhanced in large hEBs compared to the hESCs and small hEBs. (B) In quantitative data of real time RT-PCR, the endodermal and mesodermal differentiation indicated by relative expression level of *SOX17*, *Brachyury* and *RUNX1* significantly increased in large hEBs when compared with small hEBs. * indicates $p < 0.05$ and ** indicates $p < 0.01$.

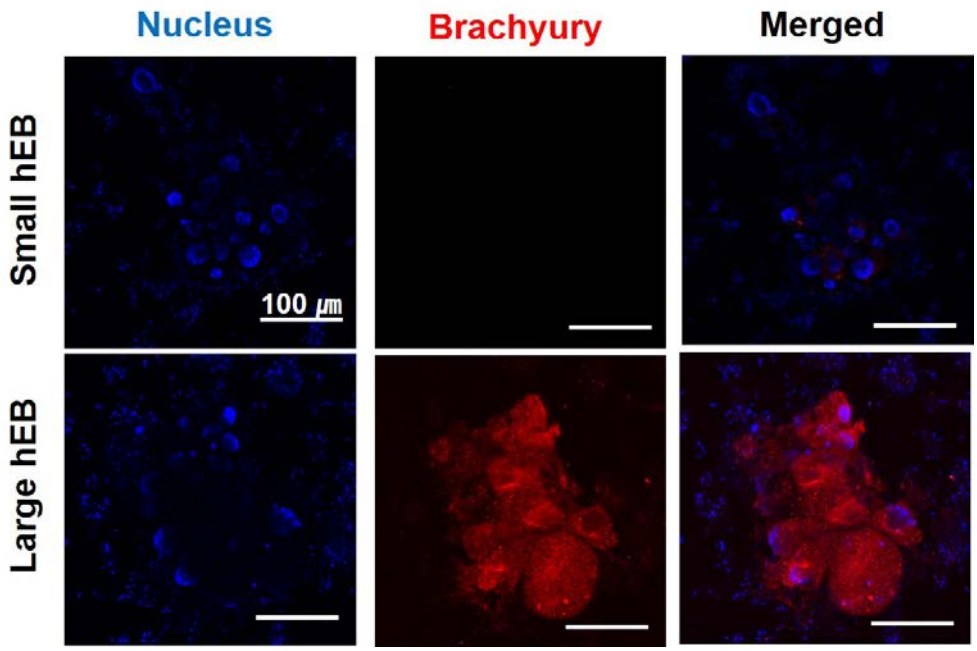

Figure 5.4.2 ICC of endodermal and mesodermal differentiation in small and large hEBs. The endodermal and mesodermal differentiation represented by protein expression of Brachyury (red fluorescence) obviously enhanced in the large hEBs compared with small hEBs. The nuclei were stained as blue. Scale bars indicate 100 μm.

5.5 Effect of hEB size on cell death and lineage-specific differentiation

By aggregating the hESCs using MNPs and the concentrated magnetic force system, they were spontaneously differentiated in the form of hEBs. The pluripotency of the hESCs was significantly down-regulated and lineage-specific differentiation was observed according to hEB size in the hEB culture medium, which does not determine the direction of differentiation. As a result, small hEBs showed enhanced ectodermal differentiation compared with the large hEBs, and large hEBs showed improved endodermal and mesodermal differentiation relative to the small hEBs.

To verify the differences between these hEBs of two sizes, core cell death aspects was investigated depending on diameter of the hEBs (Figure 5.5.1). It was predicted that the core part of the hEBs would have limitations in transfer of the nutrient and oxygen according to the hEB size. In small and large hEBs, live hESCs were shown as green, whereas dead cells were shown as red, respectively. There was significant cell death in the core of large hEBs while almost all cells were alive in small hEBs. In the large hEBs, fluorescence is not expressed at the core, and thus it appears black because dye could not penetrate the thick cell layer, resulting in failure of reaching inside of the center.

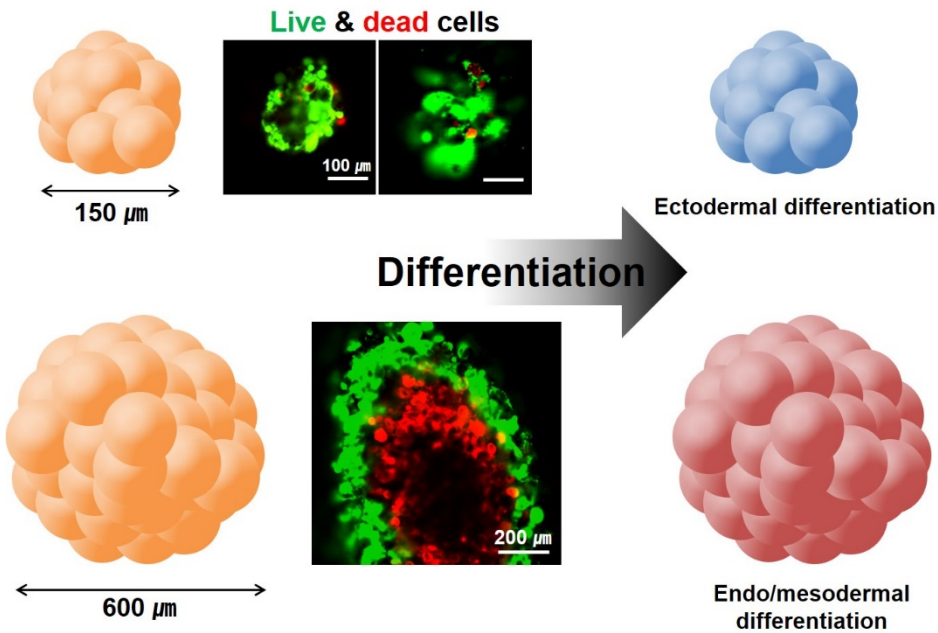

Figure 5.5.1 Cell death patterns in hEBs depending on their size. The cell death was investigated in both small and large hEBs. Live and dead hESCs were shown as green and red fluorescence, respectively. There was significant cell death in the core of large hEBs while almost all cells were alive in the small hEBs. Scale bars indicate 100 μm and 200 μm, respectively.

5.6 Conclusions

By gathering the cells and forming hEBs, the hESCs lose pluripotency, which is an intrinsic feature of the hESCs, regardless of the hEB sizes. In hEB culture medium without any inducer directing differentiation lineage, hEBs of both sizes were spontaneously differentiated. After 3-day-long spontaneous differentiation in suspended condition, the differentiation patterns of the small and large hEBs were investigated.

The expression of ectodermal genes represented as *GFAP*, *SOX1*, *OTX2* and *PAX6*, was significantly enhanced in small hEBs compared with large hEBs. And ectodermal protein GFAP were intensively expressed in small hEBs compared to large hEBs.

On the other hand, the expression of endodermal and mesodermal genes represented as *SOX17*, *Brachyury*, *RUNX1*, *PDX1* and *CD31*, was significantly increased in large hEBs relative to small hEBs. And the expression of mesodermal protein Brachyury was up-regulated in large hEBs compared to small hEBs.

To identify the cause of these differences in differentiation direction depending on the hEB size, cell death in hEBs was investigated. The diameter of the hEBs had a significant effect on cell viability in core part of the hEBs. Many cells were found to be dead in the center of large hEBs and led to formation of lumens.

Thus, as described in Figure 5.6.1, the initial size of the hEBs was crucial for localized cell death and the lineage-specific differentiation. So, this work indicates

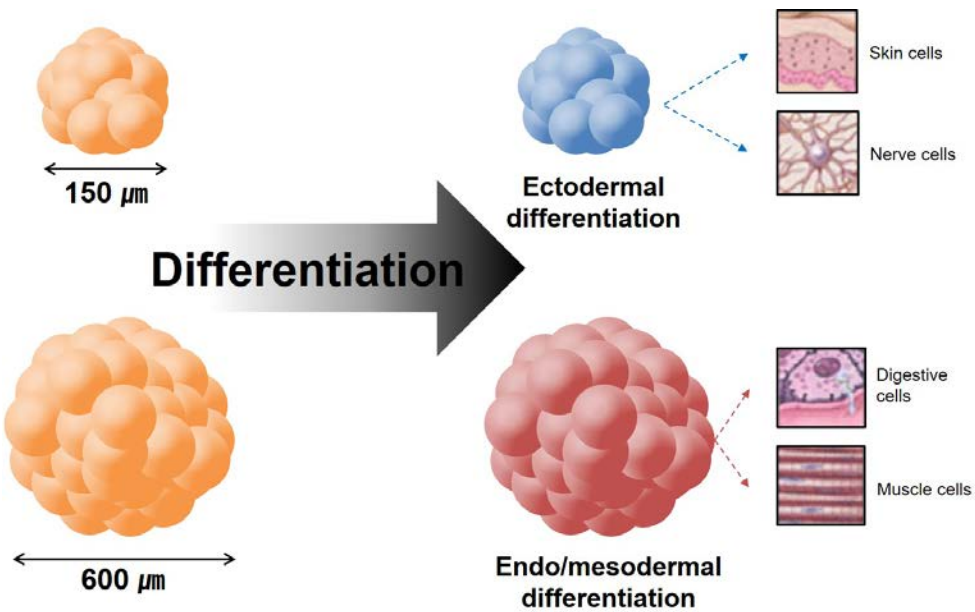

Figure 5.6.1 Lineage-specific differentiation of hEBs depending on their size. Small hEBs (150 μm in diameter) were differentiated into ectodermal lineage, while the large hEBs (600 μm in diameter) were differentiated into endodermal and mesodermal lineage.

that through various chemical and biological factors induced by the hEB size-dependent signals, the small hEBs began to differentiate into ectodermal lineages, which should be preceded for the differentiation into skin cells and nerve cells, whereas the large hEBs differentiated into endodermal and mesodermal lineages, which have to be preceded before differentiation into digestive cells and muscle cells.

Chapter 6.

Neural induction of small-sized human embryoid bodies

Chapter 6. Neural induction of small-sized human embryoid bodies (hEBs)

6.1 Introduction

Nerve cells are largely divided into two groups; neurons and non-neurons [115-117]. Nerve cells that perform the neurological functions which are actively involved in neuronal transmission are neurons [118, 119]. On the other hand, non-neuronal cells, called glial cells, help the neurons with their proper function. They maintain the homeostasis of the nervous system, support the structures of nervous system, and protect the neurons [120, 121]. In neurogenesis with the human embryonic stem cells (hESCs), the ultimate targets are usually neurons with the function of neurotransmission, though various glial cells such as oligodendrocytes could be the differentiation purpose.

In the hESC-based neurodevelopmental studies, it is common to utilize the human embryoid body (hEB) forms, called neurospheres, for the improved differentiation (Table 6.1) [122]. This seems to be due to the fact that the hEBs mimic the stiffness of the brain tissue which is very soft among the body tissues (Figure 6.1.1) [123, 124]. In other words, it is a worthy strategy to facilitate neural induction by providing similar physical environment.

In the previous chapter, a successful technology for hEB generation was developed and the effect of hEB size on the direction of initial differentiation of the hESCs was investigated. Based on the standard point of the diameter, 300 μm,

Table 6. 1 Conventional neurogenesis of hESCs.

Time	3 ~ 4 weeks	1 ~ 2 weeks	3 months	1 ~ 3 weeks
Medium	Neural progenitor **induction medium**	**Early** neuro-ectodermal differentiation medium	**Mature** neuro-ectodermal differentiation medium	**Neuronal** differentiation medium
				Glial differentiation medium
				Astrocytal differentiation medium
Condition	**Monolayer** w/o feeder	**Monolayer**	**Neurosphere suspension**	**Attached** onto dishes
Phase	**Induced neural progenitor cells**	**Early neuro-ectodermal cells**	**Mature neuro-ectodermal cells**	**Three fundamental neural cells w/ function**

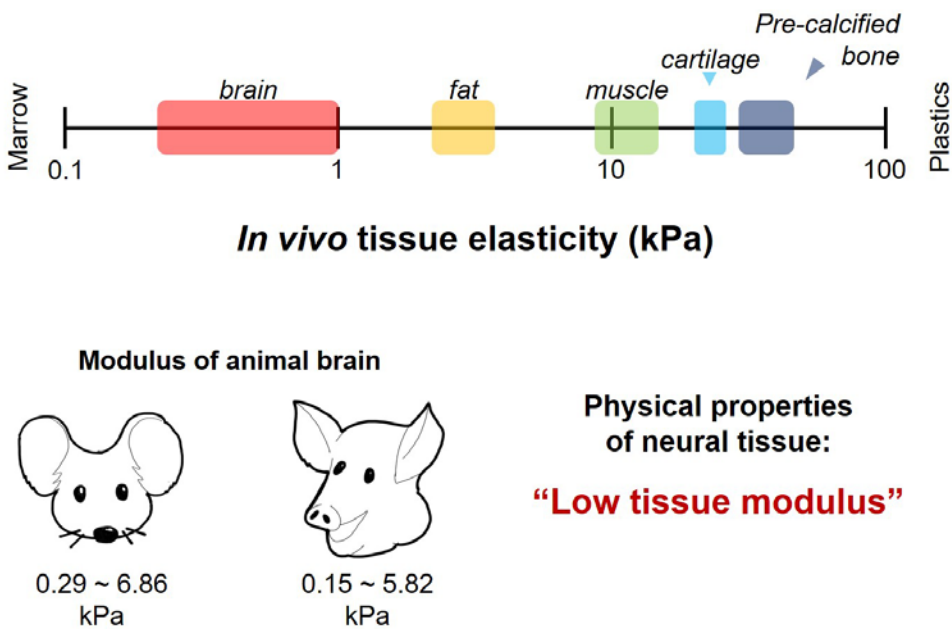

Figure 6.1.1 Physical properties of brain tissue and neurosphere.

the ectodermal differentiation was promoted in small hEBs with a diameter of 150 μm, and endodermal and mesodermal differentiation was improved in large hEBs of 600 μm in diameter. This lineage-specific differentiation occurred spontaneously in the hEB medium without any inducers for specific differentiation. The spontaneously differentiated small hEBs in hEB medium were ectodermally induced and they showed enhanced glial fibrillary acidic protein (GFAP) expression. Moreover, some of these GFAP-positive cells showed neurite-like outgrowth (Figure 6.1.2). Therefore, in this chapter, the hESCs were neurally induced in the form of the small-sized hEBs using the magnetic nanoparticles (MNPs) and the concentrated magnetic force system.

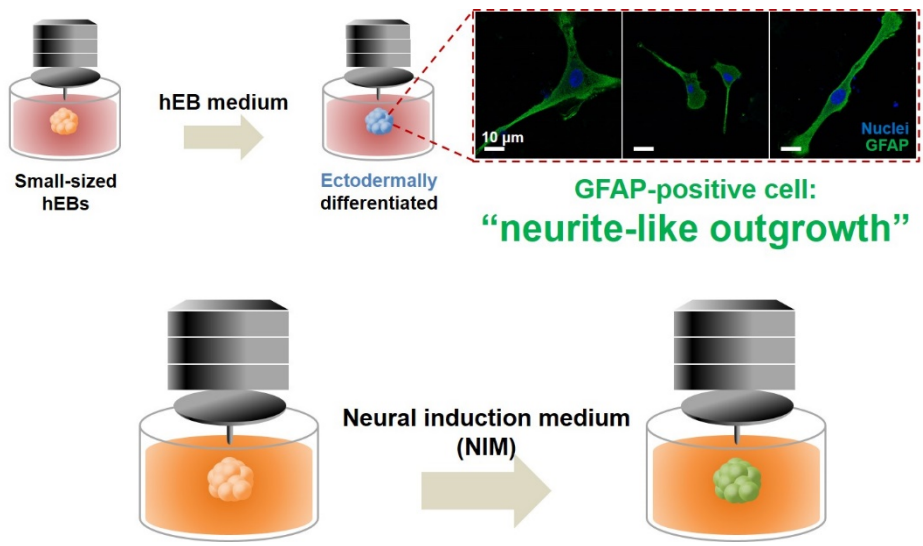

Figure 6.1.2 Spontaneous neurite-like outgrowth of small-sized hEBs. Some of the ectodermally differentiated small hEBs, which were positive to GFAP expression, showed neurite-like outgrowth. So, the improvement of neural induction of the hESCs was conducted in the form of hEBs using the MNPs and the concentrated magnetic force sysem. Scale bars indicate 10 μm.

6.2 Neural induction method for hESCs using MNPs

6.2.1 Neural induction of small-sized hEBs

In this study, the hESCs were neurally induced in the form of small-sized hEBs using the MNPs and the concentrated magnetic force system. Through previous work, it was already revealed that the initial size of hEBs is important for the lineage-specific differentiation of the hESCs in early stage and that the small-sized hEBs, 150 μm in diameter, is spontaneously differentiated into ectodermal lineages. Because ectodermal differentiation should be preceded for the neural induction [125, 126], the small-sized hEBs were used for the improved neural induction (Figure 6.2.1.1). And the hEB culture medium which was utilized for spontaneous differentiation of the hEBs in former chapter, was replaced to neural induction medium (NIM) for the improved neural induction. Furthermore, duration of the cultivation for the hESC differentiation was 3 days for the spontaneous induction but in the neural induction, the duration of cultivation was increased to 5 days. So, the small-sized hEBs generated using the MNP were neurally induced in NIM for 5 days.

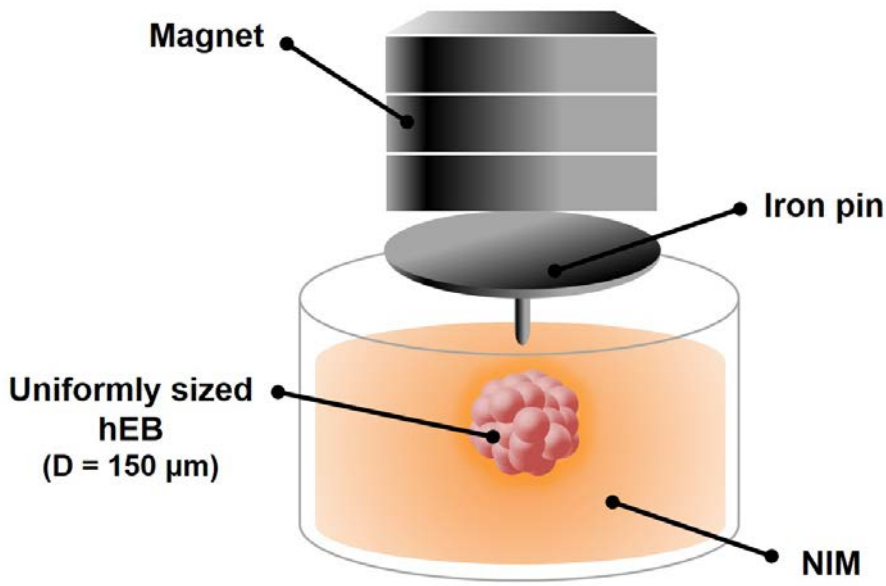

Figure 6.2.1.1 Neural induction of small-sized hEBs. In order to neurally induce the hESCs, hEB generation method utilizing the MNPs and the concentrated magnetic force system was applied for small-sized hEB (150 μm in diameter) production. And the hEB medium used in spontaneous differentiation was replaced to NIM and the cultivation time increased from 3 days to 5 days.

6.2.2 Experimental groups

To investigate the improvement of the neural induction of small-sized hEBs cultured in NIM under suspended condition for 5 days (IV), comparable groups were set as follows (Figure 6.2.2.1); undifferentiated hESCs (I), conventionally differentiated hESCs with NIM (II), and conventionally differentiated hESCs with NIM and MNPs (III). The undifferentiated hESCs (I), which were maintained in pluripotency state, became a control group. The neurally induced hESCs using only the NIM (II), following the most general method of neural induction, became the comparative test group. Because there were two different factors, such as addition of the MNPs and three-dimensional (3D) cultivation in group IV, compared with II, a new experimental group, two-dimensionally (2D) cultured hESCs differentiated with NIM and the MNPs (III), was added. As a result, the effect of the small-sized hEB generation method using the MNPs and the concentrated magnetic force system on neural induction was examined; comparing the improvement of neural induction in IV with other groups. And also the effect of 3D culture on the improvement of neural induction could be investigated by comparing IV and III. Furthermore, by comparing the III with I and II, the synergic neural inductivity of the MNPs when treated with NIM, could be detected.

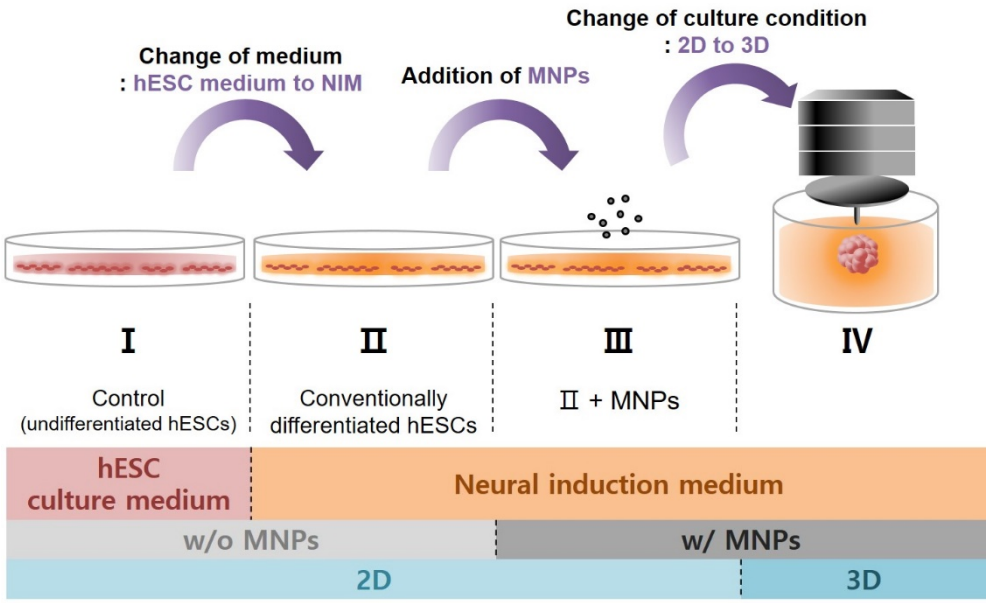

Figure 6.2.2.1 Schematics for experimental groups. The undifferentiated hESCs were the control (I), and conventionally differentiated hESCs with NIM were group II. The hESCs differentiated with NIM and the MNPs were III. And the small-sized hEBs which were neurally induced in NIM were the group IV.

6.3 Morphological analysis

6.3.1 Morphology of hESCs

As an indicator detecting the neural induction of 4 experimental groups, morphological analysis was performed to observe, compare and analyze the appearance of the hESCs. Thus, the superficial morphology of the cells and the number and length of the neurites sprouted from the cells were investigated.

First, morphological differences among the cells were observed. The morphological characteristics of the natural hESCs are that the shape of the cells is round and the size of the cells is very small compared to the other mammalian cells; less than 10 μm in diameter [9, 16]. The hESCs, which are cultured with feeder cells, grow in compact colonies. The feeder-free hESCs grow in colony-shapes either, though the colonies are made loose slightly. A significant change in the progression of neuronal differentiation is the formation of tiny projections on cells, called “neurites” [127-130]. When a hESC becomes a neuron, the morphology becomes sharp-pointed like a star. In the process of differentiation into such a neuron, neurites are necessarily found. In general, neurons do not colonize like the hESCs. Instead of forming compact colonies, there is enough intercellular space between the neuronal cells. But when the neurons are matured, intercellular interactions could be active, which leads to the improvement of intercellular connections.

Based on these, shape of the cells in 4 experimental groups was investigated

(Figure 6.3.1.1). In the control group, undifferentiated hESCs (I), the typical appearance of hESCs described above, was observed. The cells formed a colony and maintained a round-shaped appearance. However, it was observed that the rounded cells and the triangular cells with pointed parts co-existed in II, in which the angular cells existed where the cell density was low, far from the colony. In III and IV, many of the angular cells were observed and prominent neurite protrusions were shown. It was possible to observe not only one neurite but also several neurites sprouting from one cell, and some of the neurites were extremely long, resulting in enlarge the length of the whole cell. Also in group IV, I observed cell aggregates, which were some parts of the attached hEBs. To investigate the morphology of the suspending hESCs in the form of 3D, the hEBs were made sunk to the bottom of the wells, resulting in not only the adherence of the hEBs but also the migration of the exterior cells away from the center. The squares with the yellow dotted lines indicated cells that migrated away from the adhered hEB mass, whereas the squares with red dotted lines represented some of the attached masses of hEBs and the surrounding cells.

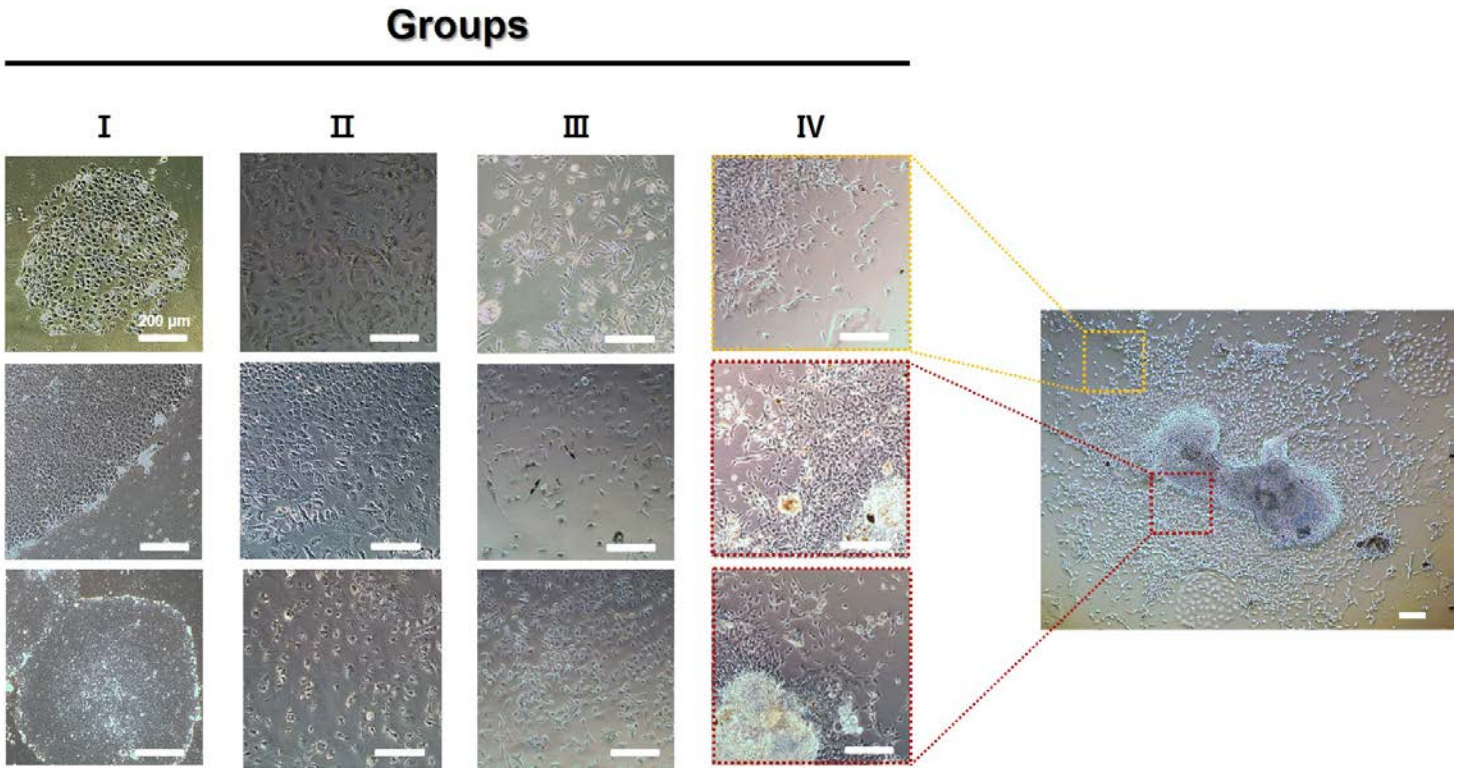

Figure 6.3.1.1 Morphology of hESCs in 4 experimental groups. The shape of cells was observed in all of the experimental group by microscope. Scale bars indicate 200 μm.

6.3.2 Number of neurites per cell

To quantify the neurite-related cell morphology, which was observed through microscope above, the number of neurites per cell was examined. To determine the number of neurites from the hESCs, 150 cells per each experimental group were analyzed. According to the Table 6.2, proportion of the cells according to the number of neurites was investigated. Then the average number of neurites per cell was calculated in Figure 6.3.2.1.

In the control group, undifferentiated hESCs (I), all of the cells remained spherical, resulting in the absence of neurite-extending cells.

In the hESCs conventionally differentiated using NIM for 5 days (II), more than half of the cells existed without any neurites (64.1%), but the neurites were found in rest of the cells, and the hESCs with more than two neurites were also found. The percentage of cells with one neurite per cell was 18.9%, two neurites per cell was 6.8%, and the ratio of the cells with three or more neurites was 10.2%. The calculated average number of neurites per cell was 0.45, when total cells, including the hESCs without neurite, were investigated. However, except for the cells without neurite (64.1%), the average number of neurites per cell was 1.90.

In the hESCs neurally induced using NIM and the MNPs (III), the proportion of neurite-free cells was only 9.6%, and thus 90.4% of the cells were observed to possess neurites. In group III, 33.8% of the cells had one neurite per cell, 25.0% of cells had two neurites, and 31.6% of the cells had three or more neurites per cell. When the average number of neurites per cell was calculated, it was analyzed to be

Table 6.2 Proportion of cells according to number of neurites.

Proportion of cells (%)

Number of neurites	I	II	III	IV
0	100	64.1	9.6	10.5
1	0	18.9	33.8	14.3
2	0	6.8	25.0	30.5
≥ 3	0	10.2	31.6	44.7

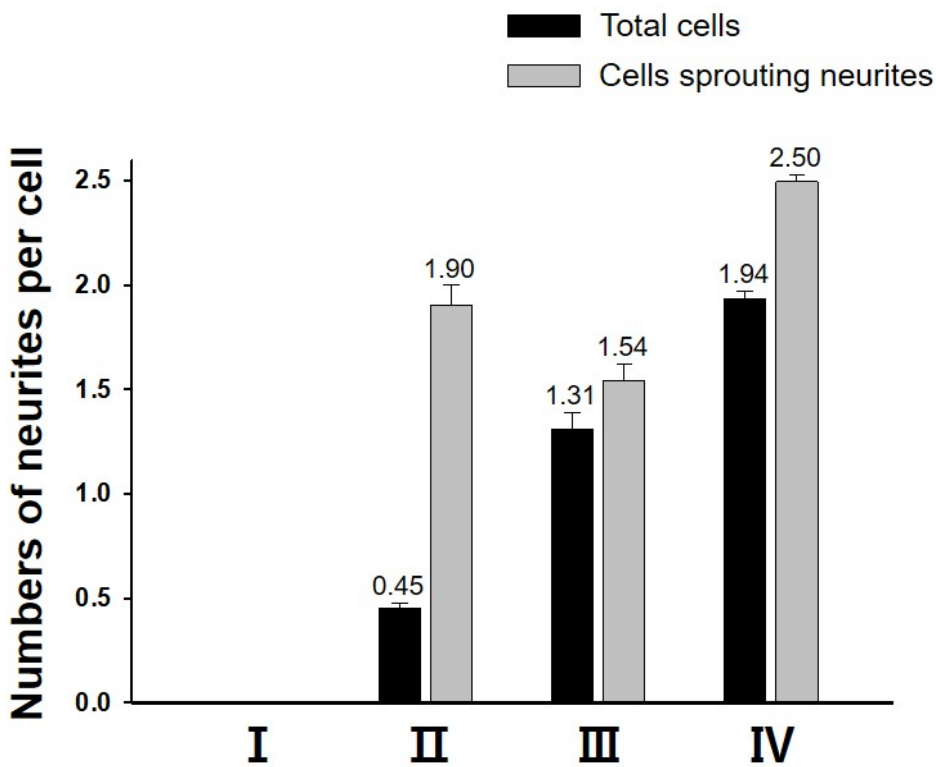

Figure 6.3.2.1 Average number of neurites per cell. Both in total cells, including the cells without neurites, and in cells sprouting neurites, the average number of neurites was largest in neurally induced hEBs (IV), compared to the other experimental groups.

1.31 in total cells including neurite-free cells, whereas the average value of only neurite-observed cells was 1.54.

In the neurally induced hEBs using NIM (IV), the percentage of cells without neurite was only 10.5%, similar to III. The percentage of cells with one neurite per cell was 14.3%, the cells with two neurites was 30.5%, and the cells with three or more neurites was 44.7%. The ratio of three or more neurites out of one cell was highest in IV compared to the other groups. The average number of neurites per cell was calculated to be 1.94 for total cells containing the cells without neurite in IV, and 2.50 for only the cells with neurites.

As a result, from experimental group I to IV, the ratio of neurite-free cells significantly decreased, while the proportion of cells with neurites increased remarkably. In particular, the ratio of cells with more than one neurite has been greatly improved. In addition, the average number of neurites per cell also increased toward the end group. When calculating the total cells, number of neurites per cell in III was statistically increased compared with II, resulting in 2.9-fold to the group II ($p < 0.001$). And the average number of neurites of total cells in IV was significantly increased compared to III, resulting in 1.5-fold of III and 4.3-fold of II ($p < 0.001$). Meanwhile, calculating only the cells with neurites, number of neurites per cell in IV showed statistically significant increase compared with both II and III, resulting in 1.3-fold to II and 1.6-fold to III ($p < 0.001$, respectively). Therefore, the average number of neurites per cell was highest in both total cells and cells sprouting neurites in IV compared to the other experimental groups. And the

difference in the number of neurites of total cells and of the cells sprouting neurites decreased from 1.45 in II to 0.56 in IV, as the proportion of cells without neurites was reduced.

6.3.3 Length of neurites per cell

In 4 experimental groups, not only the number of neurites per cell which was described above, but also the length of the neurites was analyzed. As the analysis of average neurite numbers, 150 cells for each experimental groups were used to measure the length of neurites. The length of all the neurites sprouted from each cell was measured one by one and the following values were calculated (Figure 6.3.3.1); the length of primary neurites (which were the longest in each cell), sum of the length of primary neurites and secondary neurites (which were second longest in each cell), and sum of the length of total neurites extending from one cell.

According to the analysis, the length of primary neurite, secondary neurite, and the total neurites were all zero in the control group, undifferentiated hESCs (I), since neurites were not observed in any of the cells in I.

In 2D hESCs neurally induced using NIM (II), the mean length of the primary neurites was 31.57 μm. And in III, the 2D hESCs neurally induced using NIM and the MNPs, the mean length of the primary neurites was 53.68 μm, which was 1.7-fold of II. The mean value of the primary neurite length in the experimental group IV, the hEBs which were neurally induced with NIM, was 57.27 μm, 1.8-fold of II. As a result, the length of primary neurites in experimental group III and IV increased statistically significantly compared to II ($p < 0.001$).

The sum of length of the primary and secondary neurites in one cell was calculated and then compared among the experimental groups. The mean length of this value in II was 56.81 μm. And the mean value in III was 96.12 μm, 1.7-fold to II, while

A

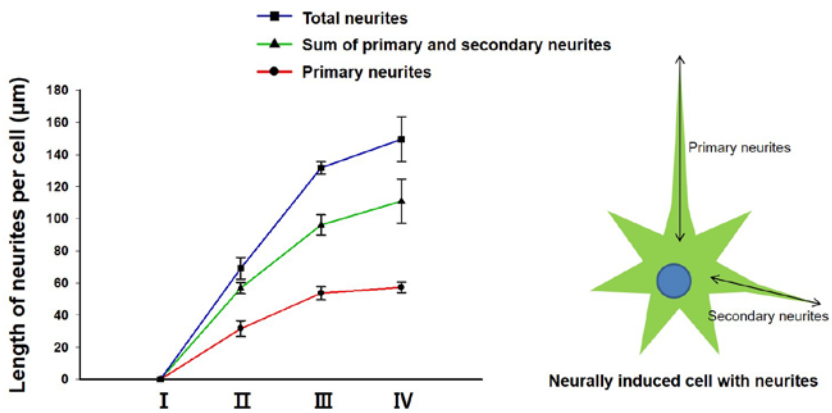

B

Neurites	Length of neurites per cell (μm) Mean ± SD		
	Ⅱ	Ⅲ	Ⅳ
Primary	31.57±4.90	53.68±4.05	57.27±3.24
Primary + secondary	56.81±3.46	96.12±6.29	111.00±13.78
Total	69.14±6.70	131.76±3.79	149.51±13.88

Figure 6.3.3.1 Length of the neurites per cell. The length of primary neurites, sum of primary and secondary neurites, and total neurites was investigated. The mean value of each length was highest in the experimental group IV, compared to the other groups. SD means standard deviation.

111.00 μm in IV, nearly twice of II. As a result, the sum of the primary neurite and secondary neurite length in the experimental group III and IV remarkably increased compared to the group II ($p < 0.001$).

Finally, the sum of length of the total neurites sprouted from one cell was calculated and the investigated between the experimental groups. In II, the mean value of total neurite length was 69.14 μm. On the other hand, in III 131.76 μm and in IV 149.51 μm, which were 1.9-fold and 2.2-fold compared with the group II, respectively. In conclusion, the length of total neurites in the experimental group III and IV was statistically enlarged when compared to II ($p < 0.001$).

From the experimental group I to IV, the length of the primary neurite, sum of primary and secondary neurites, and total neurites increased, respectively. In addition, the subtract between the length of total neurites and the length of primary neurite was increased toward the end group, either.

6.4 Immunocytochemical analysis (ICC)

6.4.1 ICC of pluripotency markers

To compare and analyze the neural induction in 4 experimental groups, expression of several related proteins was investigated through immunocytochemical analysis (ICC). The representative markers for ICC were described with their related functions in Table 6.3. First, the expression of the pluripotency, which is a unique property of the hESCs, was detected by representative pluripotency markers, and then whether or not the differentiation occurred was verified. As the representative pluripotency marker proteins, NANOG and sex determining region Y-box 2 (SOX2) were used. On the other hand, the neural induction markers used were as follows; glial fibrillary acidic protein (GFAP), indicating the growth of intermediate filament and the maintenance of cell shape; paired box 6 (PAX6), indicating the development of brain during embryogenesis; and prospero homeobox protein 1 (PROX1), indicating the development of white matter of the brain during embryogenesis process.

First, the expression of pluripotency markers was investigated *via* fluorescence images obtained from ICC. In Figure 6.4.1.1, the nuclei of the cells were labeled as blue fluorescence, and NANOG was labeled with green fluorescence. In the control group, the pluripotent hESCs (I), NANOG expression was clearly observed, while there was not any expression of NANOG in the other groups. And the nuclei shown as blue in I represented the cells in colonies and the nuclei in IV indicated that cells existed in the form of cell aggregates. Likewise, in Figure 6.4.1.2, the

Table 6.3 Representative markers for ICC.

Pluripotency marker	NANOG	Self-renewal of pluripotent stem cell
	SOX2	Self-renewal of pluripotent stem cell, Mammalian development
Neural induction marker	GFAP	Intermediate filament growth, Shape maintenance
	PAX6	Brain development
	PROX1	White matter development

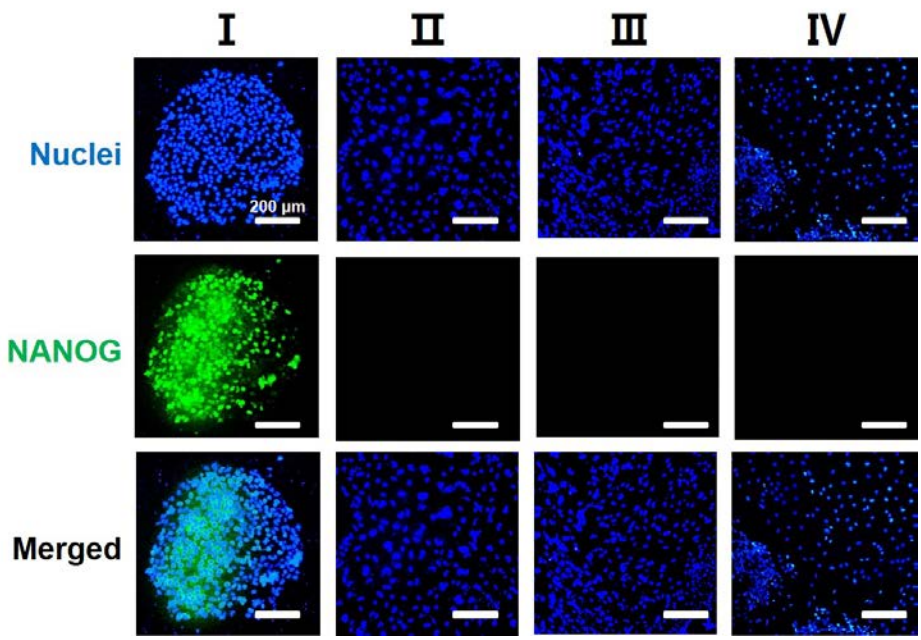

Figure 6.4.1.1 ICC of pluripotency marker NANOG. The nuclei were represented as blue and a pluripotency marker protein NANOG was shown as green in 4 experimental groups. Only in the control group, undifferentiated hESCs, NANOG was expressed contrary to the other groups. Scale bars indicate 200 μm.

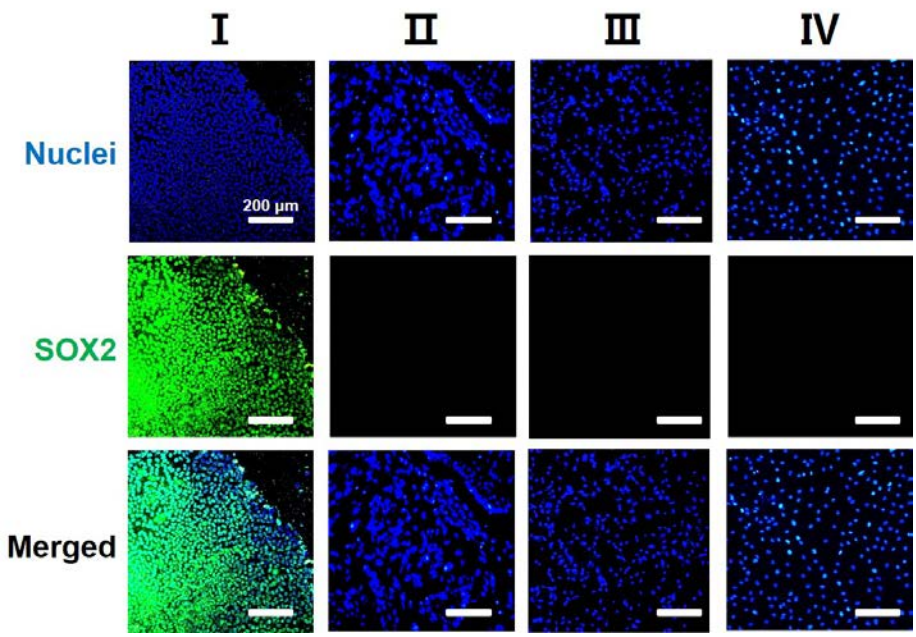

Figure 6.4.1.2 ICC of pluripotency marker SOX2. The nuclei were represented as blue and a pluripotency marker protein SOX2 was shown as green in 4 experimental groups. Only in the control group, undifferentiated hESCs, SOX2 was expressed contrary to the other groups. Scale bars indicate 200 μm.

control group showed obvious green fluorescence which indicating SOX2, different from the other groups. As a result, the hESCs remained pluripotent only in the control group, and the cells existed in the form of colonies, when confirmed by blue fluorescence. On the other hand, the hESCs lost pluripotency due to the differentiation in experimental group II, III and IV, and the intercellular distance was enlarged, resulting in loss of the colony form.

The fluorescence in the images above was quantified depending on the intensity and then the calculated values were compared among the experimental groups (Figure 6.4.1.3). The expression level of pluripotency markers was quantitated on the basis of the control group, the undifferentiated hESCs (I), which showed the maximum expression of the pluripotency markers compared to the other experimental groups. When the relative fluorescent intensity of the control group was 100%, the values of the other groups were statistically significantly lower, resulting in under the 0.5%, in the comparison of the expression level of NANOG ($p < 0.001$). Likewise, the expression level of SOX2 was significantly reduced in experimental group II, III and IV, resulting in 0.5%, 0.4% and 0.4% respectively, compared with the control group, in which the relative fluorescent intensity was 100% ($p < 0.001$). In conclusion, the expression of both NANOG and SOX2, the representative pluripotency markers, was significantly decreased in II, III and IV different from I, as shown in the ICC images above. Therefore, the pluripotency of the control group, as well as the differentiation of the other experimental groups could be quantitatively investigated.

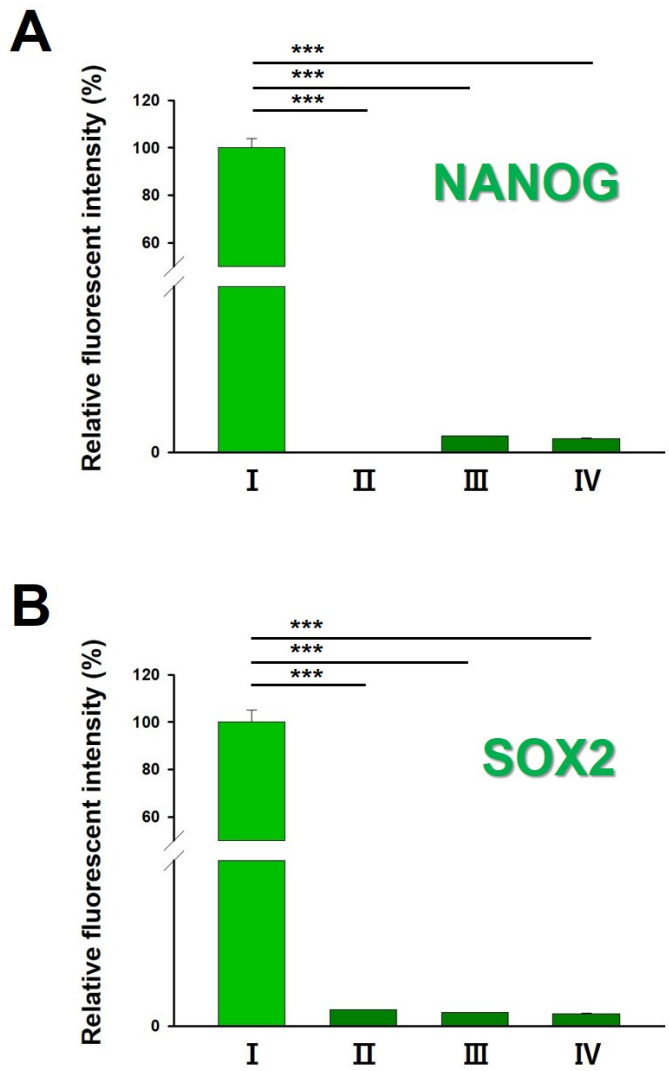

Figure 6.4.1.3 Quantified fluorescent intensity of pluripotency markers. The expression level of the pluripotency markers was quantified relative to the control group (100%), which showed maximum expression in both NANOG (A) and SOX2 (B). The relative expression of NANOG and SOX2 in group II, III and IV was statistically down-regulated compared with the control group. *** indicates $p < 0.001$.

6.4.2 ICC of neural induction markers

The expression of neural induction markers was investigated *via* fluorescence images obtained from ICC, as the expression of pluripotency markers described above.

In Figure 6.4.2.1, the nuclei of the cells were labeled as blue fluorescence, and GFAP was labeled with red fluorescence. In the control group, the undifferentiated hESCs (I), nuclei were observed as blue in the form of cell colonies, while GFAP expression was not observed at all. Similarly, in the experimental group II, conventionally differentiated hESCs with NIM, only the nuclei were shown as blue, but there was not any expression of GFAP. On the other hand, both in the hESCs neurally induced with NIM and the MNPs (III), and the neurally induced hEBs (IV), the GFAP was expressed as red. And the expression of the red fluorescence representing GFAP was remarkably enhanced in the experimental group IV, compared with III.

The expression of another neural induction marker, PAX6, was investigated as shown in Figure 6.4.2.2. As mentioned in GFAP expression of the control group, the pluripotent hESCs (I) did not show any red fluorescence which indicating PAX6, different from the other groups. However, the experimental group II, III and IV showed obvious PAX6 expression through red fluorescence. In the group II than I, also in group III compared to II, and in the last group IV than III, red fluorescence was enhanced, and thus intensity of the purple fluorescence in merged image also increased. Furthermore, according to the red fluorescence in IV, the morphology

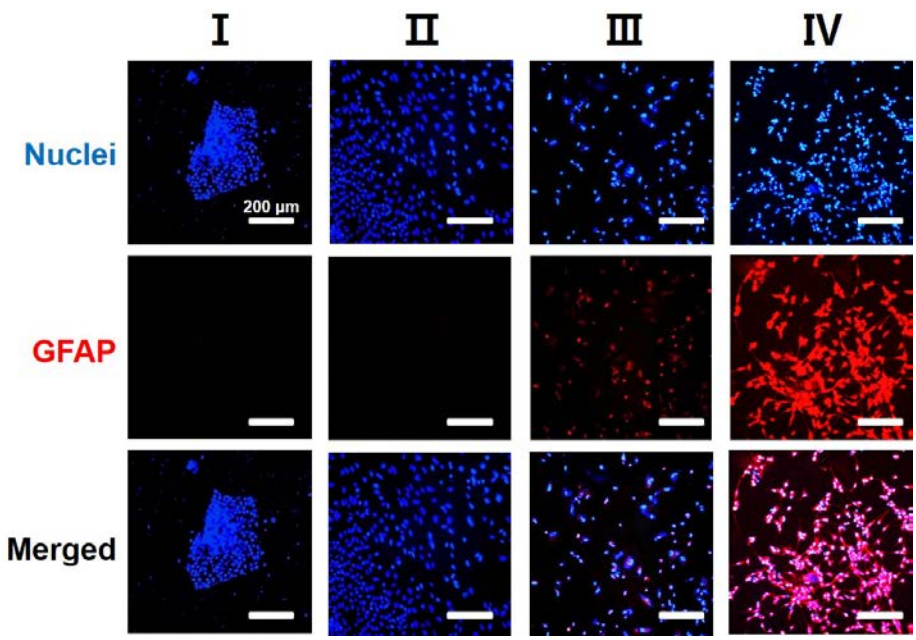

Figure 6.4.2.1 ICC of neural induction marker GFAP. The nuclei were represented as blue and a neural induction marker protein GFAP was shown as red in 4 experimental groups. Contrary to the control group and group II, GFAP was expressed in III and IV. Scale bars indicate 200 μm.

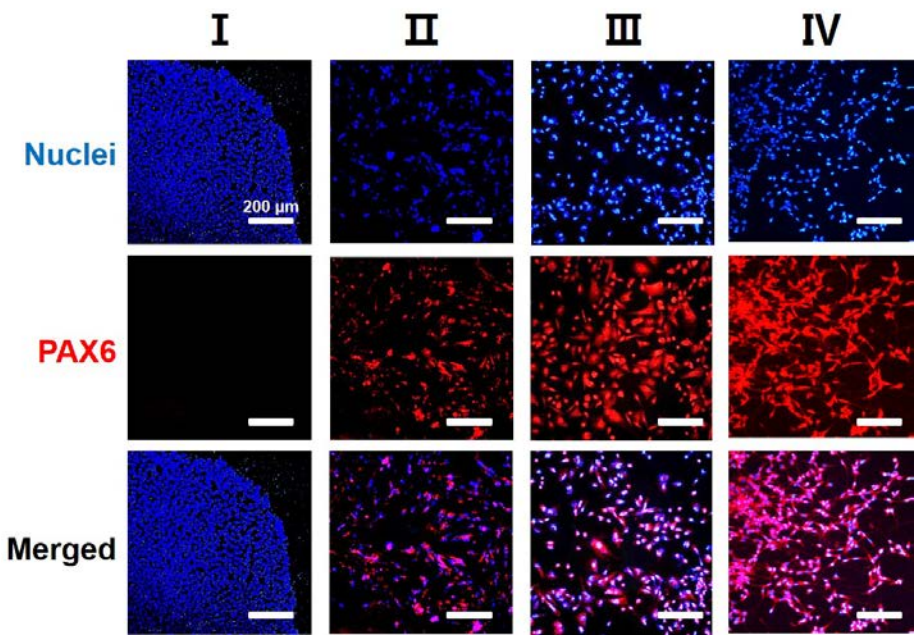

Figure 6.4.2.2 ICC of neural induction marker PAX6. The nuclei were represented as blue and a neural induction marker protein PAX6 was shown as red in 4 experimental groups. Contrary to the control group, PAX6 was expressed in the experimental group II, III and IV. And compared with the other groups, the fluorescence was much brighter in IV. Scale bars indicate 200 μm.

of the cells was elongated linear, and the neurites extended from each cell seemed to connect the cells with other cells.

Finally, the expression of the last neural induction marker, PROX1, was observed in Figure 6.4.2.3. In the control group and the group II, red fluorescence representing PROX1 was not observed. Only nuclei were observed as blue in the form of cellular colonies in I, and in both compact cellular colony-like forms and distanced cells in II, respectively. Meanwhile, PROX1 was expressed as red in the hESCs differentiated with NIM and the MNPs (III), and also in neurally induced hEBs (IV).

As a result, the undifferentiated hESCs did not show neural induction at all, and remained pluripotent in the form of cellular colonies. On the other hand, the hESCs lost pluripotency and neurally induced in experimental group II, III and IV, and the differentiation degree, represented as red fluorescence of neural induction markers, increased toward the end group.

The fluorescence in the images obtained was quantified depending on the intensity and then the calculated values were compared among the experimental groups (Figure 6.4.2.4). The expression level of neural induction markers was quantitated on the basis of the last group, neurally induced hEBs (IV), which showed the maximum expression of the neural induction markers compared to the other experimental groups.

In the comparison of the expression level of GFAP, the values of the control group and group II were both under 1.0%, when the relative fluorescent intensity of group

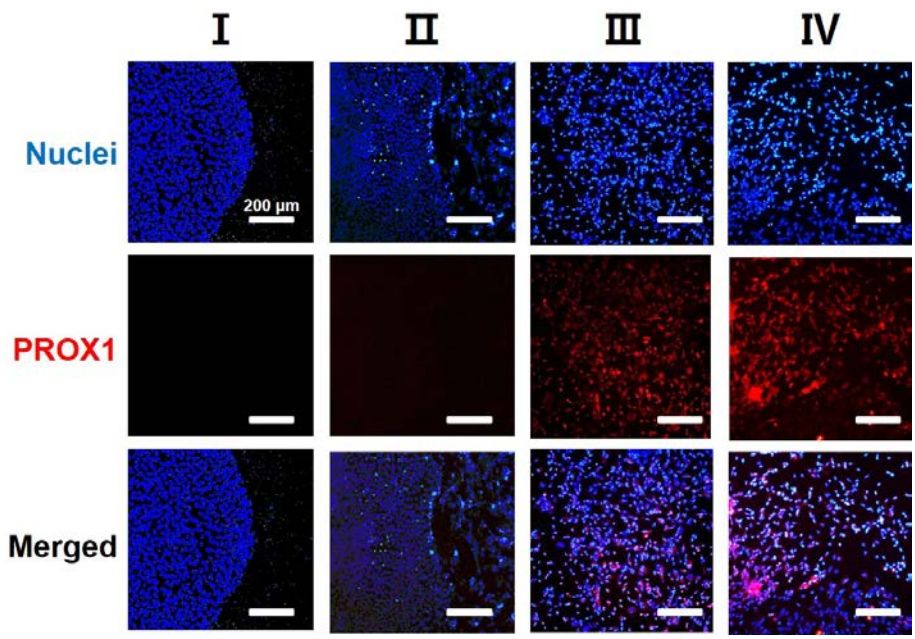

Figure 6.4.2.3 ICC of neural induction marker PROX1. The nuclei were represented as blue and a neural induction marker protein PROX1 was shown as red in 4 experimental groups. Contrary to the control group and the group II, PROX1 was expressed in III and IV. Scale bars indicate 200 μm.

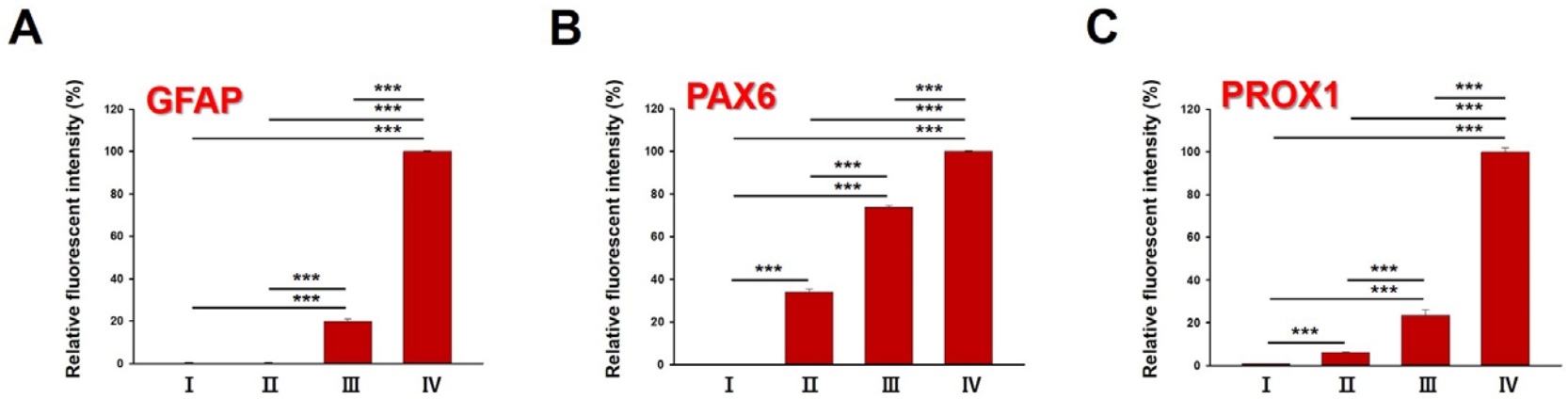

Figure 6.4.2.4 Quantified fluorescent intensity of the neural induction markers. The expression level of the neural induction markers was quantified relative to the group IV (100%), which showed maximum expression in GFAP (A), PAX6 (B) and PROX1 (C). The relative expression of GFAP, PAX6 and PROX1 in group IV was statistically up-regulated compared with the other groups. *** indicated $p < 0.001$.

IV was 100% and the value of group III was 19.8%. Thus, the quantitative GFAP expression in the control group and II did not show any statistical significance, while the expression in III was significantly enhanced compared to both I and II ($p < 0.001$, respectively). Furthermore, the expression of GFAP in IV increased statistically compared with the other groups ($p < 0.001$, respectively), resulting in more than 5.0-fold to III.

Regarding the expression of PAX6, the quantified value of the control group was under 1.0%, value of the group II was 33.9%, and the value of the III was 73.7%, respectively. Thus, the expression level of PAX6 was statistically enhanced toward the end group. The level of II was significantly increased compared with the control group ($p < 0.001$), and the value of III, which was 2.2-fold of II, was statistically increased than the group II ($p < 0.001$). Moreover, the PAX6 expression level of IV was significantly improved when compared to the group III, resulting in 1.4-fold to III ($p < 0.001$).

In the analysis of the PROX1 expression, the control group showed the value under 1.0%, as the other neural induction marker proteins in group I. However, in the group II, the expression level of PROX1 was 6.1%, and in III, it was 23.5%. The statistical significance was similar to the expression of PAX6. The value of the experimental group II was statistically enhanced compared with the control group ($p < 0.001$), and the expression in III was significantly increased than II, resulting in 3.9-fold of the group II ($p < 0.001$). Furthermore, the expression level in IV, which was 4.3-fold to III, was statistically emhanced compared with III ($p < 0.001$).

In conclusion, the expression of neural induction markers, GFAP, PAX6 and PROX1, was significantly increased toward end group (IV), as shown in the ICC images above.

6.5 Genetical analysis

To investigate neural induction in 4 experimental groups, genetic analysis was performed to measure the expressed mRNA levels according to the expression of related genes. Each of the expressed genes was normalized by glyceraldehyde 3-phosphate dehydrogenase (*GAPDH*), an endogenous reference gene, and then they were analyzed using relative quantification methods. All the data were compared with each value of the control group, the undifferentiated hESCs (I), which was marked as 1 for the relative fold induction (RFI). As a pluripotency marker gene, octamer-binding transcription factor 4 (*OCT4*) was utilized, and neural induction marker genes used were as follows; growth associated protein 43 (*GAP43*), related to the neuronal growth and the neurite formation; β3-tubulin (*TUBB3*), indicating microtubule formation; nestin (*NES*), related to the intermediate filament growth and the axon growth; and *GFAP*, indicating the intermediate filament growth and the cellular shape maintenance. The primer sequences of each gene for real time RT-PCR were listed in Table 6.4.

According to the Figure 6.5.1, the expression of *OCT4*, a pluripotency marker, was statistically decreased in experimental group II, III and IV, resulting in 0.6, 0.3 and 0.2 respectively, compared to the control group in which the RFI value was 1 ($p < 0.001$). And a neural induction marker, *GAP43*, was significantly increased in II, III and IV, compared with the control group I ($p < 0.001$). In the expression of *NES* and *GFAP*, neural induction markers, there was no significant difference in II from

Table 6.4 Primer sequences for genetical analysis.

	Marker	Sequence (5' → 3') Forward / Reverse
Endogenous reference	***GAPDH***	ccatgacaactttggcatcg / cctgcttcaccaccttctt
Pluripotency	***OCT4***	agcgaaccagtatcgagaac / ctctcgttgtgcatagtcg
Neural induction	***GAP43***	gatgatgtccaagctgctga / ttctcctctgaggatgcag
	TUBB3	ttgctgatgagcaacgtgc / ggaaccatggacagtgtc
	NES	aaggaaaccgtcattgtagagg / agctggtgacttggcctc
	GFAP	gagaacaacctggctgccta / ctcatactgcgtgcggatct

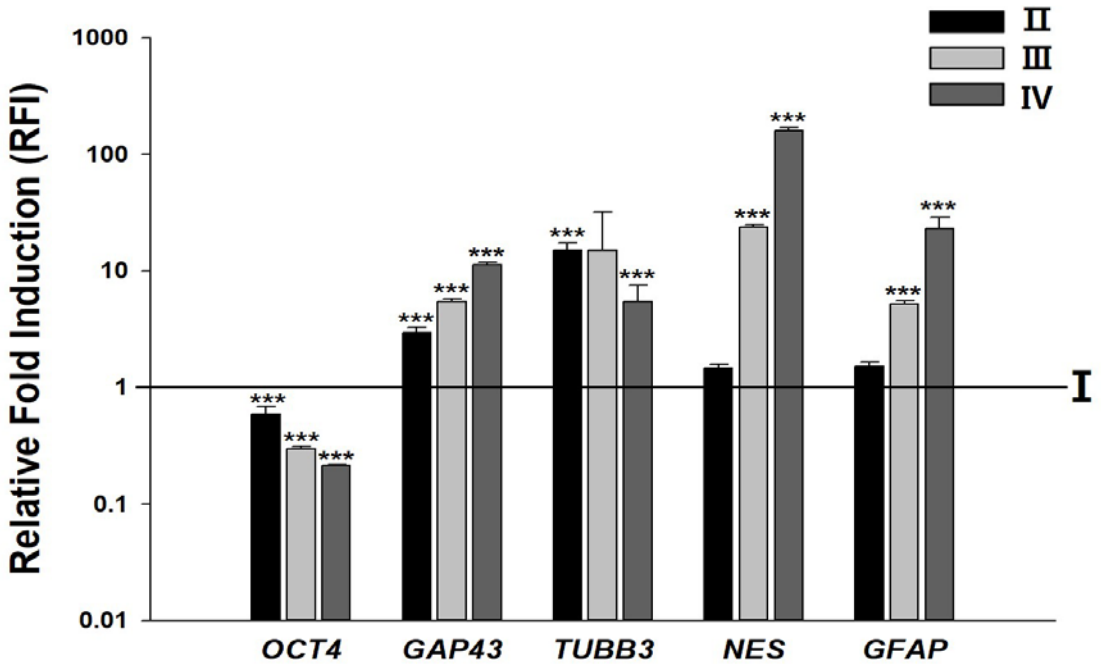

Figure 6.5.1 Genetical analysis of a pluripotency marker and neural induction markers. The expression of all the genes was normalized by each value of the control group. The relative expression of the neural induction marker genes increased in group II, III and IV compared with the control group. *** indicates $p < 0.001$.

the control group, while in III and IV, their expression significantly increased ($p < 0.001$).

For more detailed comparisons between the experimental groups, the graphs were divided and then analyzed depending on each gene (Figure 6.5.2). According to the comparison of the *GAP43* expression (Figure 6.5.2 A), there was a statistically significant increase in experimental group II compared to the control group, also in group III compared to II, and in the last group, IV compared with III ($p < 0.001$, respectively). The relative value of the expression in II was 3.0, which was 3.0-fold of the control group, and in III was 5.4, which was 1.8-fold to II. Moreover, the RFI of IV was 11.2, which was 3.7-fold of II, and 2.1-fold to III, respectively. Thus, the expression of *GAP43* was most prominent in the last group (IV).

In the comparison of *NES* and *GFAP* expression through Figure 6.5.2 C and D respectively, there was no significant difference between the control group and the experimental group II. The relative value of II was 1.5 in both *NES* and *GFAP* expression. On the other hand, the expression of both genes was significantly increased in III compared to II, and in IV compared with III ($p < 0.001$, respectively). In the expression of *NES*, the RFI of III was 23.6, which was 15.7-fold of II, and the value of IV was 158.3, which was 105.5-fold to II and 6.7-fold of III, respectively. Meanwhile, in *GFAP* expression the RFI value of III was 5.2, which was 3.5-fold of II, and the value of IV was 22.9, which was 15.3-fold to II and 4.4-fold of III, respectively.

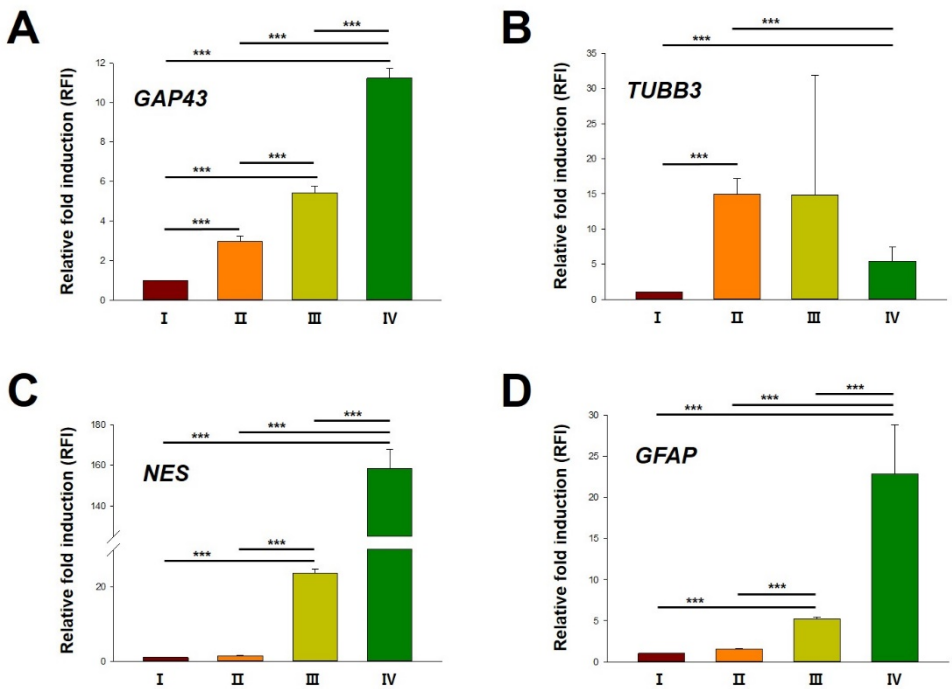

Figure 6.5.2 Comparison of neural induction marker expression through genetical analysis. The relative expression of the neural induction markers, *GAP43* (A), *TUBB3* (B), *NES* (C) and *GFAP* (D), was compared between the experimental groups. The expression of *GAP43*, *NES* and *GFAP*, showed statistically significant increase in IV, compared with the other groups. *** indicates $p < 0.001$.

Therefore, the expression of these three genes resulted in significant neural induction of the hESCs differentiated with NIM and the MNPs (III) and also neurally induced hEBs (IV), contrary to the undifferentiated hESCs (I) and conventionally differentiated hESCs with NIM (II).

However, when the expression level of *TUBB3* was compared, a slightly different tendency was observed (Figure 6.5.2 B). Although the standard deviation of the experimental group III was quite large, it was confirmed that *TUBB3* expression level in II and III was higher than that of group IV. The relative value in IV was 5.4, the RFI in II was 15.0, which was 2.8-fold of IV, and the value in III was 8.1, 1.5-fold to IV. This was a very specific phenomenon as compared to the expression pattern of the other neural induction markers, increasing toward the end group (IV) as described above. That is to say, the expression of *TUBB3* was down-regulated in the experimental group IV, a 3D cell culture and differentiation, when compared with II and III, 2D cell culture and differentiation.

6.6 Conclusions

The small-sized hEBs (150 μm in diameter), generated by the MNPs and the concentrated magnetic force system, were spontaneously differentiated into ectodermal lineage in hEB culture medium for 3 days, and some of those cells showed neurite-like outgrowth. So, I decided to improve the neural induction of the hESCs in the form of the small-sized hEBs replacing the hEB culture medium to NIM, and increasing the duration for differentiation from 3 days to 5 days. To investigate the improvement of the neural induction of the small-sized hEBs (IV), comparable groups were set as follows; undifferentiated hESCs (I), conventionally differentiated hESCs with NIM (II), and conventionally differentiated hESCs with NIM and MNPs (III).

To detect the neural induction of 4 experimental groups, the superficial morphology of the cells was observed. The intrinsic shape of natural hESCs was small (less than 10 μm in diameter) and round, in the form of cellular colonies. According to the morphological analysis, neurally induced hESCs in group II, III and IV were changed in their appearance, resulting in formation of tiny projections on cells, called neurites. Therefore, the neurally induced hESCs became sharp-pointed, and the compact colonies were disrupted, producing enough intercellular distance between cells.

The hESCs were divided by number of neurites per cell; cells without any neurites, cells with one neurite, cells with 2 neurites, and the cells with 3 or more neurites. And then the proportion of each type was investigated. In the control group,

undifferentiated hESCs (I), all of the cells existed without neurite, and in group II more than half of the cells existed without neurites. However, in both III and IV, about 90% of the cells existed with neurites, and the hESCs with 3 or more neurites per cell were more than 30%, respectively. And the average number of the neurites per cell was also calculated. In total cells, including the cells without neurites, number of neurites was 0 in the control group, 0.45 in II, 1.31 in III, and 1.94 in group IV. Meanwhile, in only the cells sprouting neurites, the number of neurites per cell was 0 in the control group, 1.90 in II, 1.54 in III, and 2.50 in IV. Both the number of neurites per cell in total cells and in the cells with neurites increased toward the end group (IV).

Also the length of all the neurites sprouted from each cell was measured one by one, and the following values were calculated; the length of primary neurites (which were the longest in each cell), sum of the length of primary neurites and secondary neurites (which were second longest in each cell), and sum of the length of total neurites extending from one cell. From the experimental group I to IV, the length of the primary neurite, sum of primary and secondary neurites, and total neurites increased, respectively. In addition, the difference between the total neurite length and the length of primary neurites enhanced toward the end group, either.

According to ICC and the quantification of fluorescent intensity, only the control group, undifferentiated hESCs (I), possess pluripotency, whereas the other groups did not show any expressions of pluripotency markers, represented as NANOG and SOX2. On the other hand, the expression of neural induction markers, represented

as GFAP, PAX6, and PROX1, was detected in the experimental group II, III and IV, contrary to the control group. And the expression level of those neural induction marker proteins significantly increased toward the end group.

According to genetical analysis, the expression of a pluripotency marker gene, *OCT4*, significantly decreased in the experimental group II, III and IV, compared with the control group. However, the expression of neural marker genes, represented as *GAP43*, *NES* and *GFAP*, showed statistically significant increase in IV compared to the other groups. Among the neural induction marker genes, only the *TUBB3* showed different result; its expression was reduced in IV compared to the group II and III.

In conclusion, the hEBs in NIM for 5 days were successfully differentiated, resulting in the improvement of the hESC neural induction and the acceleration of initial neural differentiation. The time required for initial neural induction and neurite outgrowth was reduced from 2 to 3 weeks to 5 days, compared with previous work [122]. And this improved neural inductivity was statistically confirmed through morphological analysis, ICC and genetical analysis, comparing with the undifferentiated hESCs, conventionally differentiated hESCs with NIM, and conventionally differentiated hESCs with NIM and the MNPs.

Chapter 7.

Mechanisms of accelerated neural induction of small-sized human embryoid bodies

Chapter 7. Mechanisms of accelerated neural induction of small-sized human embryoid bodies (hEBs)

7.1 Introduction

In the previous chapter, the neural induction of human embryonic stem cells (hESCs) was investigated and compared in 4 experimental groups. According to the results (Figure 7.1.1), the neural induction was improved in the group II, in which the culture medium of the undifferentiated hESCs (I) was changed to neural induction medium (NIM). Furthermore, neural induction was more enhanced when the magnetic nanoparticles (MNPs) were treated with NIM (III), compared with group II. And when the hESCs gathered by the concentrated magnetic force system and then formed the human embryoid bodies (hEBs) (IV), three-dimensional (3D) cell aggregates, with NIM and the MNPs, the neural differentiation was most accelerated, compared with the other groups. The differentiation patterns were investigated statistically through morphological analysis, related protein analysis and the representative gene analysis. In other words, it was confirmed that the neural differentiation was improved from the control group to the experimental groups II, III, and IV.

In this chapter, in order to analyze these phenomenon, the related signaling pathways which happen inside the cells, leading particular cell fate, were identified. To reveal the mechanisms related to the neural differentiation of the hESCs, the

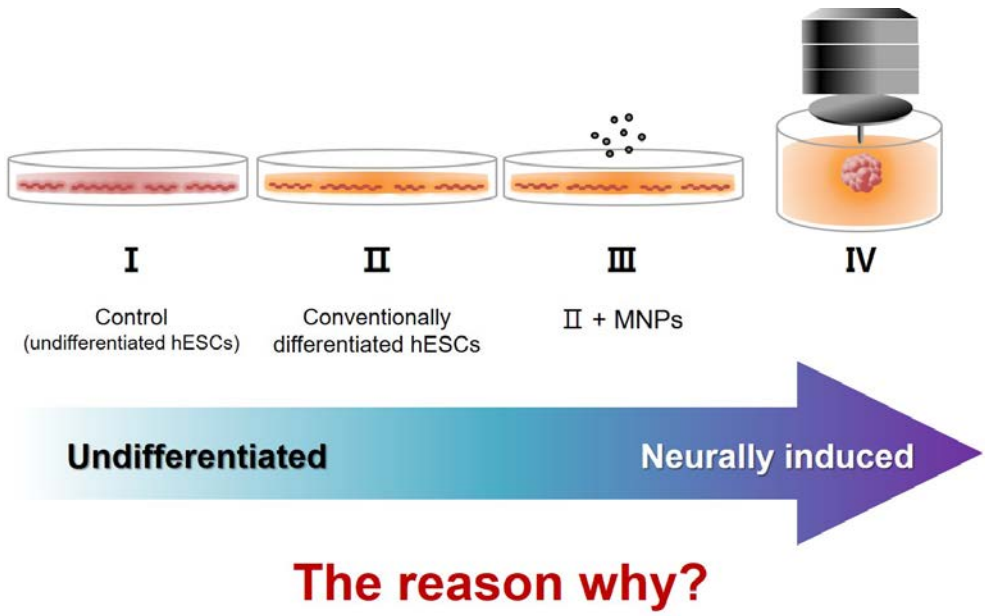

Figure 7.1.1 Schematics for accelerated neural induction. The neural induction of small-sized hEBs (IV) was most accelerated compared to the other groups. From the undifferentiated hESCs (I) to the experimental group II, III and IV, the neural induction was improved.

expression of cascading proteins was investigated and compared between the experimental groups.

7.2 WNT signaling pathways

WNT proteins encoded by *WNT* genes, which express various types of cystein-rich glycoproteins, regulate various behaviors of the cells, represented as cell death, carcinogenesis, migration and cell differentiation [131-133]. According to former studies, among WNT family proteins, WNT3 and WNT5α possess important effects on the regulation of cell fate during embryological development (Figure 7.2.1) [134-139]. That is to say, those proteins are necessary for the differentiation of the hESCs. The activation of WNT3 proteins results in differentiation of pluripotent stem cells (PSCs) into neural progenitor cells (NPCs), and then differentiation of the NPCs into mature neurons [134-136]. Moreover, the WNT3 has known to be concerned with the conversion of non-neuronal nerve cells, such as glial cells, into neuron-like cells. Meanwhile, the expression of WNT5α has known to be lead to induction of PSCs into NPCs, and the differentiation of the NPCs into neurons and glial cells [137-139].

Based on this, in order to verify the activated signaling pathways during neural induction of the hESCs, I investigated these WNT3 and WNT5α expression in 4 experimental groups through Western blotting (Figure 7.2.2). When β-actin was used as a reference protein, which is expressed constantly in all groups, the expression of WNT3 and WNT5α was analyzed and compared. The expressed WNT3 was remarkably observed in group IV, when compared with the other groups. WNT5α was expressed only in group II. In group III, the hESCs were neurally induced with NIM and MNPs, both WNT3 and WNT5α were not expressed. The

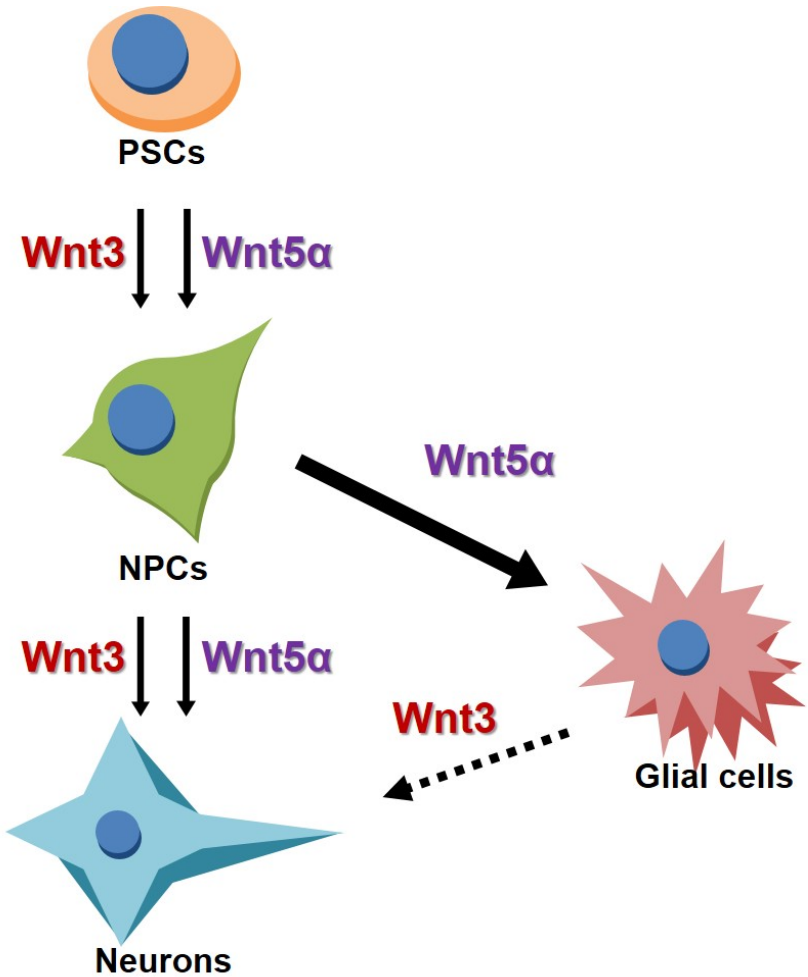

Figure 7.2.1 Schematics for WNT signaling pathways. Both WNT3 and WNT5α affect differentiation of the hESCs during embryogenesis and neuronal development.

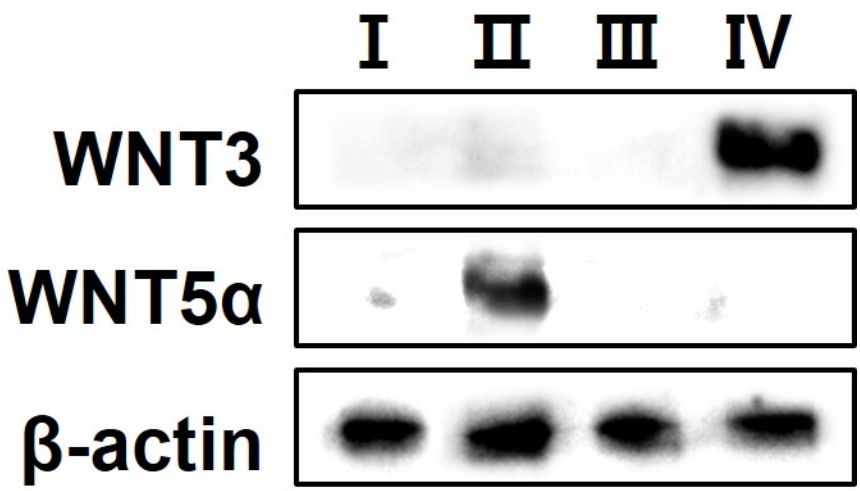

Figure 7.2.2 Western blotting of WNT proteins. As a reference protein, β-actin was used. WNT3 was expressed only in the experimental group IV compared with the other groups. On the other hand, WNT5α was expressed only in group II compared to the other groups.

experimental group III is related to the group II in terms of NIM use, and also related to the group IV in terms of MNP application. In addition, according to the results of chapter 6, neural differentiation of group III was verified, like group II and IV. However, according to Figure 7.2.2, neural induction in group III seems to follow other signaling pathways different from WNT3 and WNT5a. Accordingly, the accelerated neural induction of the hESCs in IV was considered to follow WNT3 signaling pathway. Whereas, the neural induction of group II followed WNT5α signaling pathway.

7.3 Dopaminergic neuronal pathways

7.3.1 Expression of glial cell line-derived neurotrophic growth factor (GDNF)

Among the various neuronal factors, one of the most important is glial cell line-derived neurotrophic growth factor (GDNF), which is a distantly related member of the transforming growth factor-β (TGF-β) superfamily [140, 141]. Therefore, it is a kind of multifunctional cytokine regulating pathway proteins by activating various downstream substrates in signaling cascades. The GDNF is expressed in a dynamic pattern in the anterior neuroectoderm during early stages of neurogenesis [142-148]. Significant roles of the GDNF are to promote the survival and development of the neurons which have high affinity with dopamine (Figure 7.3.1.1) [145, 146]. Thus, the GDNF prevents apoptosis of motor neurons and improves differentiation of dopaminergic neurons.

In order to detect the dopaminergic neuronal pathways in the experimental groups, the expression of GDNF was observed through immunocytochemical analysis (ICC) in neurally induced hESCs (Figure 7.3.1.2). Because the experimental group II (conventionally differentiated hESCs with NIM), group III (neurally induced hESCs with NIM and MNPs), and the group IV (neurally induced hEBs with NIM and MNPs) were neurally differentiated, GDNF expression in these three groups was investigated. The nuclei were shown as blue fluorescence in group II, III and IV, while GDNF was observed as red (Figure 7.3.1.2 A). Different from the group II

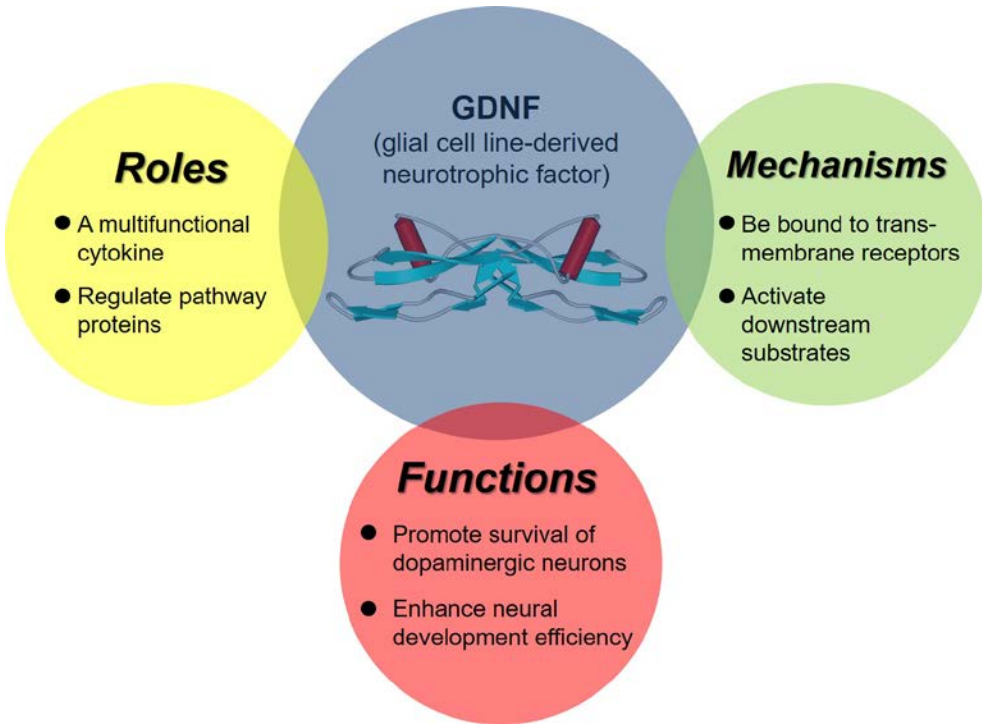

Figure 7.3.1.1 Schematics for GDNF structure and functions.

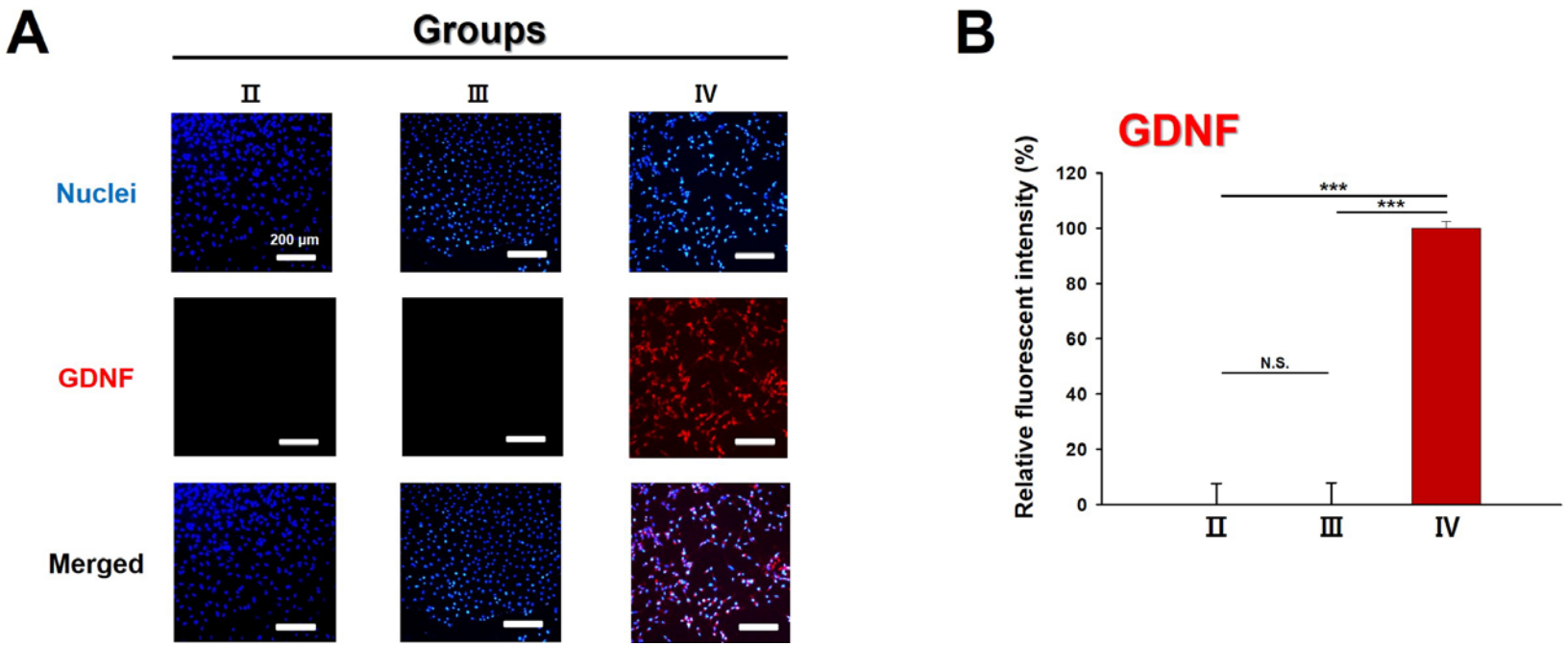

Figure 7.3.1.2 GDNF expression. (A) The expression of dopaminergic neuronal pathway protein, GDNF was investigated through ICC. Nuclei were observed as blue and GDNF was shown as red. Scale bars indicate 200 μm. (B) The fluorescent intensity of GDNF was quantified. N.S. indicated not significant, and *** indicated $p < 0.001$.

and III, the expression of red fluorescence, representing GDNF, was remarkably observed in group IV. And the morphology of the cells in IV was linear and sharpen with neurites sprouted from the cell body. The fluorescence in the images was quantified depending on the intensity and then calculated values were compared among the experimental groups (Figure 7.3.1.2 B). The expression level of GDNF was quantitated relative to group IV, which showed the maximum expression of GDNF compared to the other experimental groups. When the relative fluorescent intensity of group IV was 100%, the values of group II and III were statistically significantly lower ($p < 0.001$), while there was no significant difference in the values between group II and III.

According to the results, the hESCs in the form of small-sized hEBs with NIM and MNPs (IV) were neurally differentiated expressing GDNF, different from other groups. Therefore, some of the neurally induced hESCs in group IV were considered to possess affinity with dopamine. However, the dopamine-related function of mature neurons and dopaminergic signaling pathway should be verified with additional analysis.

7.4 Intracellular communications

7.4.1 Expression of neural cell adhesion molecule (NCAM)

There are several groups of the cell adhesion molecules which mediate cell-to-cell and cell to extracellular matrix (ECM) interactions; the immunoglobulin superfamily, the cadherin family, the integrin superfamily, the selection family and the epidermal growth factor family [149, 150]. Among those cell adhesion molecules, the neural cell adhesion molecule (NCAM), a member of the immunoglobulin superfamily, is responsible for not only neural cell adhesion and recognition but also the neural development (Figure 7.4.1.1) [151, 152]. The NCAM is a cell surface glycoprotein which mediates adhesions and then interactions between the neuron to neuron, neuron to glial cell, and neuron to ECM. And NCAM is highly expressed during the developmental processes of the nervous system. Furthermore, according to the related studies, the significant role of NCAM in the central nervous system is associated with not only neural development, but also with adult functions, such as the processing system of sensory information and neuronal plasticity [151-156]. Regarding the effect of NCAM on neurite outgrowth, it has been proposed that improvement of the neurite outgrowth occurs above the threshold value of the NCAM expression.

To detect cell adhesions and intercellular communications, the expression of NCAM was investigated through ICC in neurally induced hESCs (Figure 7.4.1.2). The expression of NCAM was analyzed and compared in the group II, III and IV, in

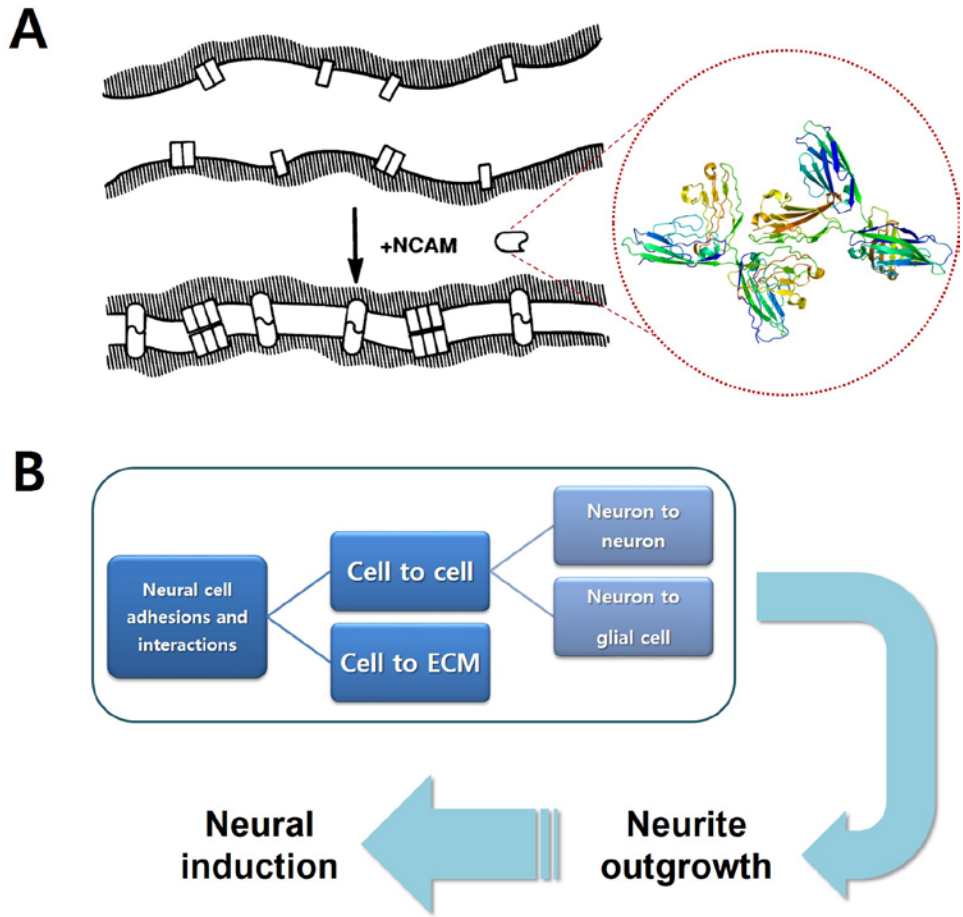

Figure 7.4.1.1 Schematics for NCAM structure and functions.

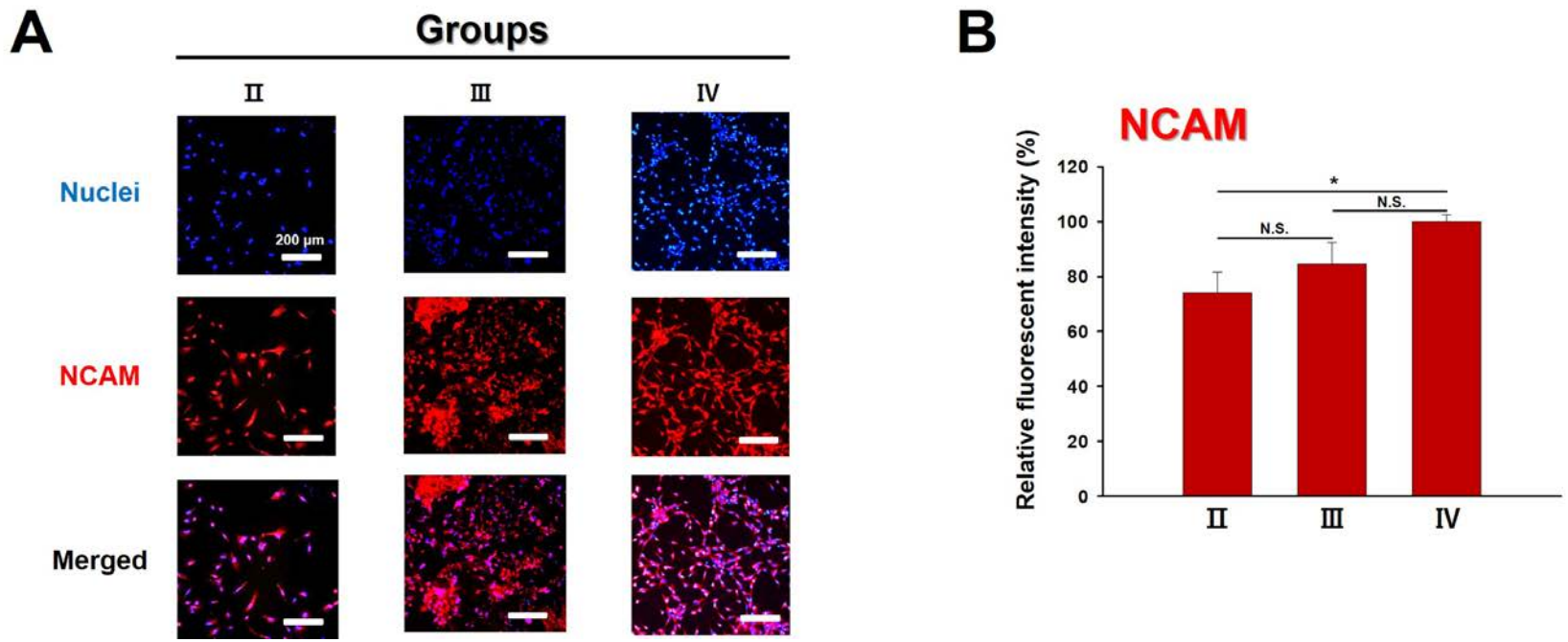

Figure 7.4.1.2 NCAM expression. (A) The expression of intercellular communication protein, NCAM was investigated through ICC. Nuclei were observed as blue and NCAM was shown as red. Scale bars indicate 200 μm. (B) The fluorescent intensity of NCAM was quantified. N.S. indicated not significant, and * indicated $p < 0.05$.

which physical condition of cell cultivation was different; two-dimension (2D) in the experimental group II and III, and 3D in the group IV. The nuclei were represented as blue, NCAM was observed as red, and the merged images showed bright purple fluorescence in the group II, III and IV (Figure 7.4.1.2 A). In both group II and III, the hESCs adhered to the bottom of flask in 2D condition expressed NCAM. In the group IV, though the cells were cultured in suspended condition, in which cell adhesion to bottom was inhibited, the expression of NCAM was obviously observed. The fluorescence was quantified depending on the intensity and the values were calculated relative to group IV, which showed maximum expression of NCAM (Figure 7.4.1.2 B). When the relative fluorescent intensity of IV was 100%, the values of group II was 74.0±7.6%, and group III was 84.5±7.9%, respectively. There was no statistical significance in NCAM expression between group II and III, and group III and IV, either. However, NCAM expression of group IV showed statistical improvement compared to group II ($p < 0.05$).

Accordingly, it was confirmed that the expression of NCAM did not to depend on the application of MNPs, when comparing the results of group II and III. In addition, by comparing the experimental group III and IV, it was evaluated that NCAM expression was not impeded when external stimulation derived from concentrated magnetic force was applied, even when the cells were cultured in 3D condition. Consequently, the hESCs differentiated in suspended condition (IV) expressed sufficient NCAM when compared with neurally induced hESCs in 2D condition (II and III). This result indicated that cell-to-cell adhesions and

interactions were enhanced in 3D suspended culture condition, though cell to bottom adhesions and interactions were prohibited.

7.5 Mechanotransduction

7.5.1 Expression of microtubule-associated protein 2 (MAP2)

To maintain cellular morphology, proteins involved in the cytoskeletons exist inside the cells and complex structures are formed from those cytoskeletal proteins [66]. There are three categories of the cytoskeletal proteins present throughout the cell; microtubules, intermediate filaments, and actin filaments [157, 158]. Interactions and changes between them enable important cellular actions, such as cell contraction, migration and cleavage. In addition, these cytoskeletal proteins act as receptors for external stimuli.

The microtubule-associated protein 2 (MAP2) is a member of MAP family, which is known to be involved in microtubule assembly and neurite genesis [159, 160]. The MAP2 stabilizes growth of microtubules by crosslinking them with intermediate filaments and other microtubules (Figure 7.5.1.1) [161, 162]. Also MAP2 forms neuron-specific cytoskeletons, determining and stabilizing the shape of nerve cells during neuronal development. Therefore, MAP2 is a protein that sensitively responses to physical stimuli externally applied to cells. When an external force is applied to cells, this stimulation could be transmitted inside the cells by cytoskeletons which are mediated by MAP2 [163, 164]. And this process facilitates neuronal differentiation through transfer of the mechanical stimuli.

In this chapter, in order to verify the effect of magnetic force and the 3D circumstances on neural induction of the neurally induced hEBs (IV), expression of

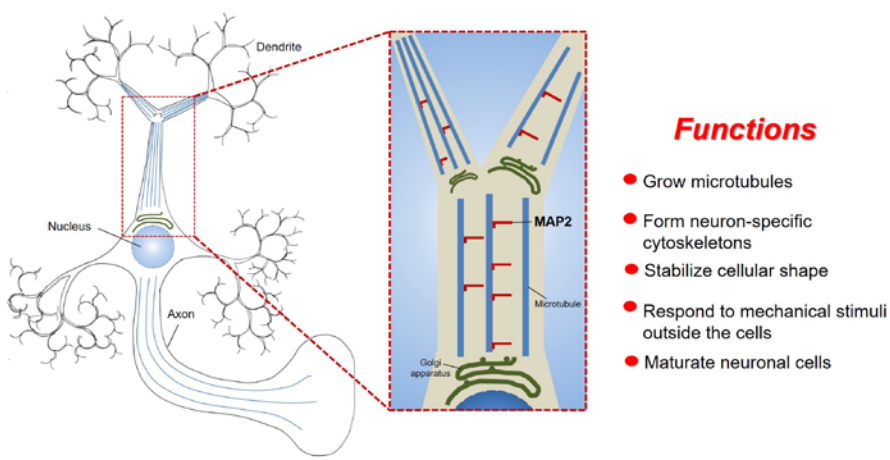

Figure 7.5.1.1 Schematics for MAP2 structure and functions.

the proteins related to the mechanotransduction was investigated.

By observing the expression level of MAP2, microtubule growth and neural development promoted through mechanotransduction was analyzed in neurally induced hESCs (Figure 7.5.1.2). The nuclei were represented as blue, MAP2 was observed as red, and the merged images showed bright purple fluorescence in the experimental group II, III and IV (Figure 7.5.1.2 A). In three experimental groups, the expression of MAP2 was observed similarly. By quantifying the relative fluorescent intensity, it was evaluated that there was no statistical significance of MAP2 expression among all the groups (Figure 7.5.1.2 B).

Although the results of microtubule growth and genesis, which were represented by red fluorescence seemed not to be different, the circumstances of cell cultivation were distinguishable; 2D for group II, 2D with MNPs for group III, and 3D with MNPs and the concentrated magnetic force for the group IV. Therefore, the cause and process of the microtubule generation would be different in those experimental groups. In group II and III, the cells adhered to bottom enlarging the contact area of cell bodies, thus cytoskeletal proteins such as microtubules were expressed sufficiently. However, in group IV, the cells were suspended and only cell-to-cell adhesions were available, thus cytoskeletons would be generated through these intercellular communications.

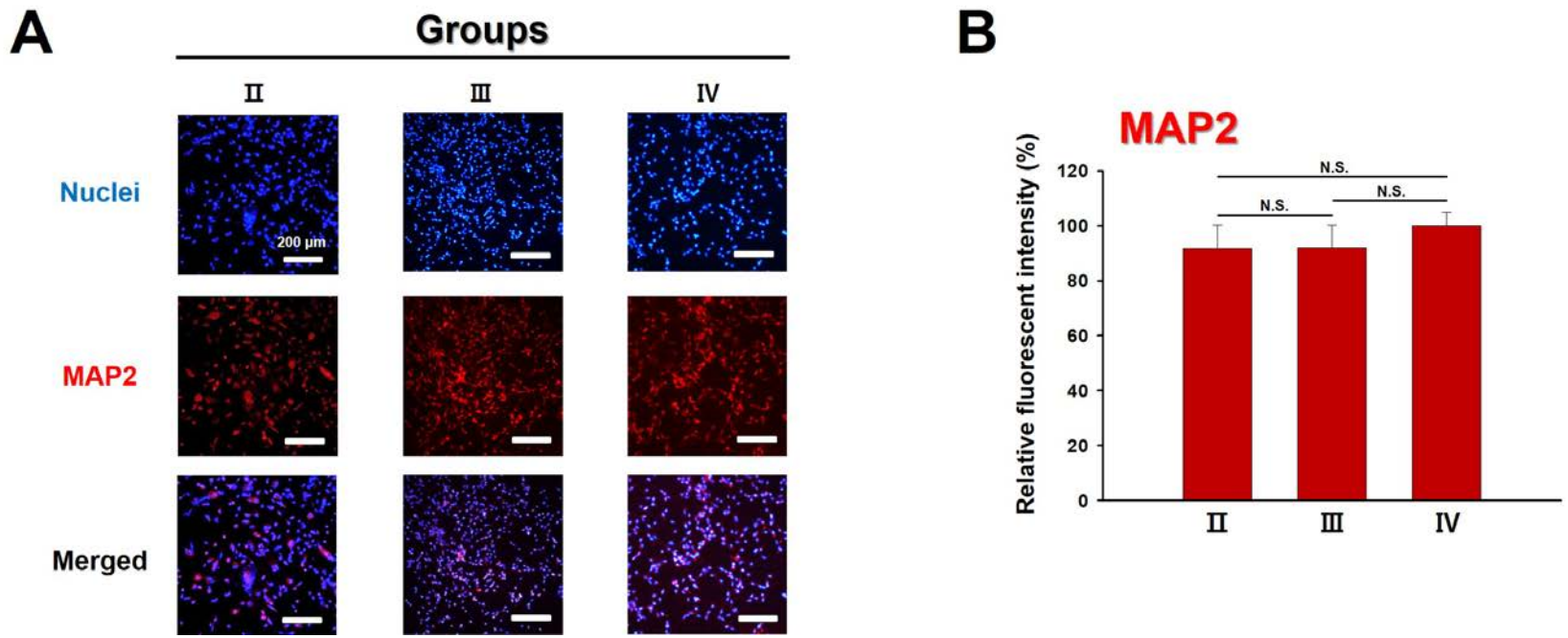

Figure 7.5.1.2 MAP2 expression. (A) The expression of cytoskeleton-related protein, MAP2 was investigated through ICC. Nuclei were observed as blue and MAP2 was shown as red. Scale bars indicate 200 μm. (B) The fluorescent intensity of MAP2 was quantified. N.S. indicated not significant.

7.5.2 Expression of focal adhesion kinase (FAK)

An important question in cell biology is how the receptors in cellular membrane transmit extracellular signals inside the cells [165, 166]. Focal adhesion kinase (FAK) is a crucial signaling component, which is activated by various stimuli, as a biosensor or integrator to modulate cell adhesions and motility. The activated FAK is a highly tyrosine-phophorylated protein involved in the cytoskeletons, structures of cell adhesion sites, called focal contacts, and membrane protrusions (Figure 7.5.2.1) [167]. FAK pays a key role at early steps in reception of mechanical stimulation outside the cells [167, 168]. Through the FAK activation, intracellular signal transduction pathways could be turned on. Thus, the activated form of FAK is necessary during the stem cell development, for recognizing the exterior physical factors.

In order to detect the mechanical stimuli-induced neural differentiation of the hESCs, the expression of FAK in neurally induced hESCs was estimated (Figure 7.5.2.2). The nuclei were shown as blue and FAK was detected by red fluorescence (Figure 7.5.2.2 A). All the neurally induced hESCs in the experimental group II to IV expressed the FAK. According to the quantitated results, there was no significant differences of FAK expression between the group II and III, between group III and IV, and also between II and IV (Figure 7.5.2.2 B). Although the hESCs in group IV were cultivated in suspended condition, in which cell adhesion to bottom was hindered, the cells expressed sufficient FAK, compared with group II and III, in which cells adhered to bottom.

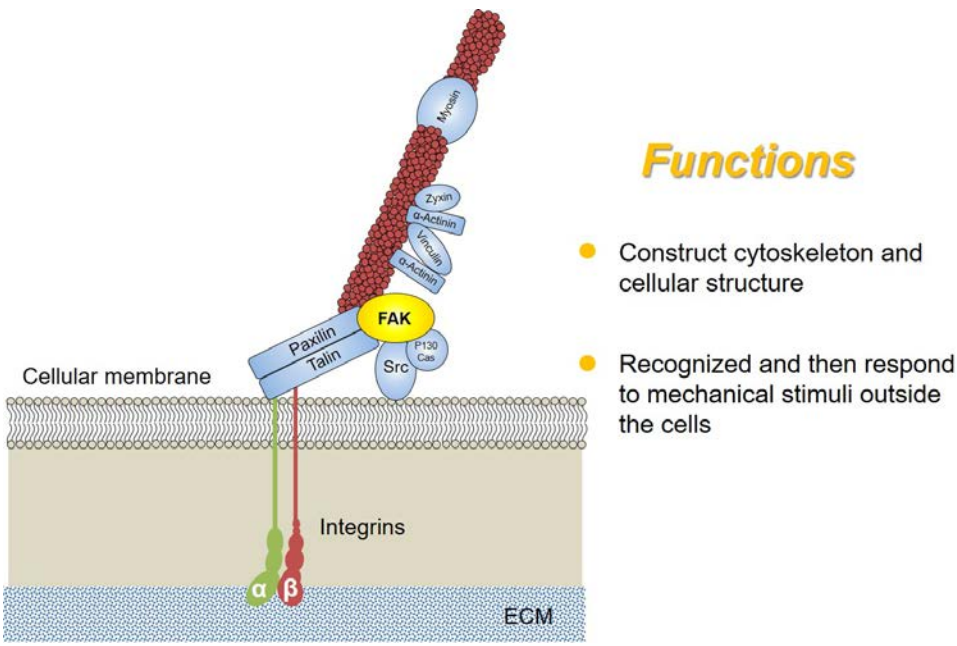

Figure 7.5.2.1 Schematics for FAK structure and functions.

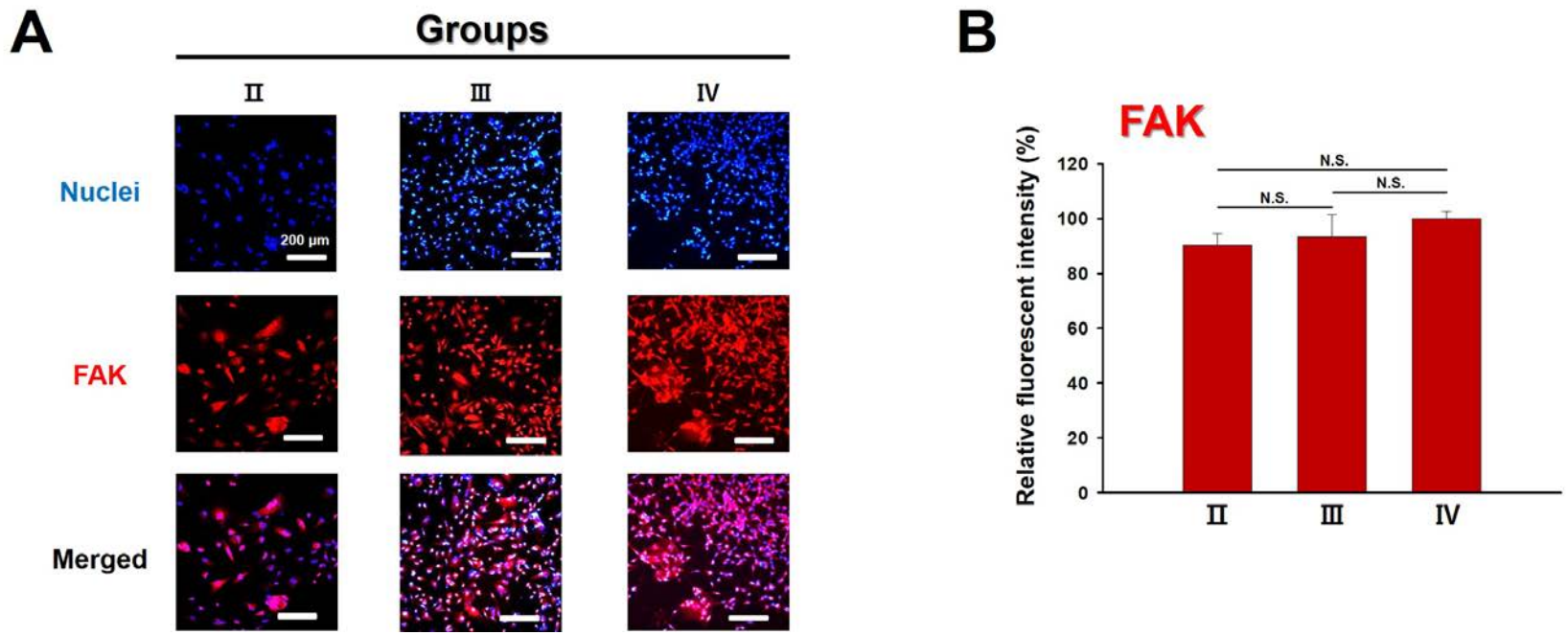

Figure 7.5.2.2 FAK expression. (A) The expression of mechanotransduction protein, FAK was investigated through ICC. Nuclei were observed as blue and FAK was shown as red. Scale bars indicate 200 μm. (B) The fluorescent intensity of FAK was quantified. N.S. indicated not significant.

Therefore, it was verified that the neurally differentiated hESCs in the experimental group IV underwent focal adhesion stimuli in suspended condition, like adhesive cells did. And this physical stimulation, which was detected and then transmitted intracellularly by FAK, is considered to result from the concentrated magnetic force system, an especial cell culture condition of IV.

7.6 Conclusions

In previous chapter, the accelerated neural induction of the small-sized hEBs was investigated. So, in order to find the cause of this result, several signaling pathways, which were considered to be related, were analyzed.

First, WNT signaling pathways were investigated through Western blotting of WNT3 and WNT5α proteins in 4 experimental groups. According to the immunoblotting, the accelerated neural induction of small-sized hEBs (IV) followed WNT3 signaling pathway rather than WNT5α pathway. On the other hand, the neurally induced hESCs using conventional method (II) followed the WNT5α signaling pathway.

According to the expression of GDNF in neurally induced hESCs (group II to IV), GDNF expression was remarkably enhanced in group IV, compared with group II and III. It was evaluated that some of the neurally differentiated hESCs in IV possess affinity with dopamine, different from the group II and III.

And the NCAM expression, which was not significant between group II and III, and also between group II and IV, indicated that cell-to-cell adhesions and interactions were improved in the hESCs differentiated in 3D suspended condition (IV), in which cell adhesion to bottom was prohibited.

Regarding the MAP2 expression, there was no statistical difference among all the neurally induced groups. In group IV, cytoskeletons were generated and organized

like in group II and III, adhesive condition. Enhanced cell-to-cell communications were considered to induce those microtubule growth and genesis.

The expression of FAK was not different among the groups, either. It indicated that the neurally induced hESCs in suspended condition (IV) underwent focal adhesive stimuli like the cells in group II and III did.

As a result, the accelerated neural induction of the small-sized hEBs (IV) followed WNT3 signaling pathway and some possessed dopamine-affinity, represented as the expression of GDNF. Those results were considered to result from the enhanced cell-to-cell adhesions and interactions, which were indicated by NCAM expression, and also from the concentrated magnetic force-derived mechanical stimuli, which was verified by the expression of MAP2 and FAK.

Chapter 8.

Overall discussion and further suggestions

Chapter 8. Overall discussion and further suggestions

Human embryonic stem cells (hESCs) have been used in tissue engineering and regenerative medicine due to their ability to differentiate into various cell types [1-7]. The use of hESCs in such studies requires precise control over differentiation of the hESCs into specific types of cells [10-14]. Recently, researchers have focused on novel methods to selectively differentiate the hESCs *via* physical factors, contrary to conventional differentiation depending on chemical factors [21-23]. Accordingly, the generation of the human embryoid bodies (hEBs), three-dimensional (3D) cell aggregates of the hESCs morphologically mimicking embryos, has been suggested as an ideal method for efficient differentiation [15, 24-27]. Furthermore, the effect of the initial hEB size on early lineage specification of the hESCs has been extensively studied [109-113].

In this thesis, I hypothesized that the size of hEBs is an important mechanical cue to direct the fate of the hESCs. As embryological development proceeds, the volume and mass of the cell aggregates are enlarged with increase in the cell amount [169, 170]. From this point of view, I could imitate the specific stage of gastrulation by regulating the size of the hEBs. The initial stage of gastrulation, which forms the ectoderm, could be mimicked by generating small hEBs, whereas the latter stage of gastrulation forming the endoderm and mesoderm could be imitated by a large hEB generation.

I considered a diameter of 300 μm for the hEB as a reference point, as reported in previous works [110, 111]. The related studies indicated that hEBs smaller than

300 μm in diameter exhibit enhanced dermal or neural differentiation, while hEBs larger than 300 μm exhibited enhanced myocardial differentiation. Thus, the hESC commitment was controlled by adjusting the size of the hEBs to be smaller or larger than the standard of 300 μm. The uniformly size-controlled hEBs were efficiently generated using the magnetic nanoparticles (MNPs) and the concentrated magnetic force system, by regulating the number of cells added in a well. 1×10^4 cells were added for small hEBs with a diameter of 150 μm, and 16×10^4 cells were added per well for large hEBs with a diameter of 600 μm. In contrast with previous studies, the hEBs were induced to differentiate in hEB culture medium without any chemical inducers, which are regarded as vital for stem cell differentiation. By excluding other complex factors influencing the hESC differentiation, I could investigate the practical effect of the hEB size itself on the early hESC lineage decision.

In chapter 4, during the experimental process, the MNPs were directly applied to the hESCs for intracellular incorporation without any superficial modifications [23, 171]. The MNPs are covered with lipid layers, which contribute to endocytosis, originating from magnetic bacteria, and they showed no significant cytotoxicity to the hESCs over all concentrations (up to 50 μg/ml). However, there was a statistically proven cell death in human mesenchymal stem cells (hMSCs) with highly concentrated MNPs (higher than 30 μg/ml). The difference in the cell viability with identical MNPs was attributed to the different rate of intracellular incorporation according to the cell types. Unlike other types of stem cells, represented as hMSCs and mouse embryonic stem cells (mESCs), the hESCs showed a low MNP incorporation because the single cell size of the hESCs is much smaller

than that of the others, and the nuclei may account for a large portion of the total area of the cells, resulting in a hindrance to the MNP incorporation in cytosol. As a result, the poor efficiency of the MNP incorporation led to not only low cytotoxicity, but also improved cell proliferation, even at high concentrations of MNPs in the hESCs. Some related studies have reported that the intracellular metabolism of the iron ion would influence cell proliferation signals at limited range of MNP concentrations [172-176], and such studies can explain the extremely low cytotoxicity and increased cell number of the hESCs, even at high concentrations of the MNPs.

Highly magnetized hESCs were required for use in this concentrated magnetic force system because successful hEB generation depends on the magnetization of the cells interacting with the magnetic forces at the pinpoints. To improve the accumulation efficiency of the MNPs in cytosols, I applied a feeder-free system in the last step of the hESC cultivation. Conventionally, the hESCs were cultured with feeder cells on gelatin-coated tissue culture dishes in hESC growth medium and could keep their pluripotency [9]. However, recent studies on stem cells have shown that feeder-free cultivation methods of hESCs with various dish coating materials, such as Geltrex™, are an alternative technique without side effects on the intrinsic characteristics of the pluripotent hESCs [107]. When cultured with feeder cells, the hESC colonies were compactly constructed, and the tight cell-to-cell contact diminished the cytosolic volume of the single cells, resulting in poor accumulation of the MNPs in cytosols. On the other hand, the hESC colonies were loosely woven when cultured without feeders, and hence, the MNPs were efficiently

accumulated in hESC cytosols. Thus, the highly magnetized hESCs could be obtained by utilizing a feeder-free culture system during the MNP treatment of the hESCs.

In the spheroid generation using hMSCs and mESCs, 3D cell aggregates were generated within seconds. And the resulted spheroids were compactly organized. However, the hEB generation consumed more time due to the innate characteristics of the hESCs in terms of the vulnerability during self-organization. When the hESCs are separated into single cells, the cell-to-cell interactions diminish, and the apoptotic signals begin to accelerate, resulting in failure for the spontaneous hEB generation [177, 178]. Thus, the rho-associated protein kinase (ROCK) inhibitor can assist in enhancing the intercellular interactions and the agglomeration of single hESCs into clusters [179]. In this work, the concentrated magnetic force system facilitated the efficient hEB generation diminishing the cell death of the single hESCs without the assistance of ROCK inhibitor. Accordingly, it could be regarded as an alternative to conventional hEB generation methods relying on the ROCK-inhibitor.

In chapter 5, it was revealed that the size of the hEBs is a significant parameter to direct the hESC commitments, excluding the need for adjusting other factors as chemical inducers. Such chemical factors have been previously regarded as vital to differentiate the hESCs into specific cell types of tissues and organs. In this research, I tried to provide the natural environment of embryogenesis to the hESCs, thus the exact effect of the initial size of the hEBs on the generation of 3 germ layers

could be determined without any growth factors. And it was also suggested that the exact size obtained from a theoretical basis for each germinal layer was 150 μm for ectoderm and 600 μm for endoderm and mesoderm.

Some of the small-sized hEBs, which were spontaneously differentiated into ectodermal lineage in hEB medium, showed neurite-like outgrowth. So, **in chapter 6,** the neural induction of the hESCs in the form of hEBs, generated using the MNPs and the concentrated magnetic force system, was performed by replacing the hEB medium to neural induction medium (NIM). According to the former studies regarding neurogenesis of the hESCs [122], 3 to 4 weeks were needed to produce induced neural progenitor cells from the hESCs. Then 1 to 2 more weeks were required to generate early neuro-ectodermal cells, and 3 more months were needed to differentiate the cells to mature neuro-ectodermal cells. After 1 to 3 more weeks, the cells were finally matured to three fundamental neural cells, represented as neuronal cells, glial cells and astrocytal cells, with functions. In this process of neurogenesis from hESCs, suspension culture of the cells in the form of 3D cell aggregates, called “neurosphere”, was considered to be essential. It seems to be due to the fact that the suspending cell aggregates mimic the physical properties, represented as stiffness, of the brain tissue, which is very soft among the body tissues [123, 124]. Thus, in my study, it was reasonable to facilitate neural induction of the hESCs by generating hEBs, 3D hESC aggregates.

A marked change in the cell shape observed through the morphological analysis was related to the neurites, which are tiny projections on neuronal cells. And not

only the number of neurites per cell but also the length of neurites per cell increased in neurally induced hEBs, the experimental group IV, compared to the other groups.

I calculated the average number of neurites per cell in two different cases; calculating the average number of neurites of the total cells, including the cells without neurites; calculating the number of neurites of only the cells with neurites. The calculated values in two cases were quite different, and the gaps were variant depending the experimental groups. In group II, neurally induced hESCs with NIM, the number of neurites of total cells was 0.45, while the neurite number of cells with neurites was 1.90. The gap between two values was 1.45. Meanwhile, in group III, neurally induced hESCs with NIM and the MNPs, the number of neurites was 1.31 when total cells were calculated, whereas the neurite number was 1.54 when cells sprouting neurites were calculated. The gap between the values was 0.23. Finally, in the last group (IV), neurally induced hEBs, the average number of neurites per cell of total cells was 1.94 and number of cells with neurites was 2.50. The gap between two values was 0.56. Compared to group III and IV, the gap of II was largest due to the biggest proportion of the cells without neurites. According to Table 6.2, more than half of the cells (64.1%) did not possess any neurites in group II, while about only 10% of the cells lack of neurites in III and IV.

Concerning the length of neurites per cell, I measured every single neurite of all the cells and calculated such values below. First, the length of primary neurite was evaluated in all of the cells with neurites. The mean value of the length in group II was much shorter than in III and IV. Based on the number of neurites per cell

discussed above, it indicated that the length of primary neurites could be short when there was only a single neurite per cell, while the length of primary neurites would be longer when there were 2 or more neurites per cell. Second, the length of sum of primary and secondary neurites was estimated when there were 2 or more neurites per cell. The tendency among 3 groups was similar to the length of primary neurites. Sum of primary and secondary neurites increased from group II to IV. Third, the length of total neurites was measured in all of the cells sprouting neurites. Likewise, the length increased toward end group (IV).

Additionally, I compared the difference in the length of total neurites and the length of primary neurites among the experimental groups. The difference between the two lengths represents the length of sum of neurites except for primary neurites. That is to say, the value indicates sum of secondary, third, and shorter neurites. The subtract in group II was 37.57 μm, in III was 78.08 μm, and in IV was 92.24 μm, respectively. The value was smallest in group II. Accordingly, in addition to the length of primary neurites, the length of shorter neurites was much longer in the group III and IV compared with II. Thus, it implies that as the number of neurites per cell increases, the length of each neurite enhances, either.

In genetical analysis of the hESCs for detecting neural induction, I investigated representative neural induction marker genes such as growth associated protein 43(*GAP43*), β3-tubulin (*TUBB3*), nestin (*NES*) and glial fibrillary acidic protein (*GFAP*). However, only *TUBB3* showed different tendency in expression contrary to the other genes. All the neural induction markers except for *TUBB3* were

statistically up-regulated in the experimental group III and IV compared with I and II. Especially, in group IV, the expression of each gene was enhanced than III. But *TUBB3* expression in IV decreased compared to group II and III. Based on the fact that the role of *TUBB3* is related to microtubule formation [180-182], the 3D culture condition, in which cells were cultivated in the suspended condition, may have a negative effect on producing microtubules, as compared with the two-dimensional (2D) culture condition, in which the cells adhere to the bottom and generate cytoskeletons as well.

In chapter 7, the mechanisms of accelerated neural induction of the small-sized hEBs were investigated. First, WNT signaling pathway was analyzed in 4 experimental groups. The WNT5α and WNT3 were expressed in group II and IV, respectively. Though both WNT proteins are known to be involved in neural induction of the pluripotent stem cells (PSCs) into neural progenitor cells (NPCs) [134-139], exact function of each protein is different. According to the related studies, the activation of WNT3 results in not only induction of the PSCs into NPCs, but also differentiation of the NPCs into mature neurons [134-136], whereas the WNT5α mediates the differentiation of NPCs into both neurons and glial cells [137-139]. Therefore, the experimental group IV, in which the WNT3 protein expressed remarkably, was induced to neuronal direction following WNT3 signaling pathway, while the group II was differentiated following WNT5α signaling pathway. According to the genetical analysis of the 4 experimental groups in chapter 6.5, the expression of *GFAP* was enhanced in group IV compared with other groups. Regarding that *GFAP* indicates the glial fibrillary acidic protein, improved *GFAP*

expression in group IV would be considered as the differentiation of hESCs into glial cells. However, through the WNT3 expression in the experimental group IV, it was evaluated that the hESCs in IV were induced to neuronal direction. Thus, it could be inferred that increased *GFAP* expression in group IV would be related to intermediate filament growth, which is one of the important roles of *GFAP* gene, and the hESCs in group IV were neurally induced through WNT3 signaling pathway [183-185]. Regarding group III, both WNT3 and WNT5α did not show any expression. The signaling pathway related to III should be revealed.

Since the cell culture condition was different as 2D and 3D, depending on the experimental groups, the expression of the related proteins affected by this physical environment was investigated in neurally induced hESCs (group II to IV). The expression of neural cell adhesion molecule (NCAM), microtubule-associated protein 2 (MAP2), and focal adhesion kinase (FAK) has been considered to be suppressed in 3D suspended cell culture condition. However, according to the results, there was no statistical difference in the expression of NCAM, MAP2, and FAK between adhesive cells, cultured in 2D condition, and suspended cells, cultured in 3D condition. Consequently, it indicates that cell-to-cell adhesions and interactions were improved in the hESCs differentiated in 3D suspended condition (IV), in which cell adhesion to bottom was inhibited. Accordingly, by these enhanced intercellular communications, growth of cytoskeletons was sufficient in the suspended cells (IV) and the neurally induced hESCs of IV underwent focal adhesive stimulations, like cells in 2D (II and III) did. It is considered to result from

a particular cell culture condition of the group IV, in which magnetic driven force was applied under the concentrated magnetic force system.

According to the genetical analysis of the 4 experimental groups in chapter 6.5, the expression of *TUBB3* decreased in group IV compared with group II and III. Regarding that *TUBB3* gene expresses microtubules, down regulated *TUBB3* expression in group IV would be considered as failure of cytoskeleton formation. However, according to the MAP2 expression in the experimental group IV, it was verified that the hESCs in IV generated and organized sufficient cytoskeletons such as microtubules, like the hESCs in the group II and III did. Thus, it could be inferred that decreased *TUBB3* is one of the genes regulate the growth and genesis of microtubules, and the final complexed cytoskeletons would be produced by the interaction of various related genes [186-188]. Therefore, though *TUBB3* gene expression in group IV was suppressed compared with other groups, practical generation of cytoskeletons represented as microtubules in group IV was not significantly different when comparing with the group II and III.

In this thesis, the key issue is to identify the critical difference that directs the fate of the hESCs between small and large hEBs. The physically defined difference in the hEB size is associated with a restriction in the area of mass transfer. As the size of the hEBs increases, the region of restricted mass transfer would increase from the core, and indeed core part underwent cell death in the large hEBs, resulting in the formation of a large lumen. Because the cavitation that occurs through central apoptosis has been regarded as a significant cue for embryological process [189,

190], the difference in the scale and moment of the cavitation would induce separate mechanisms sequentially, resulting in distinct lineage specification. However, it is still unclear how the hESC clusters recognize their size and which mechanisms are engaged as a result. In the case of bacteria, they coordinate certain behaviors in response to their local cell density using innate cell-to-cell communication, called quorum sensing [191, 192]. As such, it is necessary to investigate the change in intercellular communication and subsequent signaling of the hESCs in various forms. Also, further studies are needed to elucidate the underlying biology of the hESC behavior depending on the hEB size and related factors to better understand the direction of the hESC fate.

In spontaneous differentiation of the hESCs in the form of hEBs, generated using the MNPs and the concentrated magnetic force system, the MNPs themselves did not have significant effect on directing the hESC fate. According to related studies, the MNPs did not influence on specific differentiation of PSCs [193, 194]. However, when the MNPs were applied to particular progenitor cells with differentiation condition, such as differentiation medium with growth factors, it seemed that the MNPs induce or help some differentiation. In this research, according to the comparison of neural induction through ICC and genetical analysis, the group III showed statistically enhanced neural inductivity when compared with I and II. Though the MNPs themselves do not regulate the differentiation of hESCs, the MNPs could synergically affect specific differentiation when treated with chemical inducers, as in NIM. In previous works, the behavior and change of intracellularly delivered MNPs have been discussed [84, 86, 171]. The

endocytosed MNPs would be ionized producing iron ion in intracellular organelles, in which pH is low and the environment is acidic. And this iron ion could affect particular cell commitments in various ways. The detailed mechanisms related to the synergic effect of the MNPs on neural induction should be revealed and thus the exact role and function of the MNPs on neural induction of the hESCs have to be established.

Through the analysis of several signaling pathways, I tried to find the cause of accelerated neural induction of small-sized hEBs compared with conventionally differentiated hESCs. As a result, the improved neural induction of the hEBs followed WNT3 signaling pathways and possessed dopamine affinity. Furthermore, enhanced cell-to-cell interactions resulted from magnetic force-derived mechanical stimuli affected the results. Although I compared two groups in the expression of those signaling pathway proteins, in order to clarify the related mechanisms, it is considered that numerous proteins should be investigated according to significant cascades.

To summarize, in my research during Ph.D., I have devised a technique to efficiently generate hEBs and regulate their sizes using MNPs and the concentrated magnetic force system. Through the method, I could reveal the effect of hEB size on the hESC fate. In addition, I successfully improved neural induction of the hESCs by generating small-sized hEBs, and also reduced the time required for early neural induction. Furthermore, I confirmed the related signaling pathways affecting the accelerated neural induction of the hESCs. Therefore, the MNP-based

hEB size control method proposed in this study would be useful for inducing lineage-specific differentiation of hESCs and determining the cell fate. If this technique could be used to induce the differentiation of hESCs into various cell types, application to tissue engineering and simulations of embryogenesis would be possible.

Bibliography

[1] I.G. Faragher, I.M. Chaitowitz, D.A. Stupart, Long-term results of palliative stenting or surgery for incurable obstructing colon cancer, Colorectal Dis 10(7) (2008) 668-72.

[2] T.C. McDevitt, R.L. Carpenedo, C.Y. Sargent, G.Y. Berguig, R.A. Marklein, S. Seaman, Engineering the 3D microenvironment of embryonic stem cells undergoing differentiation, Biomed Mater Eng 18(4-5) (2008) 179-81.

[3] J. Niclis, A.O. Trounson, M. Dottori, A. Ellisdon, S.P. Bottomley, Y. Verlinsky, D. Cram, Human embryonic stem cell models of Huntington disease, Reprod Biomed Online 19(1) (2009) 106-13.

[4] S.D. Schwartz, J.P. Hubschman, G. Heilwell, V. Franco-Cardenas, C.K. Pan, R.M. Ostrick, E. Mickunas, R. Gay, I. Klimanskaya, R. Lanza, Embryonic stem cell trials for macular degeneration: a preliminary report, Lancet 379(9817) (2012) 713-20.

[5] S.D. Schwartz, C.D. Regillo, B.L. Lam, D. Eliott, P.J. Rosenfeld, N.Z. Gregori, J.P. Hubschman, J.L. Davis, G. Heilwell, M. Spirn, J. Maguire, R. Gay, J. Bateman, R.M. Ostrick, D. Morris, M. Vincent, E. Anglade, L.V. Del Priore, R. Lanza, Human embryonic stem cell-derived retinal pigment epithelium in patients with age-related macular degeneration and Stargardt's macular dystrophy: follow-up of two open-label phase 1/2 studies, Lancet 385(9967) (2015) 509-16.

[6] M. Amit, M.K. Carpenter, M.S. Inokuma, C.P. Chiu, C.P. Harris, M.A. Waknitz, J. Itskovitz-Eldor, J.A. Thomson, Clonally derived human embryonic stem cell lines maintain pluripotency and proliferative potential for prolonged periods of culture, Dev Biol 227(2) (2000) 271-8.

[7] N.S. Hwang, S. Varghese, J. Elisseeff, Controlled differentiation of stem cells, Adv Drug Deliv Rev 60(2) (2008) 199-214.

[8] M. Alvarez-Dolado, R. Pardal, J.M. Garcia-Verdugo, J.R. Fike, H.O. Lee, K. Pfeffer, C.

Lois, S.J. Morrison, A. Alvarez-Buylla, Fusion of bone-marrow-derived cells with Purkinje neurons, cardiomyocytes and hepatocytes, Nature 425(6961) (2003) 968-73.

[9] J.A. Thomson, J. Itskovitz-Eldor, S.S. Shapiro, M.A. Waknitz, J.J. Swiergiel, V.S. Marshall, J.M. Jones, Embryonic stem cell lines derived from human blastocysts, Science 282(5391) (1998) 1145-7.

[10] L.A. Boyer, T.I. Lee, M.F. Cole, S.E. Johnstone, S.S. Levine, J.P. Zucker, M.G. Guenther, R.M. Kumar, H.L. Murray, R.G. Jenner, D.K. Gifford, D.A. Melton, R. Jaenisch, R.A. Young, Core transcriptional regulatory circuitry in human embryonic stem cells, Cell 122(6) (2005) 947-56.

[11] M. Kyba, R.C. Perlingeiro, G.Q. Daley, HoxB4 confers definitive lymphoid-myeloid engraftment potential on embryonic stem cell and yolk sac hematopoietic progenitors, Cell 109(1) (2002) 29-37.

[12] O. Lindvall, Z. Kokaia, A. Martinez-Serrano, Stem cell therapy for human neurodegenerative disorders-how to make it work, Nat Med 10 Suppl (2004) S42-50.

[13] O. Caspi, A. Lesman, Y. Basevitch, A. Gepstein, G. Arbel, I.H. Habib, L. Gepstein, S. Levenberg, Tissue engineering of vascularized cardiac muscle from human embryonic stem cells, Circ Res 100(2) (2007) 263-72.

[14] J.S. Lebkowski, J. Gold, C. Xu, W. Funk, C.P. Chiu, M.K. Carpenter, Human embryonic stem cells: culture, differentiation, and genetic modification for regenerative medicine applications, Cancer J 7(2) (2001) S83-93.

[15] A.M. Bratt-Leal, R.L. Carpenedo, T.C. McDevitt, Engineering the embryoid body microenvironment to direct embryonic stem cell differentiation, Biotechnol Prog 25(1) (2009) 43-51.

[16] B.E. Reubinoff, M.F. Pera, C.Y. Fong, A. Trounson, A. Bongso, Embryonic stem cell lines from human blastocysts: somatic differentiation in vitro, Nat Biotechnol 18(4) (2000)

399-404.

[17] M. Borowiak, R. Maehr, S. Chen, A.E. Chen, W. Tang, J.L. Fox, S.L. Schreiber, D.A. Melton, Small molecules efficiently direct endodermal differentiation of mouse and human embryonic stem cells, Cell Stem Cell 4(4) (2009) 348-58.

[18] T. Touboul, N.R. Hannan, S. Corbineau, A. Martinez, C. Martinet, S. Branchereau, S. Mainot, H. Strick-Marchand, R. Pedersen, J. Di Santo, A. Weber, L. Vallier, Generation of functional hepatocytes from human embryonic stem cells under chemically defined conditions that recapitulate liver development, Hepatology 51(5) (2010) 1754-65.

[19] S. Yao, S. Chen, J. Clark, E. Hao, G.M. Beattie, A. Hayek, S. Ding, Long-term self-renewal and directed differentiation of human embryonic stem cells in chemically defined conditions, Proc Natl Acad Sci U S A 103(18) (2006) 6907-12.

[20] S.C. Zhang, M. Wernig, I.D. Duncan, O. Brustle, J.A. Thomson, In vitro differentiation of transplantable neural precursors from human embryonic stem cells, Nat Biotechnol 19(12) (2001) 1129-33.

[21] F. Guilak, D.M. Cohen, B.T. Estes, J.M. Gimble, W. Liedtke, C.S. Chen, Control of stem cell fate by physical interactions with the extracellular matrix, Cell Stem Cell 5(1) (2009) 17-26.

[22] C.M. Metallo, M.A. Vodyanik, J.J. de Pablo, Slukvin, II, S.P. Palecek, The response of human embryonic stem cell-derived endothelial cells to shear stress, Biotechnol Bioeng 100(4) (2008) 830-7.

[23] B. Son, H.D. Kim, M. Kim, J.A. Kim, J. Lee, H. Shin, N.S. Hwang, T.H. Park, Physical Stimuli-Induced Chondrogenic Differentiation of Mesenchymal Stem Cells Using Magnetic Nanoparticles, Adv Healthc Mater 4(9) (2015) 1339-47.

[24] P.W. Burridge, D. Anderson, H. Priddle, M.D. Barbadillo Munoz, S. Chamberlain, C. Allegrucci, L.E. Young, C. Denning, Improved human embryonic stem cell embryoid

body homogeneity and cardiomyocyte differentiation from a novel V-96 plate aggregation system highlights interline variability, Stem Cells 25(4) (2007) 929-38.

[25] S. Gerecht-Nir, S. Cohen, J. Itskovitz-Eldor, Bioreactor cultivation enhances the efficiency of human embryoid body (hEB) formation and differentiation, Biotechnol Bioeng 86(5) (2004) 493-502.

[26] J. Itskovitz-Eldor, M. Schuldiner, D. Karsenti, A. Eden, O. Yanuka, M. Amit, H. Soreq, N. Benvenisty, Differentiation of Human Embryonic Stem Cells into Embryoid Bodies Comprising the Three Embryonic Germ Layers, J Mol Med 6(2) (2000) 88-95.

[27] N.S. Hwang, M.S. Kim, S. Sampattavanich, J.H. Baek, Z. Zhang, J. Elisseeff, Effects of three-dimensional culture and growth factors on the chondrogenic differentiation of murine embryonic stem cells, Stem Cells 24(2) (2006) 284-91.

[28] A.T. Clark, M.S. Bodnar, M. Fox, R.T. Rodriquez, M.J. Abeyta, M.T. Firpo, R.A. Pera, Spontaneous differentiation of germ cells from human embryonic stem cells in vitro, Hum Mol Genet 13(7) (2004) 727-39.

[29] K. Osafune, L. Caron, M. Borowiak, R.J. Martinez, C.S. Fitz-Gerald, Y. Sato, C.A. Cowan, K.R. Chien, D.A. Melton, Marked differences in differentiation propensity among human embryonic stem cell lines, Nat Biotechnol 26(3) (2008) 313-5.

[30] R.Z. Lin, H.Y. Chang, Recent advances in three-dimensional multicellular spheroid culture for biomedical research, Biotechnol J 3(9-10) (2008) 1172-84.

[31] R.L. Carpenedo, C.Y. Sargent, T.C. McDevitt, Rotary suspension culture enhances the efficiency, yield, and homogeneity of embryoid body differentiation, Stem Cells 25(9) (2007) 2224-34.

[32] R. Nair, A.V. Ngangan, T.C. McDevitt, Efficacy of solvent extraction methods for acellularization of embryoid bodies, J Biomater Sci Polym Ed 19(6) (2008) 801-19.

[33] A.V. Ngangan, T.C. McDevitt, Acellularization of embryoid bodies via physical

disruption methods, Biomaterials 30(6) (2009) 1143-9.

[34] A. Khademhosseini, R. Langer, J. Borenstein, J.P. Vacanti, Microscale technologies for tissue engineering and biology, Proc Natl Acad Sci U S A 103(8) (2006) 2480-7.

[35] P.E. Murray, F. Garcia-Godoy, K.M. Hargreaves, Regenerative endodontics: a review of current status and a call for action, J Endod 33(4) (2007) 377-90.

[36] T.J. Lee, S. Park, S.H. Bhang, J.K. Yoon, I. Jo, G.J. Jeong, B.H. Hong, B.S. Kim, Graphene enhances the cardiomyogenic differentiation of human embryonic stem cells, Biochem Biophys Res Commun 452(1) (2014) 174-80.

[37] J. Wu, D. Okamura, M. Li, K. Suzuki, C. Luo, L. Ma, Y. He, Z. Li, C. Benner, I. Tamura, M.N. Krause, J.R. Nery, T. Du, Z. Zhang, T. Hishida, Y. Takahashi, E. Aizawa, N.Y. Kim, J. Lajara, P. Guillen, J.M. Campistol, C.R. Esteban, P.J. Ross, A. Saghatelian, B. Ren, J.R. Ecker, J.C. Izpisua Belmonte, An alternative pluripotent state confers interspecies chimaeric competency, Nature 521(7552) (2015) 316-21.

[38] M.F. Pittenger, A.M. Mackay, S.C. Beck, R.K. Jaiswal, R. Douglas, J.D. Mosca, M.A. Moorman, D.W. Simonetti, S. Craig, D.R. Marshak, Multilineage potential of adult human mesenchymal stem cells, Science 284(5411) (1999) 143-7.

[39] S. Kern, H. Eichler, J. Stoeve, H. Kluter, K. Bieback, Comparative analysis of mesenchymal stem cells from bone marrow, umbilical cord blood, or adipose tissue, Stem Cells 24(5) (2006) 1294-301.

[40] S. Kim, B.S. Kim, Control of adult stem cell behavior with biomaterials, Tissue Eng Regen Med 11(6) (2014) 423-30.

[41] F.H. Gage, Mammalian neural stem cells, Science 287(5457) (2000) 1433-8.

[42] M.J. Bissell, W.C. Hines, Why don't we get more cancer? A proposed role of the microenvironment in restraining cancer progression, Nat Med 17(3) (2011) 320-9.

[43] M.P. Lutolf, P.M. Gilbert, H.M. Blau, Designing materials to direct stem-cell fate, Nature

462(7272) (2009) 433-41.

[44] R.A. Marklein, J.A. Burdick, Controlling stem cell fate with material design, Adv Mater 22(2) (2010) 175-89.

[45] D.A. Fletcher, R.D. Mullins, Cell mechanics and the cytoskeleton, Nature 463(7280) (2010) 485-92.

[46] J.M. Kyriakis, J. Avruch, Protein kinase cascades activated by stress and inflammatory cytokines, Bioessays 18(7) (1996) 567-77.

[47] H. Metzger, The receptor with high affinity for IgE, Immunol Rev 125 (1992) 37-48.

[48] T.J. Lee, J. Jang, S. Kang, M. Jin, H. Shin, D.W. Kim, B.S. Kim, Enhancement of osteogenic and chondrogenic differentiation of human embryonic stem cells by mesodermal lineage induction with BMP-4 and FGF2 treatment, Biochem Biophys Res Commun 430(2) (2013) 793-7.

[49] B.S. Kim, D.J. Mooney, Development of biocompatible synthetic extracellular matrices for tissue engineering, Trends Biotechnol 16(5) (1998) 224-30.

[50] B.S. Kim, C.E. Baez, A. Atala, Biomaterials for tissue engineering, World J Urol 18(1) (2000) 2-9.

[51] J.M. Kang, J.K. Yoon, S.J. Oh, B.S. Kim, S.H. Kim, Synergistic Therapeutic Effect of Three-Dimensional Stem Cell Clusters and Angiopoietin-1 on Promoting Vascular Regeneration in Ischemic Region, Tissue Eng Part A 24(7-8) (2018) 616-30.

[52] Y.S. Torisawa, B.H. Chueh, D. Huh, P. Ramamurthy, T.M. Roth, K.F. Barald, S. Takayama, Efficient formation of uniform-sized embryoid bodies using a compartmentalized microchannel device, Lab Chip 7(6) (2007) 770-6.

[53] B. Patra, Y.H. Chen, C.C. Peng, S.C. Lin, C.H. Lee, Y.C. Tung, A microfluidic device for uniform-sized cell spheroids formation, culture, harvesting and flow cytometry analysis, Biomicrofluidics 7(5) (2013) 54114.

[54] N. Kumar, A multicentre study on suicide outcomes following subthalamic stimulation for Parkinson's disease, Brain 131(10) (2009) 83-4.

[55] H. Qi, Y. Du, L. Wang, H. Kaji, H. Bae, A. Khademhosseini, Patterned differentiation of individual embryoid bodies in spatially organized 3D hybrid microgels, Adv Mater 22(46) (2010) 5276-81.

[56] Y.Y. Choi, B.G. Chung, D.H. Lee, A. Khademhosseini, J.H. Kim, S.H. Lee, Controlled-size embryoid body formation in concave microwell arrays, Biomaterials 31(15) (2010) 4296-303.

[57] J.C. Mohr, J. Zhang, S.M. Azarin, A.G. Soerens, J.J. de Pablo, J.A. Thomson, G.E. Lyons, S.P. Palecek, T.J. Kamp, The microwell control of embryoid body size in order to regulate cardiac differentiation of human embryonic stem cells, Biomaterials 31(7) (2010) 1885-93.

[58] S. Sun, H. Zeng, Size-controlled synthesis of magnetite nanoparticles, J Am Chem Soc 124(28) (2002) 8204-5.

[59] C.R. Vestal, Z.J. Zhang, Synthesis and magnetic characterization of Mn and Co spinel ferrite-silica nanoparticles with tunable magnetic core, Nano Letters 3(12) (2003) 1739-43.

[60] N.A. Frey, S. Peng, K. Cheng, S. Sun, Magnetic nanoparticles: synthesis, functionalization, and applications in bioimaging and magnetic energy storage, Chem Soc Rev 38(9) (2009) 2532-42.

[61] A.K. Gupta, R.R. Naregalkar, V.D. Vaidya, M. Gupta, Recent advances on surface engineering of magnetic iron oxide nanoparticles and their biomedical applications, Nanomedicine 2(1) (2007) 23-9.

[62] J.L. Corchero, A. Villaverde, Biomedical applications of distally controlled magnetic nanoparticles, Trends Biotechnol 27(8) (2009) 468-76.

[63] A.H. Lu, E.L. Salabas, F. Schuth, Magnetic nanoparticles: synthesis, protection, functionalization, and application, Angew Chem Int Ed Engl 46(8) (2007) 1222-44.

[64] L. Ferreira, J.M. Karp, L. Nobre, R. Langer, New opportunities: the use of nanotechnologies to manipulate and track stem cells, Cell Stem Cell 3(2) (2008) 136-46.

[65] A.W. Orr, B.P. Helmke, B.R. Blackman, M.A. Schwartz, Mechanisms of mechanotransduction, Dev Cell 10(1) (2006) 11-20.

[66] N. Wang, J.P. Butler, D.E. Ingber, Mechanotransduction across the cell surface and through the cytoskeleton, Science 260(5111) (1993) 1124-7.

[67] M. Glogauer, J. Ferrier, C.A. McCulloch, Magnetic fields applied to collagen-coated ferric oxide beads induce stretch-activated Ca2+ flux in fibroblasts, Am J Physiol 269(5) (1995) C1093-104.

[68] C.R. Vestal, Z.J. Zhang, Atom transfer radical polymerization synthesis and magnetic characterization of MnFe2O4/polystyrene core/shell nanoparticles, J Am Chem Soc 124(48) (2002) 14312-3.

[69] R.J. Mannix, S. Kumar, F. Cassiola, M. Montoya-Zavala, E. Feinstein, M. Prentiss, D.E. Ingber, Nanomagnetic actuation of receptor-mediated signal transduction, Nat Nanotechnol 3(1) (2008) 36-40.

[70] D. MacGlashan Jr, IgE receptor and signal transduction in mast cells and basophils, Curr Opin Immunol 20(6) (2008) 717-23.

[71] R. Sensenig, Y. Sapir, C. MacDonald, S. Cohen, B. Polyak, Magnetic nanoparticle-based approaches to locally target therapy and enhance tissue regeneration in vivo, Nanomedicine 7(9) (2012) 1425-42.

[72] J.M. Kanczler, H.S. Sura, J. Magnay, D. Green, R.O. Oreffo, J.P. Dobson, A.J. El Haj, Controlled differentiation of human bone marrow stromal cells using magnetic nanoparticle technology, Tissue Eng Part A 16(10) (2010) 3241-50.

[73] B. Hu, A.J. El Haj, J. Dobson, Receptor-targeted, magneto-mechanical stimulation of osteogenic differentiation of human bone marrow-derived mesenchymal stem cells, Int J Mol Sci 14(9) (2013) 19276-93.

[74] B. Hu, J. Dobson, A.J. El Haj, Control of smooth muscle alpha-actin (SMA) up-regulation in HBMSCs using remote magnetic particle mechano-activation, Nanomedicine 10(1) (2014) 45-55.

[75] D.E. Jaalouk, J. Lammerding, Mechanotransduction gone awry, Nat Rev Mol Cell Biol 10(1) (2009) 63-73.

[76] V. Vogel, M. Sheetz, Local force and geometry sensing regulate cell functions, Nat Rev Mol Cell Biol 7(4) (2006) 265-75.

[77] V. Vogel, Mechanotransduction involving multimodular proteins: converting force into biochemical signals, Annu Rev Biophys Biomol Struct 35 (2006) 459-88.

[78] B. Geiger, A. Bershadsky, R. Pankov, K.M. Yamada, Transmembrane crosstalk between the extracellular matrix and the cytoskeleton, Nat Rev Mol Cell Bio 2(11) (2001) 793-805.

[79] N. Wang, J.D. Tytell, D.E. Ingber, Mechanotransduction at a distance: mechanically coupling the extracellular matrix with the nucleus, Nat Rev Mol Cell Bio 10(1) (2009) 75-82.

[80] D.E. Ingber, Cellular tensegrity: defining new rules of biological design that govern the cytoskeleton, J Cell Sci 104(3) (1993) 613-27.

[81] N.J. Sniadecki, R.A. Desai, S.A. Ruiz, C.S. Chen, Nanotechnology for cell-substrate interactions, Ann Biomed Eng 34(1) (2006) 59-74.

[82] S. Hughes, A.J. El Haj, J. Dobson, Magnetic micro- and nanoparticle mediated activation of mechanosensitive ion channels, Med Eng Phys 27(9) (2005) 754-62.

[83] A.R. Bausch, F. Ziemann, A.A. Boulbitch, K. Jacobson, E. Sackmann, Local

measurements of viscoelastic parameters of adherent cell surfaces by magnetic bead microrheometry, Biophys J 75(4) (1998) 2038-49.

[84] J.A. Kim, J.H. Choi, M. Kim, W.J. Rhee, B. Son, H.K. Jung, T.H. Park, High-throughput generation of spheroids using magnetic nanoparticles for three-dimensional cell culture, Biomaterials 34(34) (2013) 8555-63.

[85] C.C. Berry, A.S.G. Curtis, Functionalisation of magnetic nanoparticles for applications in biomedicine, J Phys D 36(13) (2003) R198.

[86] J.A. Kim, H.J. Lee, H.J. Kang, T.H. Park, The targeting of endothelial progenitor cells to a specific location within a microfluidic channel using magnetic nanoparticles, Biomed Microdevices 11(1) (2009) 287-96.

[87] A. Bongso, M. Richards, History and perspective of stem cell research, Best Pract Res Clin Obstet Gynaecol 18(6) (2004) 827-42.

[88] L.A. Boyer, K. Plath, J. Zeitlinger, T. Brambrink, L.A. Medeiros, T.I. Lee, S.S. Levine, M. Wernig, A. Tajonar, M.K. Ray, G.W. Bell, A.P. Otte, M. Vidal, D.K. Gifford, R.A. Young, R. Jaenisch, Polycomb complexes repress developmental regulators in murine embryonic stem cells, Nature 441(7091) (2006) 349-53.

[89] T. Reya, H. Clevers, Wnt signalling in stem cells and cancer, Nature 434(7035) (2005) 843-50.

[90] P.W. Zandstra, D.A. Lauffenburger, C.J. Eaves, A ligand-receptor signaling threshold model of stem cell differentiation control: a biologically conserved mechanism applicable to hematopoiesis, Blood 96(4) (2000) 1215-22.

[91] M.M. Wilke, D.V. Nydam, A.J. Nixon, Enhanced early chondrogenesis in articular defects following arthroscopic mesenchymal stem cell implantation in an equine model, J Orthop Res 25(7) (2007) 913-25.

[92] C. Stamm, B. Westphal, H.D. Kleine, M. Petzsch, C. Kittner, H. Klinge, C. Schumichen,

C.A. Nienaber, M. Freund, G. Steinhoff, Autologous bone-marrow stem-cell transplantation for myocardial regeneration, Lancet 361(9351) (2003) 45-6.

[93] K. Cheng, K. Malliaras, T.S. Li, B. Sun, C. Houde, G. Galang, J. Smith, N. Matsushita, E. Marban, Magnetic enhancement of cell retention, engraftment, and functional benefit after intracoronary delivery of cardiac-derived stem cells in a rat model of ischemia/reperfusion, Cell Transplant 21(6) (2012) 1121-35.

[94] M. Song, H. Jang, J. Lee, J.H. Kim, S.H. Kim, K. Sun, Y. Park, Regeneration of chronic myocardial infarction by injectable hydrogels containing stem cell homing factor SDF-1 and angiogenic peptide Ac-SDKP, Biomaterials 35(8) (2014) 2436-45.

[95] B.J. Kang, H. Kim, S.K. Lee, J. Kim, Y. Shen, S. Jung, K.S. Kang, S.G. Im, S.Y. Lee, M. Choi, N.S. Hwang, J.Y. Cho, Umbilical-cord-blood-derived mesenchymal stem cells seeded onto fibronectin-immobilized polycaprolactone nanofiber improve cardiac function, Acta Biomater 10(7) (2014) 3007-17.

[96] Z. Huang, Y. Shen, A. Sun, G. Huang, H. Zhu, B. Huang, J. Xu, Y. Song, N. Pei, J. Ma, X. Yang, Y. Zou, J. Qian, J. Ge, Magnetic targeting enhances retrograde cell retention in a rat model of myocardial infarction, Stem Cell Res Ther 4(6) (2013) 149.

[97] A. Chaudeurge, C. Wilhelm, A. Chen-Tournoux, P. Farahmand, V. Bellamy, G. Autret, C. Ménager, A. Hagège, J. Larghéro, F. Gazeau, Can magnetic targeting of magnetically labeled circulating cells optimize intramyocardial cell retention?, Cell Transplant 21(4) (2012) 679-91.

[98] J.R. Henstock, M. Rotherham, H. Rashidi, K.M. Shakesheff, A.J. El Haj, Remotely Activated Mechanotransduction via Magnetic Nanoparticles Promotes Mineralization Synergistically With Bone Morphogenetic Protein 2: Applications for Injectable Cell Therapy, Stem Cells Transl Med 3(11) (2014) 1363-74.

[99] Y. Sapir, S. Cohen, G. Friedman, B. Polyak, The promotion of in vitro vessel-like

organization of endothelial cells in magnetically responsive alginate scaffolds, Biomaterials 33(16) (2012) 4100-9.

[100] Y. Sapir, B. Polyak, S. Cohen, Cardiac tissue engineering in magnetically actuated scaffolds, Nanotechnology 25(1) (2014) 14009.

[101] S.W. Lane, D.A. Williams, F.M. Watt, Modulating the stem cell niche for tissue regeneration, Nat Biotechnol 32(8) (2014) 795-803.

[102] B.S. Ding, D.J. Nolan, J.M. Butler, D. James, A.O. Babazadeh, Z. Rosenwaks, V. Mittal, H. Kobayashi, K. Shido, D. Lyden, T.N. Sato, S.Y. Rabbany, S. Rafii, Inductive angiocrine signals from sinusoidal endothelium are required for liver regeneration, Nature 468(7321) (2010) 310-5.

[103] B.S. Ding, D.J. Nolan, P. Guo, A.O. Babazadeh, Z. Cao, Z. Rosenwaks, R.G. Crystal, M. Simons, T.N. Sato, S. Worgall, K. Shido, S.Y. Rabbany, S. Rafii, Endothelial-derived angiocrine signals induce and sustain regenerative lung alveolarization, Cell 147(3) (2011) 539-53.

[104] J.H. Lee, E.S. Kim, M.H. Cho, M. Son, S.I. Yeon, J.S. Shin, J. Cheon, Artificial control of cell signaling and growth by magnetic nanoparticles, Angew Chem Int Ed Engl 49(33) (2010) 5698-702.

[105] J. Chen, B. Fabry, E.L. Schiffrin, N. Wang, Twisting integrin receptors increases endothelin-1 gene expression in endothelial cells, Am J Physiol Cell Physiol 280(6) (2001) C1475-84.

[106] H. Geiger, G. de Haan, M.C. Florian, The ageing haematopoietic stem cell compartment, Nat Rev Immunol 13(5) (2013) 376-89.

[107] C. Xu, M.S. Inokuma, J. Denham, K. Golds, P. Kundu, J.D. Gold, M.K. Carpenter, Feeder-free growth of undifferentiated human embryonic stem cells, Nat Biotechnol 19(10) (2001) 971-4.

[108] S. Seong, T.H. Park, Swimming characteristics of magnetic bacterium, Magnetospirillum sp. AMB-1, and implications as toxicity measurement, Biotechnol Bioeng 76(1) (2001) 11-6.

[109] C.L. Bauwens, R. Peerani, S. Niebruegge, K.A. Woodhouse, E. Kumacheva, M. Husain, P.W. Zandstra, Control of human embryonic stem cell colony and aggregate size heterogeneity influences differentiation trajectories, Stem Cells 26(9) (2008) 2300-10.

[110] Y.S. Hwang, B.G. Chung, D. Ortmann, N. Hattori, H.C. Moeller, A. Khademhosseini, Microwell-mediated control of embryoid body size regulates embryonic stem cell fate via differential expression of WNT5a and WNT11, Proc Natl Acad Sci U S A 106(40) (2009) 16978-83.

[111] J. Park, C.H. Cho, N. Parashurama, Y. Li, F. Berthiaume, M. Toner, A.W. Tilles, M.L. Yarmush, Microfabrication-based modulation of embryonic stem cell differentiation, Lab Chip 7(8) (2007) 1018-28.

[112] J.M. Messana, N.S. Hwang, J. Coburn, J.H. Elisseeff, Z. Zhang, Size of the embryoid body influences chondrogenesis of mouse embryonic stem cells, J Tissue Eng Regen Med 2(8) (2008) 499-506.

[113] M.A. Kinney, R. Saeed, T.C. McDevitt, Systematic analysis of embryonic stem cell differentiation in hydrodynamic environments with controlled embryoid body size, Integr Biol 4(6) (2012) 641-50.

[114] N.I.o. Health, Stem cells: scientific progress and future research directions, University Press of the Pacific2004.

[115] B.A. Reynolds, S. Weiss, Generation of neurons and astrocytes from isolated cells of the adult mammalian central nervous system, Science 255(5052) (1992) 1707-10.

[116] D. Lindholm, R. Heumann, M. Meyer, H. Thoenen, Interleukin-l regulates synthesis of nerve growth factor in non-neuronal cells of rat sciatic nerve, Nature (1987) 658-9.

[117] S. Temple, The development of neural stem cells, Nature 414(6859) (2001) 112-7.

[118] R.S. Nowakowski, Stable neuron numbers from cradle to grave, Proc Natl Acad Sci U S A 103(33) (2006) 12219-20.

[119] K. Herrup, Y. Yang, Cell cycle regulation in the postmitotic neuron: oxymoron or new biology?, Nat Rev Neurosci 8(5) (2007) 368-78.

[120] K.R. Jessen, R. Mirsky, Glial cells in the enteric nervous system contain glial fibrillary acidic protein, Nature 286(5774) (1980) 736-7.

[121] A.V. Gourine, V. Kasymov, N. Marina, F. Tang, M.F. Figueiredo, S. Lane, A.G. Teschemacher, K.M. Spyer, K. Deisseroth, S. Kasparov, Astrocytes control breathing through pH-dependent release of ATP, Science 329(5991) (2010) 571-5.

[122] B.E. Reubinoff, P. Itsykson, T. Turetsky, M.F. Pera, E. Reinhartz, A. Itzik, T. Ben-Hur, Neural progenitors from human embryonic stem cells, Nat Biotechnol 19(12) (2001) 1134-40.

[123] S. Sartori, V. Chiono, C. Tonda-Turo, C. Mattu, C. Gianluca, Biomimetic polyurethanes in nano and regenerative medicine, J Mater Chem B 2(32) (2014) 5128-44.

[124] S. Galarza, N.P. Birch, L.E. Jansen, K. Bittner, J.D. Schiffman, A.J. Crosby, S.R. Peyton, A 3D biomaterial system to study breast to brain metastasis, Front Bioeng Biotechnol (2016).

[125] D.L. Turner, H. Weintraub, Expression of achaete-scute homolog 3 in Xenopus embryos converts ectodermal cells to a neural fate, Genes Dev 8(12) (1994) 1434-47.

[126] D. Acampora, S. Mazan, Y. Lallemand, V. Avantaggiato, M. Maury, A. Simeone, P. Brûlet, Forebrain and midbrain regions are deleted in Otx2−/− mutants due to a defective anterior neuroectoderm specification during gastrulation, Development 121(10) (1995) 3279-90.

[127] P. Clark, S. Britland, P. Connolly, Growth cone guidance and neuron morphology on

micropatterned laminin surfaces, J Cell Sci 105 (Pt 1) (1993) 203-12.

[128] M. Koto, M.A. Tanouye, A. Ferrus, J.B. Thomas, R. Wyman, The morphology of the cervical giant fiber neuron of Drosophila, Brain Res 221(2) (1981) 213-7.

[129] D. MacLeod, J. Dowman, R. Hammond, T. Leete, K. Inoue, A. Abeliovich, The familial Parkinsonism gene LRRK2 regulates neurite process morphology, Neuron 52(4) (2006) 587-93.

[130] L.A. Flanagan, Y.E. Ju, B. Marg, M. Osterfield, P.A. Janmey, Neurite branching on deformable substrates, Neuroreport 13(18) (2002) 2411-5.

[131] T.P. Yamaguchi, Heads or tails: Wnts and anterior-posterior patterning, Curr Biol 11(17) (2001) R713-24.

[132] T. Sadahiro, M. Isomi, N. Muraoka, H. Kojima, S. Haginiwa, S. Kurotsu, F. Tamura, H. Tani, S. Tohyama, J. Fujita, H. Miyoshi, Y. Kawamura, N. Goshima, Y.W. Iwasaki, K. Murano, K. Saito, M. Oda, P. Andersen, C. Kwon, H. Uosaki, H. Nishizono, K. Fukuda, M. Ieda, Tbx6 Induces Nascent Mesoderm from Pluripotent Stem Cells and Temporally Controls Cardiac versus Somite Lineage Diversification, Cell Stem Cell 23(3) (2018) 382-95.

[133] C.T. Lee, R.M. Bendriem, A.A. Kindberg, L.T. Worden, M.P. Williams, T. Drgon, B.S. Mallon, B.K. Harvey, C.T. Richie, R.S. Hamilton, J. Chen, S.L. Errico, S.Y. Tsai, G.R. Uhl, W.J. Freed, Functional consequences of 17q21.31/WNT3-WNT9B amplification in hPSCs with respect to neural differentiation, Cell Rep 10(4) (2015) 616-32.

[134] O. Krylova, J. Herreros, K.E. Cleverley, E. Ehler, J.P. Henriquez, S.M. Hughes, P.C. Salinas, WNT-3, expressed by motoneurons, regulates terminal arborization of neurotrophin-3-responsive spinal sensory neurons, Neuron 35(6) (2002) 1043-56.

[135] D.C. Lie, S.A. Colamarino, H.J. Song, L. Desire, H. Mira, A. Consiglio, E.S. Lein, S. Jessberger, H. Lansford, A.R. Dearie, F.H. Gage, Wnt signalling regulates adult

hippocampal neurogenesis, Nature 437(7063) (2005) 1370-5.

[136] L. Ciani, P.C. Salinas, WNTs in the vertebrate nervous system: from patterning to neuronal connectivity, Nat Rev Neurosci 6(5) (2005) 351-62.

[137] Y.K. Ryu, S.E. Collins, H.Y. Ho, H. Zhao, R. Kuruvilla, An autocrine Wnt5a-Ror signaling loop mediates sympathetic target innervation, Dev Biol 377(1) (2013) 79-89.

[138] X. Li, Y. Guan, Y. Chen, C. Zhang, C. Shi, F. Zhou, L. Yu, J. Juan, X. Wang, Expression of Wnt5a and its receptor Fzd2 is changed in the spinal cord of adult amyotrophic lateral sclerosis transgenic mice, Int J Clin Exp Pathol 6(7) (2013) 1245.

[139] G. Castelo-Branco, K.M. Sousa, V. Bryja, L. Pinto, J. Wagner, E. Arenas, Ventral midbrain glia express region-specific transcription factors and regulate dopaminergic neurogenesis through Wnt-5a secretion, Mol Cell Neurosci 31(2) (2006) 251-62.

[140] L.F. Lin, D.H. Doherty, J.D. Lile, S. Bektesh, F. Collins, GDNF: a glial cell line-derived neurotrophic factor for midbrain dopaminergic neurons, Science 260(5111) (1993) 1130-2.

[141] S. Carnicella, V. Kharazia, J. Jeanblanc, P.H. Janak, D. Ron, GDNF is a fast-acting potent inhibitor of alcohol consumption and relapse, Proc Natl Acad Sci U S A 105(23) (2008) 8114-8119.

[142] S.M. Klein, S. Behrstock, J. McHugh, K. Hoffmann, K. Wallace, M. Suzuki, P. Aebischer, C.N. Svendsen, GDNF delivery using human neural progenitor cells in a rat model of ALS, Hum Gene Ther 16(4) (2005) 509-21.

[143] M. Suzuki, J. McHugh, C. Tork, B. Shelley, S.M. Klein, P. Aebischer, C.N. Svendsen, GDNF secreting human neural progenitor cells protect dying motor neurons, but not their projection to muscle, in a rat model of familial ALS, PLoS One 2(8) (2007) e689.

[144] A. Pascual, M. Hidalgo-Figueroa, J.I. Piruat, C.O. Pintado, R. Gomez-Diaz, J. Lopez-Barneo, Absolute requirement of GDNF for adult catecholaminergic neuron survival, Nat

Neurosci 11(7) (2008) 755-61.

[145] H.L. Hellmich, L. Kos, E.S. Cho, K.A. Mahon, A. Zimmer, Embryonic expression of glial cell-line derived neurotrophic factor (GDNF) suggests multiple developmental roles in neural differentiation and epithelial-mesenchymal interactions, Mech Dev 54(1) (1996) 95-105.

[146] H.M. Young, C.J. Hearn, P.G. Farlie, A.J. Canty, P.Q. Thomas, D.F. Newgreen, GDNF is a chemoattractant for enteric neural cells, Dev Biol 229(2) (2001) 503-16.

[147] R.O. Heuckeroth, P.A. Lampe, E.M. Johnson, J. Milbrandt, Neurturin and GDNF promote proliferation and survival of enteric neuron and glial progenitors in vitro, Dev Biol 200(1) (1998) 116-29.

[148] R.H. Baloh, H. Enomoto, E.M. Johnson, Jr., J. Milbrandt, The GDNF family ligands and receptors - implications for neural development, Curr Opin Neurobiol 10(1) (2000) 103-10.

[149] H.H. Van Acker, A. Capsomidis, E.L. Smits, V.F. Van Tendeloo, CD56 in the Immune System: More Than a Marker for Cytotoxicity?, Front Immunol 8 (2017) 892.

[150] A.A. Reyes, S.J. Small, R. Akeson, At least 27 alternatively spliced forms of the neural cell adhesion molecule mRNA are expressed during rat heart development, Mol Cell Biol 11(3) (1991) 1654-61.

[151] T. Seki, Y. Arai, Distribution and possible roles of the highly polysialylated neural cell adhesion molecule (NCAM-H) in the developing and adult central nervous system, Neurosci Res 17(4) (1993) 265-90.

[152] G. Paratcha, F. Ledda, C.F. Ibáñez, The Neural Cell Adhesion Molecule NCAM Is an Alternative Signaling Receptor for GDNF Family Ligands, Cell 113(7) (2003) 867-79.

[153] A. Lüthi, J.P. Laurent, A. Figurovt, D. Mullert, M. Schachnert, Hippocampal long-term potentiation and neural cell adhesion molecules L1 and NCAM, Nature 372(6508) (1994)

777-9.

[154] D. Simmons, M.W. Makgoba, B. Seed, ICAM, an adhesion ligand of LFA-1, is homologous to the neural cell adhesion molecule NCAM, Nature 331(6157) (1988) 624-7.

[155] T. Seki, Y. Arai, Highly polysialylated neural cell adhesion molecule (NCAM-H) is expressed by newly generated granule cells in the dentate gyrus of the adult rat, J Neurosci 13(6) (1993) 2351-8.

[156] U. Rutishauser, A. Acheson, A.K. Hall, D.M. Mann, J. Sunshine, The neural cell adhesion molecule (NCAM) as a regulator of cell-cell interactions, Science 240(4848) (1988) 53-7.

[157] D. Branton, C.M. Cohen, J. Tyler, Interaction of cytoskeletal proteins on the human erythrocyte membrane, Cell 24(1) (1981) 24-32.

[158] Y.J. Wu, L.M. Parker, N.E. Binder, M.A. Beckett, J.H. Sinard, C.T. Griffiths, J.G. Rheinwald, The mesothelial keratins: a new family of cytoskeletal proteins identified in cultured mesothelial cells and nonkeratinizing epithelia, Cell 31(3) (1982) 693-703.

[159] N. Kalcheva, J. Albala, K. O'Guin, H. Rubino, C. Garner, B. Shafit-Zagardo, Genomic structure of human microtubule-associated protein 2 (MAP-2) and characterization of additional MAP-2 isoforms, Proc Natl Acad Sci U S A 92(24) (1995) 10894-8.

[160] R.L. Neve, P. Harris, K.S. Kosik, D.M. Kurnit, T.A. Donlon, Identification of cDNA clones for the human microtubule-associated protein tau and chromosomal localization of the genes for tau and microtubule-associated protein 2, Brain Res 387(3) (1986) 271-80.

[161] T.L. Yaksh, X.Y. Hua, I. Kalcheva, N. Nozaki-Taguchi, M. Marsala, The spinal biology in humans and animals of pain states generated by persistent small afferent input, Proc Natl Acad Sci U S A 96(14) (1999) 7680-6.

[162] C. Conde, A. Caceres, Microtubule assembly, organization and dynamics in axons and dendrites, Nat Rev Neurosci 10(5) (2009) 319-32.

[163] M.V. Sataric, D.L. Sekulic, B.M. Sataric, S. Zdravkovic, Role of nonlinear localized Ca(2+) pulses along microtubules in tuning the mechano-sensitivity of hair cells, Prog Biophys Mol Biol 119(2) (2015) 162-74.

[164] X.J.P.C. Georges, B. Li, Y. Du, M.K. Kutzing, M.L. Previtera, N.A. Langrana, B.L. Firestein, Cell growth in response to mechanical stiffness is affected by neuron-astroglia interactions, Neurosci J 8(1) (2007) 7-14.

[165] K.T. Chan, C.L. Cortesio, A. Huttenlocher, FAK alters invadopodia and focal adhesion composition and dynamics to regulate breast cancer invasion, J Cell Biol 185(2) (2009) 357-70.

[166] E. Andre, M. Becker-Andre, Expression of an N-terminally truncated form of human focal adhesion kinase in brain, Biochem Biophys Res Commun 190(1) (1993) 140-7.

[167] S.K. Mitra, D.A. Hanson, D.D. Schlaepfer, Focal adhesion kinase: in command and control of cell motility, Nat Rev Mol Cell Biol 6(1) (2005) 56-68.

[168] B. Geiger, A. Bershadsky, Exploring the neighborhood: adhesion-coupled cell mechanosensors, Cell 110(2) (2002) 139-42.

[169] J. Cooke, Xenopus mesoderm induction: evidence for early size control and partial autonomy for pattern development by onset of gastrulation, Development 106(3) (1989) 519-29.

[170] M.A. Power, P.P. Tam, Onset of gastrulation, morphogenesis and somitogenesis in mouse embryos displaying compensatory growth, Anat Embryol 187(5) (1993) 493-504.

[171] B. Son, J.A. Kim, S. Cho, G.-J. Jeong, B.S. Kim, N.S. Hwang, T.H.J.A.B.S. Park, Engineering, Lineage specific differentiation of magnetic nanoparticle-based size controlled human embryoid body, 3(8) (2017) 1719-1729.

[172] N.T. Le, D.R. Richardson, The role of iron in cell cycle progression and the proliferation of neoplastic cells, Biochim Biophys Acta 1603(1) (2002) 31-46.

[173] M. Cazzola, G. Bergamaschi, L. Dezza, P. Arosio, Manipulations of cellular iron metabolism for modulating normal and malignant cell proliferation: achievements and prospects, Blood 75(10) (1990) 1903-19.

[174] J. Laskey, L. Webb, H.M. Schulman, P. Ponka, Evidence that transferrin supports cell proliferation by supplying iron for DNA synthesis, Exp Cell Res 176(1) (1988) 87-95.

[175] D.M. Huang, J.K. Hsiao, Y.C. Chen, L.Y. Chien, M. Yao, Y.K. Chen, B.S. Ko, S.C. Hsu, L.A. Tai, H.Y. Cheng, S.W. Wang, C.S. Yang, Y.C. Chen, The promotion of human mesenchymal stem cell proliferation by superparamagnetic iron oxide nanoparticles, Biomaterials 30(22) (2009) 3645-51.

[176] P.P. Mueller, T. May, A. Perz, H. Hauser, M. Peuster, Control of smooth muscle cell proliferation by ferrous iron, Biomaterials 27(10) (2006) 2193-200.

[177] X. Li, R. Krawetz, S. Liu, G. Meng, D.E. Rancourt, ROCK inhibitor improves survival of cryopreserved serum/feeder-free single human embryonic stem cells, Hum Reprod 24(3) (2009) 580-9.

[178] K. Watanabe, M. Ueno, D. Kamiya, A. Nishiyama, M. Matsumura, T. Wataya, J.B. Takahashi, S. Nishikawa, S. Nishikawa, K. Muguruma, Y. Sasai, A ROCK inhibitor permits survival of dissociated human embryonic stem cells, Nat Biotechnol 25(6) (2007) 681-6.

[179] N. Okumura, M. Ueno, N. Koizumi, Y. Sakamoto, K. Hirata, J. Hamuro, S. Kinoshita, Enhancement on primate corneal endothelial cell survival in vitro by a ROCK inhibitor, Invest Ophthalmol Vis Sci 50(8) (2009) 3680-7.

[180] M.A. Tischfield, H.N. Baris, C. Wu, G. Rudolph, L. Van Maldergem, W. He, W.M. Chan, C. Andrews, J.L. Demer, R.L. Robertson, D.A. Mackey, J.B. Ruddle, T.D. Bird, I.

Gottlob, C. Pieh, E.I. Traboulsi, S.L. Pomeroy, D.G. Hunter, J.S. Soul, A. Newlin, L.J. Sabol, E.J. Doherty, C.E. de Uzcategui, N. de Uzcategui, M.L. Collins, E.C. Sener, B. Wabbels, H. Hellebrand, T. Meitinger, T. de Berardinis, A. Magli, C. Schiavi, M. Pastore-Trossello, F. Koc, A.M. Wong, A.V. Levin, M.T. Geraghty, M. Descartes, M. Flaherty, R.V. Jamieson, H.U. Moller, I. Meuthen, D.F. Callen, J. Kerwin, S. Lindsay, A. Meindl, M.L. Gupta, Jr., D. Pellman, E.C. Engle, Human TUBB3 mutations perturb microtubule dynamics, kinesin interactions, and axon guidance, Cell 140(1) (2010) 74-87.

[181] S. Ranganathan, D.W. Dexter, C.A. Benetatos, G.R. Hudes, Cloning and sequencing of human βIII-tubulin cDNA: induction of βIII isotype in human prostate carcinoma cells by acute exposure to antimicrotubule agents1, Biochim Biophys Acta 1395(2) (1998) 237-45.

[182] K. Poirier, Y. Saillour, N. Bahi-Buisson, X.H. Jaglin, C. Fallet-Bianco, R. Nabbout, L. Castelnau-Ptakhine, A. Roubertie, T. Attie-Bitach, I. Desguerre, D. Genevieve, C. Barnerias, B. Keren, N. Lebrun, N. Boddaert, F. Encha-Razavi, J. Chelly, Mutations in the neuronal ss-tubulin subunit TUBB3 result in malformation of cortical development and neuronal migration defects, Hum Mol Genet 19(22) (2010) 4462-73.

[183] J. Dahlstrand, V.P. Collins, U.J.C.r. Lendahl, Expression of the class VI intermediate filament nestin in human central nervous system tumors, 52(19) (1992) 5334-5341.

[184] R. Jing, U. Wilhelmsson, W. Goodwill, L. Li, Y. Pan, M. Pekny, O.J.J.o.c.s. Skalli, Synemin is expressed in reactive astrocytes in neurotrauma and interacts differentially with vimentin and GFAP intermediate filament networks, 120(7) (2007) 1267-1277.

[185] M. McCall, R. Gregg, R. Behringer, M. Brenner, C. Delaney, E. Galbreath, C. Zhang, R. Pearce, S. Chiu, A.J.P.o.t.N.A.o.S. Messing, Targeted deletion in astrocyte intermediate filament (Gfap) alters neuronal physiology, 93(13) (1996) 6361-6366.

[186] M. Goedert, M. Spillantini, M. Potier, J. Ulrich, R.J.T.E.j. Crowther, Cloning and

sequencing of the cDNA encoding an isoform of microtubule-associated protein tau containing four tandem repeats: differential expression of tau protein mRNAs in human brain, 8(2) (1989) 393-399.

[187] Y. Kanai, R. Takemura, T. Oshima, H. Mori, Y. Ihara, M. Yanagisawa, T. Masaki, N.J.T.J.o.c.b. Hirokawa, Expression of multiple tau isoforms and microtubule bundle formation in fibroblasts transfected with a single tau cDNA, 109(3) (1989) 1173-1184.

[188] B. Riederer, A.J.P.o.t.N.A.o.S. Matus, Differential expression of distinct microtubule-associated proteins during brain development, 82(17) (1985) 6006-6009.

[189] S.M. Dang, M. Kyba, R. Perlingeiro, G.Q. Daley, P.W. Zandstra, Efficiency of embryoid body formation and hematopoietic development from embryonic stem cells in different culture systems, Biotechnol Bioeng 78(4) (2002) 442-53.

[190] X. Li, Y. Chen, S. Scheele, E. Arman, R. Haffner-Krausz, P. Ekblom, P. Lonai, Fibroblast growth factor signaling and basement membrane assembly are connected during epithelial morphogenesis of the embryoid body, J Cell Biol 153(4) (2001) 811-22.

[191] M.B. Miller, B.L. Bassler, Quorum sensing in bacteria, Annu Rev Microbiol 55(1) (2001) 165-99.

[192] C.M. Waters, B.L. Bassler, Quorum sensing: cell-to-cell communication in bacteria, Annu Rev Cell Dev Biol 21 (2005) 319-46.

[193] J. Bulte, S.-C. Zhang, P. Van Gelderen, V. Herynek, E. Jordan, I. Duncan, J.J.P.o.t.N.A.o.S. Frank, Neurotransplantation of magnetically labeled oligodendrocyte progenitors: magnetic resonance tracking of cell migration and myelination, 96(26) (1999) 15256-15261.

[194] C. Wilhelm, L. Bal, P. Smirnov, I. Galy-Fauroux, O. Clement, F. Gazeau, J.J.B. Emmerich, Magnetic control of vascular network formation with magnetically labeled endothelial progenitor cells, 28(26) (2007) 3797-3806.

국 문 초 록

자성나노입자를 이용한 인간배아체의 크기 조절 구현 및 이를 통한 인간배아줄기세포의 분화 조절

손 보 람
서울대학교 대학원
화학생물공학부

인간배아줄기세포(human embryonic stem cells, hESCs)는 자가재생력(self-renewal) 및 분화능(differentiation)이라고 하는 고유한 특성을 가지는 세포로서, 이와 같은 성질로 인해 조직공학(tissue engineering)과 재생의학(regenerative medicine) 분야에서 유망한 재료로 널리 사용되어왔다. 아울러, 인간배아줄기세포를 3차원의 형태인 인간배아체(human embryoid

bodies, hEBs)로 구현하여 분화를 유도하는 것은 실제로 체내에서 일어나는 배아의 발생 과정(embryogenesis)과 상당부분 유사점을 가지고 있다. 이 때문에, 인간배아체는 인간의 배아 발생 과정에 대한 이해 및 통찰을 돕는 데 적합한 도구로서 이용되고 있다.

본 연구에서는 먼저, 세포 투과성(cell-penetrating) 자성나노입자(magnetic nanoparticles, MNPs)를 이용하여 인간배아체를 정해진 크기로 제작하였다. 그리고 이렇게 구현된 인간배아체의 분화 양상을 분석하였다. 그 과정에서 충분한 양의 자성나노입자를 인간배아줄기세포 안쪽으로 도입하기 위해, 피더(feeder)라고 하는 도움 세포와 함께 배양되던 인간배아줄기세포를 피더가 없는 환경에서 배양하도록 개선하였다. 그리고 자성나노입자의 도입에 의해 자화 된(magnetized) 인간배아줄기세포를 부유시켜, 자성 핀(pin) 기반의 집중된 자기력 시스템(concentrated magnetic force system)에 넣어 줌으로써 효과적으로 인간배아체로 뭉치도록 유도하였다. 이 때, 집중된 자기력 시스템의 한 개의 웰(well)에 넣어주는 세포의 개수를 조절함으로써 제작하는 인간배아체의 크기를 조절할 수 있었다. 인간배아체를 부유하는 상태로 3일간 배양한 결과, 크기가 작은 인간배아체(지름 150 μm)에서는 외배엽성 분화(ectodermal differentiation)가 증진되고, 크기가 큰 인간배아체(지름 600 μm)에서는 내배엽 및 중배엽성 분화(endodermal and mesodermal differentiation)가 증진된 것을 확인하였다.

크기가 조절된 인간배아체가 자발적으로 분화되도록 유도하는 과정에

서, 작은 크기의 인간배아체 중 신경교섬유질산성단백질(glial fibrillary acidic protein, GFAP) 염색에서 양성을 띄었던 일부 세포가 신경 돌기(neurites)를 뻗어내는 것과 같은 양상을 보였다. 실제로 많은 연구자들이 인간배아체를 가지고 신경 분화를 시키고자 연구해오고 있는데, 그 이유는 인간배아체의 탄성(elasticity)이 뇌의 조직 탄성과 비슷하고, 나아가 인간배아체에서 증진되는 세포 간 상호작용력이 실제 신경세포의 그것과 유사하기 때문이다. 이 연구에서는 앞서 제작한 작은 크기의 인간배아체를 보다 증진된 방향으로 신경 분화 시키기 위해서 신경유도배지(neural induction medium, NIM)를 5일간 사용하였다(IV). 그리고 다른 3개의 대조실험군을 설정하여 신경 분화의 증진 정도를 비교하였다; 분화시키지 않아서 분화능을 유지하고 있는 인간배아줄기세포(I), 신경유도배지를 이용해 5일간 분화시킨 인간배아줄기세포(II) 그리고 신경유도배지와 자성나노입자를 사용해 5일간 분화 유도한 인간배아줄기세포(III). 다른 실험군과 비교하여 신경 분화를 유도한 작은 크기의 인간배아체에서 통계적으로 유의미한 신경 유도의 증진 현상이 관찰되었다. 더불어, 자성나노입자가 신경유도배지와 함께 쓰였을 때, 신경 유도를 증진하는 효과가 있는 것으로 드러났다. 그리고 IV에서 증진된 신경 유도를 설명하는 신호 기전을 확인하고자 몇몇 단백질의 발현 여부를 추가적으로 확인하였다. 대표적인 단백질로는, 윈트(WNT) 단백질, 도파민반응성 신경 관련 단백질, 세포 간 상호작용과 관련된 단백질 그리고 메카노트랜스덕션

(mechanotransduction) 관련 단백질이 있다.

종합하자면, 필자는 본 연구에서 자성나노입자를 이용해 인간배아체를 효과적으로 구현하고 그것의 크기를 자유자재로 조절하는 기술을 고안하였다. 그리고 이 기술을 이용하여 인간배아줄기세포의 초기 분화 방향을 결정하는 중요한 요소 가운데 하나로서 인간배아체의 크기가 있다는 사실을 확인 할 수 있었다. 나아가, 크기가 작은 인간배아체를 구현하여 신경 유도를 시키는 연구로 심화하였는데, 신경 분화가 효과적으로 증진되어 결과적으로는 초기 신경 유도에 걸리는 시간을 대폭 단축할 수 있었다. 그리고 이 과정이 윈트(WNT) 신호전달체계 및 도파민성 신경신호전달체계를 따른다는 것을 확인할 수 있었다. 나아가, 이 같은 결과가 자성나노입자 기반의 인간배아체 구현 기술에서 기인하는 세포 간 상호작용력 증진 및 메카노트랜스덕션(mechanotransduction)에 의한 것임을 알 수 있었다. 따라서 본 연구에서 제안한 자성나노입자를 이용해 인간배아체의 크기를 조절하는 방법은 인간배아줄기세포의 특성화된 분화(lineage-specific differentiation) 유도 및 그를 통한 세포의 운명(fate) 결정에 매우 유용하고 가치 있는 기술이라고 할 수 있다. 이 기술을 이용해 인간배아줄기세포를 보다 다양한 종류의 세포로 분화 유도 할 수 있다면, 조직공학적 응용이 가능할 것이며 나아가 인간 배아의 발생과정을 모사하는 데 의미 있게 쓰일 수 있을 것이다.

주요어: 인간배아줄기세포, 인간배아체, 인간배아체 크기 조절, 특성화된 분화, 세포 운명 조절, 자성나노입자, 산화철나노입자

학번: 2012-20953